David Ian Wimpenny · Pulak M. Pandey
L. Jyothish Kumar   *Editors*

Advances in 3D Printing & Additive Manufacturing Technologies

Springer

Advances in 3D Printing & Additive Manufacturing Technologies

David Ian Wimpenny · Pulak M. Pandey
L. Jyothish Kumar
Editors

Advances in 3D Printing & Additive Manufacturing Technologies

Editors
David Ian Wimpenny
Chief Technologist – Component
  Technology
The Manufacturing Technology Centre
Coventry, Warwickshire
UK

L. Jyothish Kumar
Additive Manufacturing Society of India
Bangalore, Karnataka
India

Pulak M. Pandey
Department of Mechanical Engineering
Indian Institute of Technology Delhi
New Delhi, Delhi
India

Preface

We would like to thank the readers for taking the time to read this book, *Advances in 3D Printing & Additive Manufacturing Technologies*.

3D printing and additive manufacturing are growing at an extremely fast rate today. Additive manufacturing technology automatically fabricates components from various materials such as plastics, metals and alloys, biomaterials, and ceramics. Over the last three decades, the technology has served automotive, aerospace, manufacturing, and medical sectors. From printing parts in plastic and metals to bioprinting of transplantable organs, the technology is making a progress, which is a breakthrough innovation, garnered by the rapid growth in the core technology.

The purpose of this book is to provide the details of the latest advancements in research and developments of 3D printing and additive manufacturing processes. This book will be useful for industrial experts, entrepreneurs, university professors, and research scholars. The chapters are written by experts from across industry and academia.

Acknowledgments

Contents

Editor and Contributors

About the Editors

Prof. David Ian Wimpenny is currently appointed as the Chief Technologist at the Manufacturing Technology Centre (MTC), Coventry, UK. He joined MTC in the year 2011 as a Technology Manager, and is working as a full-time Technologist of the Component Technology Group at the MTC. He is the member of Technology Strategy Board Panel. Professor Wimpenny is Funding Advisor of National Science Foundation (NSF) since 2006. He is Chairman of the Additive Manufacturing & 3D Printing Forum for the HVM Catapult. His past roles include being head of the research at De Montfort University, Leicester, UK from 2009 to 2011 and director of Additive Manufacturing Technology Group in the Department of Engineering and Technology at De Montfort University from 2001 to 2011. Professor David Ian Wimpenny is also the member of the Additive Manufacturing Special Interest Group (AM-SIG) which was established by the Technology Strategy Board to develop a road map for the UK AM sector. He has served as an international reviewer for several international conference committees. His major activities are in the areas of additive manufacturing, rapid product development, laser printing, surface engineering, and manufacturing production tooling. He has published more than 60 papers in international/national journals and presented papers in seminars and international conferences. He has three patents to his credit and is involved with several major industries for rapid prototyping, reverse engineering, and computer-aided design. He has guided six Ph.D. students (awarded) and over 150 M.Sc. students in his capacity as a professor. He is also a member of the review committees of several reputed international journals, including Additive Manufacturing, Rapid Prototyping and Materials Processing Technology. Professor David Ian Wimpenny has two books to his credit, *Digital Model Production* and *Digital Design and Manufacturing in Dentistry.* He was also a co-editor of the *Rapid Prototyping Case Book.*

Dr. Pulak M. Pandey completed his B.Tech. degree from H.B.T.I. Kanpur in 1993 securing first position and got Master's degree from IIT Kanpur in 1995 in

Manufacturing Science specialization. He served H.B.T.I. Kanpur as faculty member for approximately 8 years and also completed Ph.D. in the area of Additive Manufacturing/3D Printing from IIT Kanpur in 2003. He joined IIT Delhi as a faculty member in 2004 and is presently continuing as Associate Professor there. In IIT Delhi, Dr. Pandey diversified his research areas in the field of micro- and nano-finishing, micro-deposition and also continued working in the area of 3D printing (Selective Laser Sintering). He has supervised 11 Ph.D.s and more than 25 M.Tech. theses in the past 10 years and also filed 10 Indian patent applications. He has approximately 60 international journal papers and 35 international/national refereed conference papers to his credit. These papers have been cited more than 1340 times with h-index as 20. He received Highly Commended Paper Award by Rapid Prototyping Journal for the paper "Experimental investigations into the effect of delay time on part strength in Selective Laser Sintering" presented in International Conference on Manufacturing Automation (ICMA 07) held at National University of Singapore during May 28–30, 2007. Many of his B.Tech. and M.Tech. supervised projects have been awarded by IIT Delhi. He is recipient of Outstanding Young Faculty Fellowship (IIT Delhi) sponsored by Kusuma Trust, Gibraltar and J.M. Mahajan Outstanding Teacher Award of IIT Delhi. Dr. Pandey is also an active reviewer of many leading international journals in the field of manufacturing science. He is Editorial Board Member of the Rapid Product Development (RPD) Magazine endorsed by RP Society of India, French RP Association, Portuguese RP Association, Standard and Industrial Research Malaysia. Recently he has been invited as an editorial member of Mechanics of Advanced Materials and Modern Processes journal published by Springer. He is an active member of Additive Manufacturing Society of India. He was the team leader of one of the assessment teams for Academic Excellence Award 2009, UP Technical University, Lucknow. Recently, he led a delegation of 10 members to UK in the area of additive manufacturing and 3D Printing sponsored by British High Commission, India. During Additive Manufacturing Society of India's recent conference-AM 2015, Dr. P.M. Pandey was awarded the award of appreciation as the leading researcher in additive manufacturing field in India.

Mr. L. Jyothish Kumar is Founder CEO of Rapitech Solutions Inc., Bangalore and also he is Founder President of Additive Manufacturing Society of India (AMSI), Bangalore. He gained his Bachelor of Engineering in Mechanical Engineering from the National Institute of Engineering, Mysore and Master's degree in Rapid Product Development from De Montfort University, UK. Mr. Kumar is currently pursuing Ph.D. research in Aerospace Applications of Additive Manufacturing Technologies. Prior to that Mr. Kumar has served in the mechanical engineering industry's different disciplines such as quality assurance, marketing, and sales and product development in India and abroad. He has a specialized experience in quality management systems and rapid product development which have been responsible in spearheading Rapitech Solutions Inc.'s efforts to streamline the business development operations for its customers. Mr. Jyothish Kumar brings credible experience and knowledge from his project work at RPMG,

UK, association with other high-scale (€9M) European Union funded projects with 33 other partners across Europe including Delcam Plc (UK), Materialise (Belgium) and Ducati (Italy), developing a new rapid prototyping process based on a combination of laser printing (electro photography) and Infrared sintering polymers. He holds Memorandum of Understanding (MOU) with international organization French Rapid Prototyping Association (APRF) and Central Manufacturing Research and Development Institute (CMRDI). Mr. Kumar is Managing Editor of Additive Manufacturing Technology Magazine (www.ammagazine.in), the only magazine in India on 3D printing and additive manufacturing technologies. He was Expert Speaker at 7th CII Annual Manufacturing Conference—Make in India: Rejuvenating Indian Manufacturing, November 14–15, 2014, Bangalore, India. He was Keynote Speaker at 19th European Forum for Additive Manufacturing Technologies, June 24–26, 2014, Paris, France. He has delivered expert talks at more than 20 engineering colleges in India and more than 12 industries including defence and private organization. He has organized and guided as a convener for 1st, 2nd, 3rd, 4th, and 5th International Conference on Additive Manufacturing Technologies and also convener for the upcoming 6th International Conference on Additive Manufacturing Technologies which is scheduled to be held during October 6–7, 2016 at Bangalore.

Contributors

B.B. Ahuja Biomedical Engineering & Technology Incubation Centre, College of Engineering Pune, Pune, India

A.R. Anwar Khan Department of Mechanical Engineering, Ghousia College of Engineering, Ramanagara, KA, India

G. Arumaikkannu Department of Manufacturing Engineering, College of Engineering Guindy, Anna University, Chennai, India

Ashutosh D. Bagde Mechanical Engineering Department, VNIT, Nagpur, India

Usaid Mohammed Baig Ghousia College of Engineering, Ramanagara, KA, India

Alok Bara Department of Mechanical Engineering, VSSUT, Burla, Odisha, India

Sébastien Begoc CNES, French Space Agency, Paris, France

Sandeep W. Dahake Mechanical Engineering Department, VNIT, Nagpur, India

Jérôme Dehouve CNES, French Space Agency, Paris, France

V. Durga Prasada Rao Mechanical Engineering Department, SRKR Engineering College, Bhimavaram, Andhra Pradesh, India

Ravi Dwivedi Department of Mechanical Engineering, Maulana Azad National Institute of Technology, Bhopal, MP, India

K. Hariharan Department of Manufacturing Engineering, College of Engineering Guindy, Anna University, Chennai, India

S.D. Hiwase Samrachana Software Solutions Ltd, Hyderabad, India

P.J. Kale Mechanical Department, Jawaharlal Darda Institute of Engineering & Technology, Yavatmal, MS, India

Ganesa Balamurugan Kannan Adhoc Faculties, Department of Production Engineering, NIT, Tiruchirappalli, India

A. Kavitha Department of Biomedical Engineering, Centre for Healthcare Technologies, SSN College of Engineering, Chennai, India

C.G. Krishnadas Nair Jain University, Governing Council, IIAEM, Bangalore, India

P.S. Krishnaveni Mechanical Engineering Department, SRKR Engineering College, Bhimavaram, Andhra Pradesh, India

L. Jyothish Kumar Jain University, Bangalore, India

T.K. Kundra Department of Mechanical Engineering, Indian Institute of Technology Delhi, New Delhi, India

Abhaykumar M. Kuthe Mechanical Engineering Department, VNIT, Nagpur, India

Sachin Maheshwari Division of Manufacturing Processes and Automation Engineering, Netaji Subhas Institute of Technology, New Delhi, India

Mahesh B. Mawale Mechanical Engineering Department, VNIT, Nagpur, India

R.M. Metkar Mechanical Department, Government College of Engineering, Amravati, India

Pragyan Paramita Mohanty Department of Mechanical Engineering, Veer Surendra Sai University of Technology, Burla, Odisha, India

A.V. Mulay Biomedical Engineering & Technology Incubation Centre, College of Engineering Pune, Pune, India

Sunita Singh Naik Department of Mechanical Engineering, VSSUT, Burla, Odisha, India

V. Navya Geethika Mechanical Engineering Department, SRKR Engineering College, Bhimavaram, Andhra Pradesh, India

Sandrine Palerm CNES, French Space Agency, Paris, France

Anjali P. Rajan Biomedical Engineering & Technology Incubation Centre, College of Engineering Pune, Pune, India

D. Ramesh Rajakumar CSIR-National Aerospace Laboratories, Bangalore, India

Dinesh Kumar Rajendran Adhoc Faculties, Department of Production Engineering, NIT, Tiruchirappalli, India

T.S. Ranjani. Department of Biomedical Engineering, Centre for Healthcare Technologies, SSN College of Engineering, Chennai, India

Sandeep Rathee Division of Manufacturing Processes and Automation Engineering, Netaji Subhas Institute of Technology, New Delhi, India

Sarat Kumar Sahoo Department of Mechanical Engineering, Veer Surendra Sai University of Technology, Burla, Odisha, India

Anshuman Kumar Sahu Department of Mechanical Engineering, Veer Surendra Sai University of Technology, Burla, Odisha, India

Raphaël Salapete SNECMA, SAFRAN Group, Vernon, France

V. Sarah Rajitha Thilagam Department of Biomedical Engineering, Centre for Healthcare Technologies, SSN College of Engineering, Chennai, India

Ankur Kumar Singh Department of Mechanical Engineering, Maulana Azad National Institute of Technology, Bhopal, MP, India

Manu Srivastava Division of Manufacturing Processes and Automation Engineering, Netaji Subhas Institute of Technology, New Delhi, India

G. Sudhir Sri Ramachandra Medical College and Research Institute, Chennai, Tamil Nadu, India

K. Swarna Lakshmi Department of Manufacturing Engineering, College of Engineering Guindy, Anna University, Chennai, India

Marie Theron CNES, French Space Agency, Paris, France

Kshitiz Upadhyay Department of Mechanical Engineering, Maulana Azad National Institute of Technology, Bhopal, MP, India

S. Vinutha Department of Biomedical Engineering, Centre for Healthcare Technologies, SSN College of Engineering, Chennai, India

Influence of Process Parameters on Tensile Strength of Additive Manufactured Polymer Parts Using Taguchi Method

K. Swarna Lakshmi and G. Arumaikkannu

Abstract Selective laser sintering (SLS) is a powder-based additive manufacturing technology in which powder particles fuse using CO_2 laser. In this work, the influence of various parameters at various levels is studied experimentally. In this work, the components were designed and fabricated as per ASTM standards. Experiments were designed based on Taguchi's design of experiment. An L27 Orthogonal array of Taguchi design was used. In order to determine the significance and contribution of each factor on the tensile strength, analysis of variance (ANOVA) was performed. The results determine that layer thickness and fill scan spacing are significant parameters that cause appreciable improvement in tensile strength.

Keywords Polyamide · Selective laser sintering · Taguchi

1 Introduction

Additive manufacturing (AM) technology has been implemented in many industrial sectors—particularly in the field of medicine and health care. SLS is one of the most popular AM process used for orthopedic and dental applications. Polymers have been widely used in the SLS process [1, 2]. Process parameters are defined variables that influence and control the SLS process. The net result of the SLS process is usually described by the geometrical and mechanical properties of the parts produced. The parts produced should possess sufficient strength to ensure functional requirements. There are several parameters contributing the strength of an SLS product. Many trials were conducted to review the consequences of process parameters on the mechanical properties of SLS parts. William and Deckard used analytical and experimental methods to understand the outcome of density and

K. Swarna Lakshmi (✉) · G. Arumaikkannu
Department of Manufacturing Engineering, College of Engineering Guindy,
Anna University, Chennai, India
e-mail: kslswarna@rediffmail.com

strength in terms of flexural modulus by varying energy density, spot diameter, and delay [2]. Gibson and Shi reviewed the consequence of laser power, hatch spacing, and scan size on strength and density of parts using fine nylon material [3]. Thompson and Crawford devised regression models to study the response of laser power, layer thickness, and build orientation on surface roughness and tensile strength [4]. Caulfield et al. investigated the importance of laser power, beam speed, and hatch spacing on the mechanical properties of polyamide components and identified that Young's modulus, yield strength, and fracture strength increases with increases in energy density [5]. Jain et al. investigated the influence of delay time on the tensile strength of SLS process keeping part bed temperature constant [6]. Jain et al. investigated the orientation on the part strength by considering the delay time [7]. Apart from the attempts made earlier in this work, various parameters were analyzed that can influence the tensile strength of the PA 12 parts.

In the present work, a trial has been made to study the outcome of fill scan spacing on the strength of SLS parts using polyamide (PA12) powder. Tensile test specimens are fabricated in various fill scan spacing ranges. Fabricated test specimens are tested for ultimate tensile strength on universal testing machines.

2 Experimental Setup

2.1 Specimen Characteristics

Polyamide powder (PA12) tensile specimen, $115 \times 6 \times 4$ mm^3, as suggested by ASTM standard of D638 was used for the experiments. This material was selected for the experiments as it can be used for medical applications. Also this has some advantages such as increased stiffness and heat resistance.

2.2 Sintering Parameters

Layer thickness, fill scan spacing, and orientation were the variables chosen for this work because from previous research [8] it was observed that these variables had the most influence on the surface roughness. A low, medium, and high level was selected for each of the sintering to have wide range of combinations.

2.3 Equipment Characteristics

SLS Sinter station 2500+ was used for the sintering operations whose build dimension is $381 \times 330 \times 457$ mm. Selective laser sintering (SLS) is an additive

manufacturing technique that uses a high-power carbon dioxide laser which selectively fuses small particles to the desired 3D shape based on the 3D CAD model.

2.4 Design of Experiments

An efficient method of experimental planning is design of experiments (DoE), which incorporates the orthogonal array developed by taguchi to collect statistically significant data with the minimum possible number of repetitions. Here L_{27} array was selected, and the levels of the parameter are displayed in Table 1.

Table 1 Levels of process parameters

Exp. no	Layer thickness (mm)	Fill scan spacing (mm)	Orientation (°)	Tensile strength (N/mm²)	S/N ratio
1	0.1	0.14	0	0.8485	−1.42696
2	0.1	0.14	30	0.7765	−2.19717
3	0.1	0.14	45	0.5645	−4.96672
4	0.1	0.15	0	0.503	−5.96864
5	0.1	0.15	30	0.9075	−0.84307
6	0.1	0.15	45	0.944	−0.50056
7	0.1	0.16	0	0.808	−1.85177
8	0.1	0.16	30	0.6845	−3.29253
9	0.1	0.16	45	0.9055	−0.86223
10	0.13	0.14	0	0.8975	−0.93931
11	0.13	0.14	30	0.936	−0.57448
12	0.13	0.14	45	1.23	0.407226
13	0.13	0.15	0	0.918	−0.62567
14	0.13	0.15	30	0.761	−2.37231
15	0.13	0.15	45	0.67925	−3.35941
16	0.13	0.16	0	0.5975	−4.47324
17	0.13	0.16	30	0.8395	−1.51959
18	0.13	0.16	45	0.909	−0.82872
19	0.15	0.14	0	0.8325	−1.59232
20	0.15	0.14	30	0.932	−0.61168
21	0.15	0.14	45	0.9485	−0.45925
22	0.15	0.15	0	0.9625	−0.33199
23	0.15	0.15	30	0.884	−1.07095
24	0.15	0.15	45	0.7825	−2.13031
25	0.15	0.16	0	0.8145	−3.39464
26	0.15	0.16	30	0.8975	−0.93931
27	0.15	0.16	45	0.8235	−1.68673
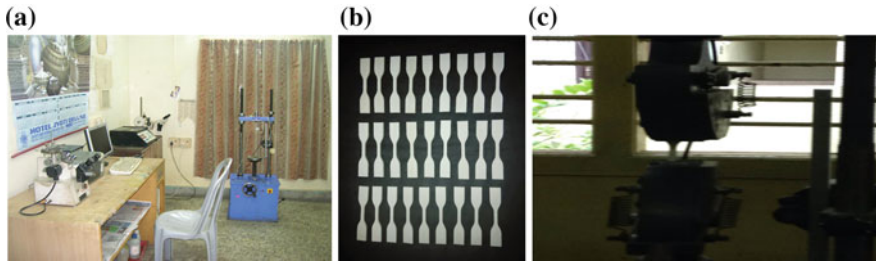
Fig. 1 **a** Experimental setup. **b** Fabricated parts. **c** Tensile test

2.5 Experimental Procedure

A tensile testing machine (Associated Scientific Engg. Works, New Delhi) with a testing load range of max 5 ton with a gear rotation speed (for gradual loading) of 0.25, 1.5, and 2.5 mm/min was used to measure the tensile strength of the specimen. Figure 1a–c shows a scheme of the experimental setup, the fabricated parts, and the testing conditions used in this work, respectively. As it is observed, once the trial concluded the change in length, area of cross section, and young's modulus are measured and calculated. The values are tabulated in Table 1. The ANOVA was performed considering the process parameters as factors and tensile strength as response.

3 Results and Discussion

Eighty one parts were fabricated with different process parameters. The experimental results are displayed in Table 1. ANOVA was performed. Analysis of variance for the response variable (Tensile strength) is displayed in Table 2. The main effects plot for tensile strength is shown in Fig. 2.

In the experimental setup, the building direction is normal to the platform (Z direction). The testing is performed parallel to the build layers. The orientation has no effect on the direction of testing. This assumption is also verified from the statistical analysis of the data. The influence of layer thickness has a greater effect

Table 2 ANOVA

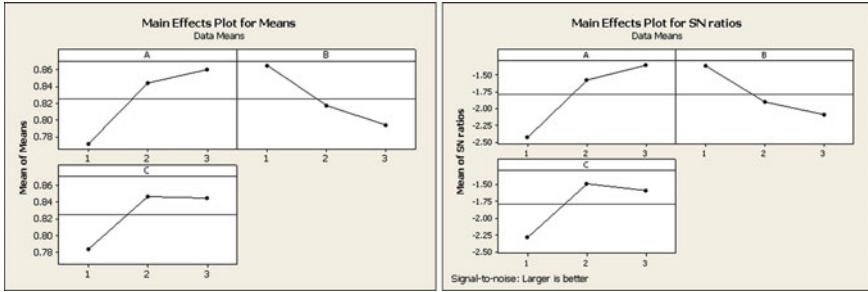| Source	DF	Seq SS	MS	F	P
Layer thickness	2	0.04025	0.02012	1.07	0.362
Fill scan spacing	2	0.02381	0.01190	0.63	0.541
Orientation	2	0.02284	0.01142	0.61	0.555
Error	20	0.37610	0.01880		
Total	26	0.46298			

Fig. 2 Main effects plot for tensile strength

on the tensile strength with statistical significance. As explained above, CO_2 laser has a trivial penetration in this process. Therefore, an increase in layer thickness will tend to weaken the bonding between layers.

4 Analysis of Results

4.1 Statistical Analysis

After the collection of data, they are to be analyzed by means of calculating S/N ratio (quality indicator). Here, the performance of the process is evaluated based on changing a particular process parameter and is displayed in Table 1. The average effect of layer thickness for levels 1, 2, and 3 are calculated using the data of layer thickness from the experiments 1–9, 10–18, and 19–27, respectively, of Table 1. Table 3 summarizes that layer thickness and fill scan spacing of the component have significant influence over tensile strength.

4.2 ANOVA

In order to evaluate the significance of ANOVA, computation was performed for evaluating the significance of the process parameters over tensile strength. From

Table 3 Response table for signal to noise ratio

Levels	A	B	C
1	−2.434	−1.373	−2.289
2	−1.587	−1.911	−1.491
3	−1.357	−2.094	−1.599
Delta	1.077	0.721	0.798
Rank	1	3	2

Table 2 it is inferred that the F ratio values of parameters layer thickness and orientation are all greater than the F ratio values drawn from table ($F2, 26 = 3.3690$).

4.3 Response Graphs

It is an organized, graphical representation of the parameters. The performance and the variation of each parameter are represented pictorially when moving from one level to another. Figure 2a, b show tensile strength response for layer thickness, fill scan spacing, and orientation.

Here, level two for $A3 = -1.357$ has the highest S/N ratio value, which indicates that the sintering performance at such level produces greater variation of tensile strength This indicates that level 3 of C in the 12th sintered part produces larger variation in tensile strength when compared to level 1 and 2 of C. It may be because the incidence of laser energy is deeper and produces complete melting of the powder material. Therefore, there is a consistent dissemination of mechanical property across the layer thickness.

5 Prediction of Optimum Performance

Optimal tensile strength values are estimated as follows:

$$\text{Predicted optimal tensile strength} = \overline{A1} + \overline{C2} - \overline{Y}$$
$$= 3.673$$

where $\overline{A1}$ is level 1 of layer thickness, $\overline{C2}$ is the level 2 of orientation, and $\overline{Y}$ is the average tensile strength.

6 Conclusion

The main intention of this work is to identify how the layer thickness, fill scan pacing, and build orientation affect the mechanical property of parts manufactured by SLS technology. In terms of mechanical property, this process is somewhat sensitive to layer thickness and orientation. An increase in layer thickness tends to temper the part in terms of tensile strength. This study provides an integrated set of experimental data addressing the mechanical property. Further, a statistical approach was used to investigate the influence of the process parameters.

References

1. Jollivet T, Darfeuille A, Verquin B, Pillot S (2009) Rapid manufacturing of polymer parts. Int J Mater Form 2(1):697–700. doi:10.1007/s12289-009-0604-8
2. Williams JD, Deckard CR (1998) Advances in modeling the effects of selected parameters on the SLS process. Rapid Prototyping J 4(2):90–100. doi:10.1108/13552549810210257
3. Gibson I, Shi D (1997) Materials Properties and fabrication parameters in selective laser sintering process. Rapid Prototyping J 3(4):129–136. doi:10.1108/13552549710191836
4. Thompson DC, Crawford RH (1997) computational quality measures for evaluation of part orientation in freeform fabrication.J. Manuf Syst 16(4):273–289
5. Caulfield B, McHugh PE, Lohfeld S (2007) Dependence of mechanical properties of polyamide components on uild parameters in the SLS process. J Mater Process Technol 182:4777–488. doi:10.1016/j.jmatprotec.2006.09.007
6. Jain PK, Pandey PM, Rao PVM (2007) Experimental investigation into delay time on part strength in selective laser sintering. In: Proceedings of international conference on manufacturing automation. National University of Singapore, Singapore, May 28–30, pp 501–506
7. Jain PK, Pandey PM, Rao PVM (2009) Effect of delay time on part strength in selective laser sintering. Int J Adv Manuf Technol 43:117–126. doi:10.1007/s00170-008-1682-3
8. Swarna Lakshmi K, Arumaikkannu G (2014) Influence of process parameters on surface finish in customized bone implant using selective laser sintering. Adv Mater Res 845(2014):862–867
9. Chokalingam K, Jawahar N, Ramanathan KN, Banerjee PS (2006) Optimization of stereolithography process parametersfor part strength using design of experiments. Int J Adv Manuf Technol 29:79–88

Determination and Comparison of the Anisotropic Strengths of Fused Deposition Modeling P400 ABS

Kshitiz Upadhyay, Ravi Dwivedi and Ankur Kumar Singh

Abstract Fused deposition modeling (FDM) is an additive layered manufacturing technique used to build prototypes and functional products out of thermoplastic materials. The properties of the FDM parts are affected by many factors like geometry of the material bead, process conditions, and orientation of the part and layers etc. The present study focuses on the effect of build direction on the mechanical properties of acrylonitrile butadiene styrene (ABS) P400 part specimens. Tensile, compressive, Izod impact, and hardness tests were performed on specimens built in the horizontal and vertical orientations with an intention to find the build direction that gives maximum strength in a particular working condition. Fractured specimens were then analyzed under the Jeol JSM 5600 Scanning Electron Microscope to study the impact failure pattern. The findings of this research can further be used to formulate product design rules for optimizing mechanical strength in layered manufacturing.

1 Introduction

Conventional manufacturing consisted mostly of subtractive and forming processes like milling, turning, coining, grinding etc., in which a part is shaped by either material removal or plastic deformation. Rapid prototyping, however, belongs to the generative or additive production processes. First emerged with the introduction of steriolithography technology in 1987, many RP technologies have been developed since then, for example fused deposition modeling, selective laser melting, selective laser sintering, laminated object manufacturing, solid ground curing etc.

K. Upadhyay (✉) · R. Dwivedi · A.K. Singh
Department of Mechanical Engineering, Maulana Azad National Institute
of Technology, Bhopal 462051, MP, India
e-mail: kshitiz.nitb@gmail.com
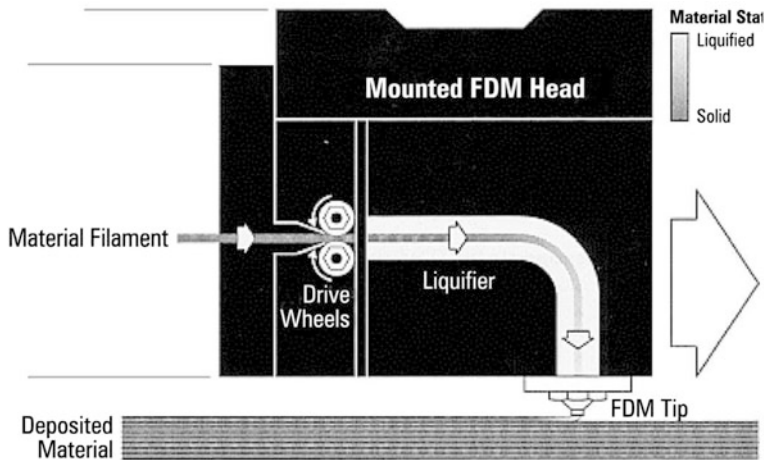
Fig. 1 Fused deposition modeling process [5]

It is a technology of huge significance in today's world because of its ability to decrease the manufacturing lead time by 30–50 %, yet maintaining part complexity [1, 2].

Fused deposition modeling (FDM) is one such RP process in which a part is fabricated by stacking layers of a molten thermoplastic material one above the other [3]. In the FDM process, first a 3D CAD model is created. This model is then exported to a slicing software like the FDM Quick Slice software using steriolithography (STL) format that tessellates the part into numerous basic triangular components. Although the part loses some resolution while exporting, STL format is advantageous because it simplifies the geometry [4]. The Quick Slice software slices the model into numerous horizontal sections. These are the two-dimensional contours that the FDM process will later generate and stack above each other. The software then uses this data to formulate a process plan for the FDM machine's hardware (Fig. 1).

During fabrication, a thermoplastic filament passes through a heating element that partially melts the filament. This semi-molten filament is then dropped through a nozzle which can move in the *XY* plane, onto a platform. The deposition takes place according to a path which is generated by the software. After completing one layer of deposition, the platform holding the part moves vertically in the *Z* plane and the process repeats. The newly fed heated filament fuses with the material in the adjacent layers of the partially constructed part. In a period of time, usually several hours, a complete part forms on the platform. An overhang or an intricate part geometry, may sometimes necessitate a support material. This material is fed through a second nozzle that is present beside the first one. The support material can be easily removed after the process by either breaking it off, or dissolving it in warm water bath. To maintain a constant heated environment, the entire process is done in a closed chamber which is also known as the envelope. This heated environment
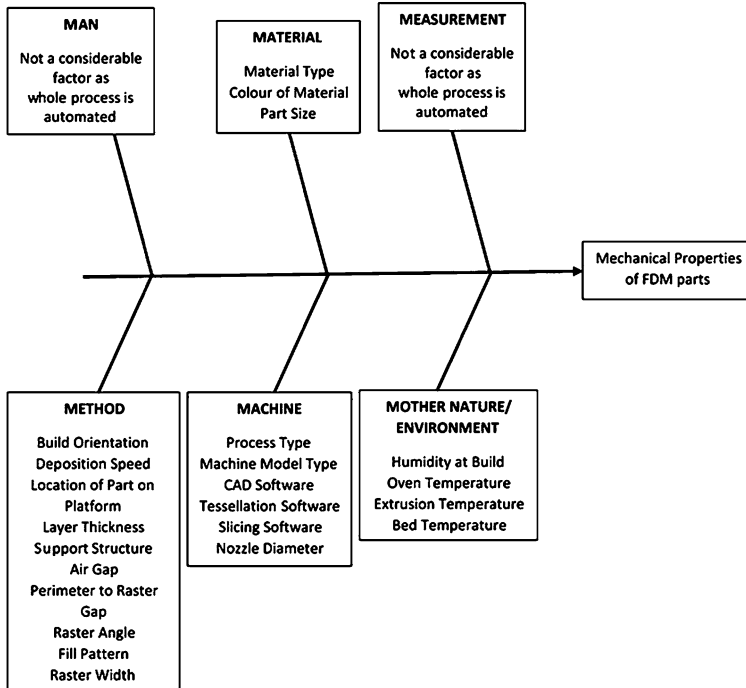
Fig. 2 Fishbone diagram (6M) showing factors that can affect the mechanical properties of the FDM prototypes/parts

helps to improve the interlayer bonding [6] and reduces shrinking, warping, and internal stresses [7].

Although the objects produced by FDM are mainly used as models and prototypes, there is a potential that these can be used as functional products. However, this would require improvements in these procedures and a sound knowledge about the material properties like mechanical, electrical, thermal properties etc. [8]. The properties of an FDM part also depend on the process parameters listed in Fig. 2. Determination of the FDM process parameters such as air gap, layer thickness, raster width and angle, and build orientation have remarkable effects on the mechanical properties and performance of the component [9, 10].

Variation in the properties of the parts produced by the FDM due to process parameters' change has also been studied in the past. Hossain et al. [11] focused on improving the tensile properties of FDM-manufactured polycarbonate parts by adjusting the parameters and analyzing the stress concentration features between the adjacent roads of material. The parameters that were changed are raster angle, contour width, raster width, and raster to raster air gap. Fatimatuzahraa et al. [12] measured and compared the tensile, bending, impact, and deflection strengths of the FDM ABS specimens manufactured in two different raster angles/orientations,

which were cross (0°/90°) and criss-cross (45°/−45°). The results of their experiments showed that the criss-cross raster orientation gave higher strengths in all the tests except the tensile strength test, in which cross raster gave a higher strength value. Anitha et al. [13] studied the effect of layer thickness, road width, and deposition speed on the surface roughness of parts produced by FDM. The experimental results concluded that the surface roughness is mostly affected by layer thickness, followed by road width and then deposition speed. Reddy et al. [14] determined that road gap, extrusion temperature, and oven temperature all had a significant impact on part strength for parts fabricated from ABS, a finding that holds for most materials. Es-Said et al. [15] studied the tensile strength, modulus of rupture, and impact resistance of ABS models produced using various raster orientations. The results suggested that the 0° raster orientation demonstrated superior strength and impact resistance among the five raster orientations examined.

In addition to the factors discussed in the previous paragraph, one important process parameter that has shown huge significance in the optimisation of FDM process is the build orientation. Build orientation (also called part orientation) is the direction along which the part is actually built on the platform. Thrimurthulu et al. [16] attempted to improve surface finish and reduce building time by optimizing part deposition orientation. They developed models to evaluate average part surface roughness and build time. Moreover, a real coded genetic algorithm was used to obtain the optimum solution. Waghchore [17] aimed at the determination of optimum-built orientation angle for minimum build time for fused deposition modeling (FDM). To achieve this, simple machine parts were manufactured at different angles from 0° to 90° in step interval of 15° and time for each orientation was taken by using the Catalyst software. Tagore et al. [3] focussed on optimizing the build orientation to get the best surface quality, part accuracy, build time, and cost. Masood et al. [18] tried to determine the optimum build orientation in FDM using volumetric error for tessellated CAD models. They formulated a generic algorithm for this purpose. Volumetric error was calculated for various build orientations and the best orientation had the least error. Byun and Lee [19] aimed at determining the optimal buildup direction of a part for different RP systems using simple additive weighting method. Factors under their consideration were average weighted surface roughness, build time, and part cost appraised by build cost, labor cost, and material cost etc.

Ahn et al. [5] compared the tensile and compressive strengths of the FDM prototypes made of ABS P400, with the injection-molded parts of the same material. The factors considered in tensile strength measurements were raster orientation, air gap, bead width, color, and model temperature. On the other hand, build orientation was the factor that was considered in compressive strength measurement. It was shown that the build orientation significantly affects the compressive strength of the FDM specimens. Lee et al. [20] compared the FDM, 3D printer, and Nanocomposite deposition (NCDS) processes by performing experiments on directionally fabricated cylindrical parts. The effect of build direction on the compressive strength of parts was examined. Anoop et al. [9] concluded that raster angle and orientation, layer thickness, raster width, and air gap are the four

significant factors that should be taken into account in an FDM process. It was stated that these parameters strongly influence the tensile, deflection, impact, and flexural strength. Bagsik et al. [21] studied the variation in the tensile properties of Ultem*9085 material FDM specimens by changing the build orientation, raster angle, filament thickness, raster to raster air gap, and perimeter to raster air gap. A total of 54 experiments were conducted each for tensile strength and strain measurement that showed that the tensile properties vary substantially by changing process parameters. Bellini et al. [22] claimed that building strategies in an FDM process affect the mechanical properties of produced parts. The authors predicted that the bond between layers is an important factor. They envisaged that when an FDM part is pulled along the build direction, the bond between layers is too weak and defects are usually present. Similar conclusion was drawn by Chakraborty et al. [23], who concluded that the mechanical strength of FDM parts suffers from anisotropy. Furthermore, they stated that as compared with the interlayer adhesive strength, the strength of continuous filaments is much greater.

Literature suggests that build orientation is an important FDM process parameter. Although extensive research has been done on the anisotropic nature of tensile and compressive properties of FDM prototypes, there is a lack of research done on other important mechanical properties like hardness and impact strength. These mechanical properties are especially more important for polymer and composite materials, where there is no general relationship between indentation hardness and tensile strength. The usage of ABS in FDM process provides the ability to conduct functional tests on fabricated part samples, by offering impact resistance, heat stability, chemical resistance, and toughness [12]. However, there is a need to quantify these properties so that build rules may be formulated. Also it can serve as a data sheet for manufacturers so that better properties may be imparted to the part even before its manufacturing begins. This paper attempts to analyze a broader spectrum of mechanical strengths of FDM ABS P400 parts. Experiments were conducted in which the effect of build orientation on the mechanical properties, namely tensile strength, compressive strength, impact strength, and the Rockwell hardness of FDM parts were examined. Fractured specimens were also analyzed under the Jeol JSM 5600 Scanning Electron Microscope to study the Impact failure pattern.

2 Build Parameter Consideration

The FDM process basically requires fixing of several build/process parameters which can affect the mechanical properties of the manufactured prototypes. These parameters were fixed for both the build orientations on which experiments were intended to perform to determine and compare their mechanical properties. The two build orientations tested in the experiments are depicted in Figs. 3 and 4. Both the
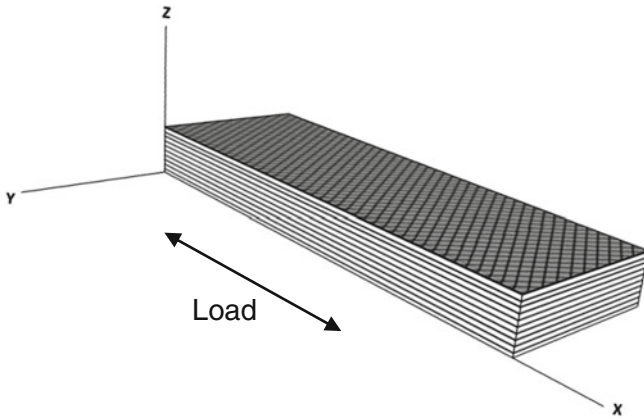
Fig. 3 Horizontal (*X*) build orientation of an FDM specimen
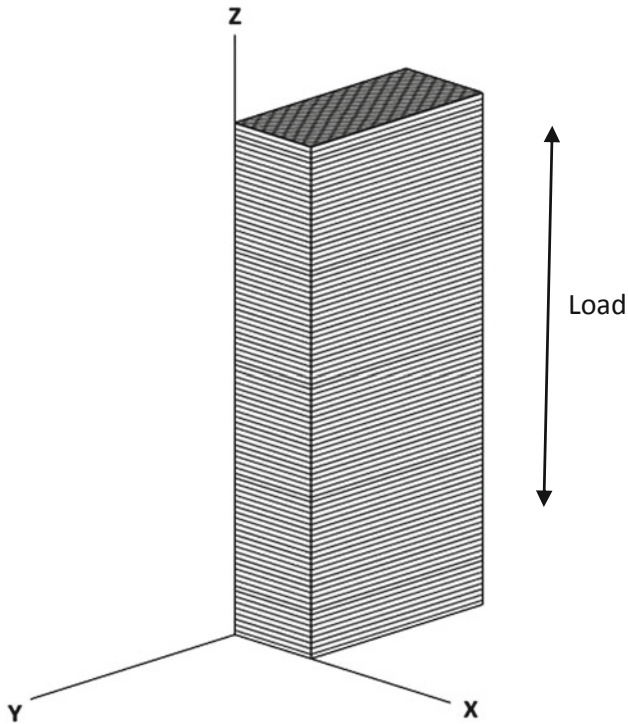

Fig. 4 Vertical (*Z*) build orientation of an FDM specimen

parts depicted in the figures have identical dimensions and are built from bottom to top (positive *Z*) in the FDM, but the orientation of fibers under stress will be different (example of a tensile load shown in the Figs. 3 and 4). In general, *X* orientation has the greatest projected footprint on the FDM bed while *Z* orientation has the least.

The research used CatalystEX slicing software for this purpose. The selected parameters are listed below.

2.1 Layer Resolution

Layer resolution is the thickness of each layer that the FDM nozzle deposits. In the FDM SST-768 machine, it can either be the standard 0.2540 mm layer or a 0.3302 mm layer. In the present research, the layer resolution selected was 0.2540 mm.

2.2 Model Interior

Model interior refers to the way in which the solid interior areas of a part get filled with material. The "Solid-normal" option in FDM is used when a strong and durable part is desired. This fill type uses more amount of material and is costlier and time-taking. The "Sparse" option creates a part that is honeycombed or hatched from inside. Sparse option creates part with lesser material and reduced time/cost. The present paper uses "Solid-normal" as its model interior.

2.3 Support Fill

An additional support material is used to provide a build substrate if the component part shows an overhang, offset, or cavity [21]. This additional material prevents the component part from collapsing during the building process. The support fill parameter can be modified to basic, sparse, minimal, and surround. The present paper used "basic" support fill for *X* orientation specimens, and "surround" fill for the *Z* orientation specimens.

2.4 Color

ABS P400 is available in white, blue, black, yellow, green, and red colors among others. Color is a qualitative parameter which has a little effect over the tensile strengths of the FDM parts [5]. The present paper used white ABS P400 polymer as a raw material.

Table 1 Build time of the FDM specimens

Specimen	Orientation	Build time (min)
Tensile	X	32
Tensile	Z	270
Compressive and hardness	X	17
Compressive and hardness	Z	48
Izod impact	X	20
Izod impact	Z	104

The build time for the specimens is given in Table 1. This data is obtained from the Catalyst EX software. It can be observed that the building time for horizontal specimens is generally lesser than that of vertical specimens. The reduction in build time can be attributed to fewer number of slices in an orientation with minimum vertical z height [17].

3 Experimental Setup

The experiment was conducted in which a number of standardized samples were built in the Dimension SST-768 FDM machine by modifying the orientation of build in CatalystEX software. Manufactured prototypes were then tested for their mechanical strengths.

3.1 Tensile Strength Test

The tensile tests were carried out according to the ASTM D638 procedure. Instron 3382 machine with 100 kN capacity was chosen for the experiments that has a measurement accuracy of ±0.5 % of the reading value. The loading rate was set to 5 mm/min. A total of five samples were made for each build orientation. The test samples were built according to the ASTM D638, type I tensile standard. Figure 5 shows the dimensions of the tensile test specimen.

3.2 Compressive Strength Test

The compression tests were carried out according to the ASTM D695 procedure. Instron 3382 machine with 100 kN capacity was chosen for the experiments that has a measurement accuracy of ±0.5 % of the reading value. The loading rate was set to 1.3 mm/min. Maximum load was noted during the test when the rupture took
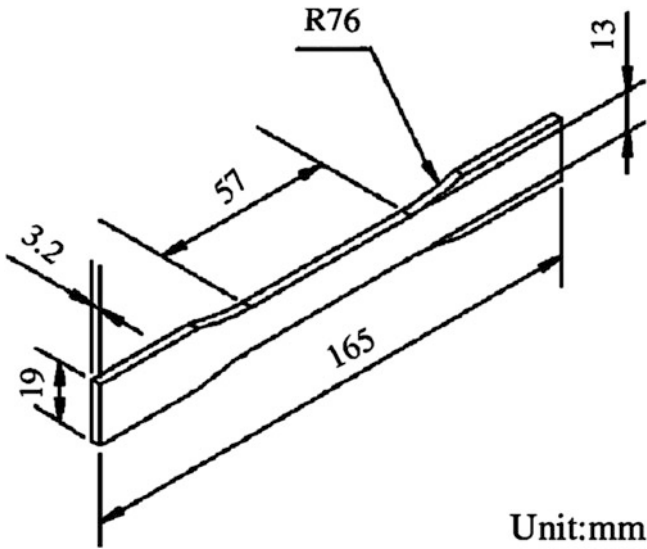
Fig. 5 ASTM D638 type I tensile bar

place. A total of five samples were made for each build orientation. The test samples were built strictly according to the ASTM D695 standard. The specimens were rectangular prisms and had a size of 12.7 mm × 12.7 mm × 25.4 mm.

3.3 Izod Impact Strength Test

The ASTM D4812 testing procedure was adopted in the experiment on a Cantilever Beam Impact machine, according to which the standard specimen size was 64 mm × 12.7 mm × 3.2 mm. The samples were un-notched and the impact blow was edgewise impact (hitting the smallest dimension). As this standard size is prone to bend or crush easily, the specimen thickness was increased from 3.2 to 6.4 mm. A total of five samples were made for each build orientation.

3.4 Rockwell Hardness Test

The ASTM D785 testing procedure was adopted for the test in which the specimens had a minimum constant thickness of 6.4 mm. Procedure A under D785 was used to find the hardness values. The scale adopted for testing was M scale, which is typically used for soft bearing metals and plastics. A minor load of 10 kgf and a temporary major load of 100 kgf was applied by a 1/4″ diameter steel ball indenter.
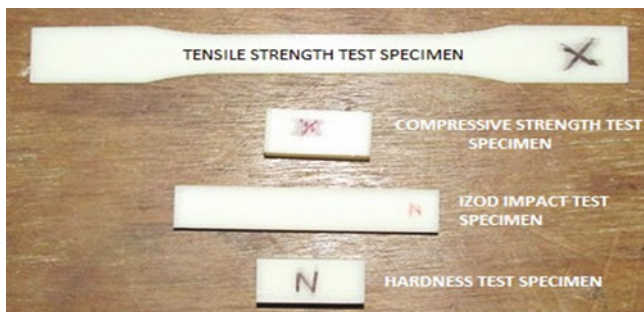
Fig. 6 Test samples used in the experiment

The 12.7 mm × 25.4 mm face was indented for both build orientations. For Z orientation, all such faces are identical. For X orientation, the indentation was made on the hatched face (parallel to the part building direction). The minor load was applied for 10 s and the major load application time was set to 15 s. Although the specimens were built identical to the compressive test specimens which had a thickness of 12.7 mm (greater than the standard of 6.4 mm), tests were performed separately. A total of five samples were made for each build orientation (Fig. 6).

4 Results

4.1 Tensile Test

Five samples of each orientation were tested for their tensile strength . Tables 2 and 3 show the results of the experiments conducted on X and Z orientation, respectively.

From the results, it can be examined that the X orientation demonstrates a greater value of ultimate tensile strength as compared to the Z orientation. The tensile strength obtained for injection-molded ABS P400 by Sung-hoon Ahn et al. was

Table 2 Tensile test results for the horizontal orientation samples

Sample No.	Width (mm)	Thickness (mm)	Failing load (kN)	Ultimate tensile strength (MPa)
X1	12.73	3.12	0.73	18
X2	13.12	3.17	0.83	20
X3	12.82	3.31	0.72	17
X4	12.85	3.22	0.78	19
X5	13.07	3.22	0.80	19

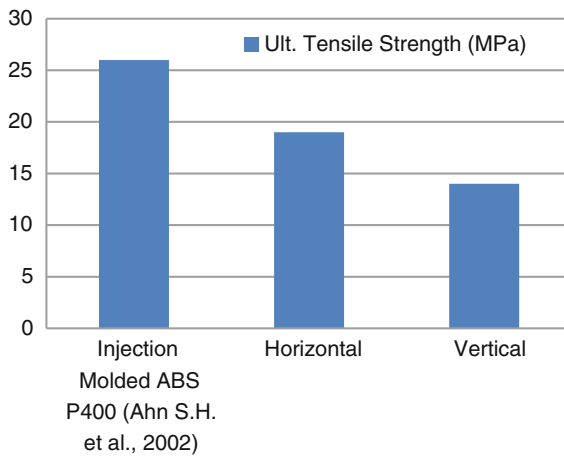Avg. Ult. tensile strength (S_{ut}) = 19 MPa
Standard Deviation (s) = 1.1

Table 3 Tensile test results for the vertical orientation samples

Sample No.	Width (mm)	Thickness (mm)	Failing load (kN)	Ultimate tensile strength (MPa)
Z1	12.67	2.93	0.56	15
Z2	12.98	3.32	0.56	13
Z3	13.21	3.36	0.58	13
Z4	12.84	2.91	0.56	15
Z5	13.28	3.05	0.59	15

Avg. Ult. Tensile strength (S'_{ut}) = 14 MPa
Standard Deviation (s) = 1.1

Fig. 7 Comparison of the Ult. tensile strength values

26 MPa [5]. We can note that the tensile strength of the oriented parts made by FDM is lesser than that of injection-molded P400 part. The difference can be observed from the chart in Fig. 7.

This difference in the values between the two orientations can be explained by the arrangement of layers in the prototypes. From Fig. 3, it can be seen that the layers in the horizontal orientation are arranged parallel to the applied load during the tensile test. On the contrary, the layers in the vertical orientation are stacked one above the other, i.e. perpendicular to the applied load. This makes the vertical orientation more vulnerable to fracture during the test. The horizontal specimens showed tensile failure of individual fibers resulting in higher tensile strength. The vertical specimens, however, resulted in lower tensile strength because the tensile load was taken by the bond between the fibers, and not the fibers themselves. The macroscopic view of six fractured specimens is presented in Fig. 8.
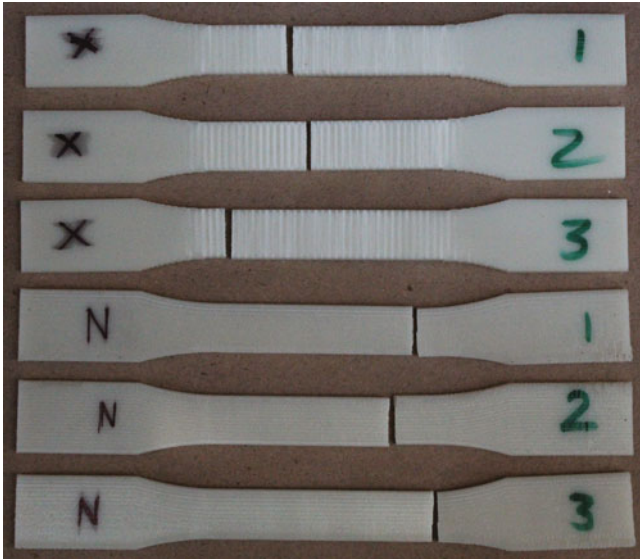
Fig. 8 Failure pattern of the fractured test samples

Table 4 Compressive test results for the horizontal orientation Samples

Sample No.	Length (mm)	Width (mm)	Failing load (kN)	Compressive strength (MPa)
X1	12.82	12.71	5.40	33.1
X2	12.80	12.67	5.24	32.3
X3	12.75	12.87	5.40	32.9
X4	12.68	12.65	5.32	33.2
X5	12.75	12.81	5.41	33.1

Avg. compressive strength = 32.9 MPa
Standard Deviation (s) = 0.36

4.2 Compressive Test

Five samples of each orientation were tested for their compressive strength. Tables 4 and 5 show the results of the experiments conducted on X and Z orientation respectively.

From the results, it can be seen that the vertical orientation demonstrates a higher value of compressive strength as compared to the horizontal orientation. This difference can be observed from the chart in Fig. 9.

It can be seen from the test results that the average compressive strength of the vertical specimens is higher than that of the horizontal specimens. Also, the compressive strength of typical bulk ABS ranges from 65 to 90 MPa [24]. So we can

Table 5 Compressive test results for the vertical orientation samples

Sample No.	Length (mm)	Width (mm)	Failing load (kN)	Compressive strength (MPa)
Z1	12.85	12.77	8.28	50.5
Z2	12.68	12.82	7.78	47.8
Z3	12.62	12.74	8.54	53.1
Z4	12.83	12.70	8.13	49.9
Z5	12.74	12.71	7.99	49.4

Avg. compressive strength = 50.1 MPa
Standard Deviation (s) = 1.9
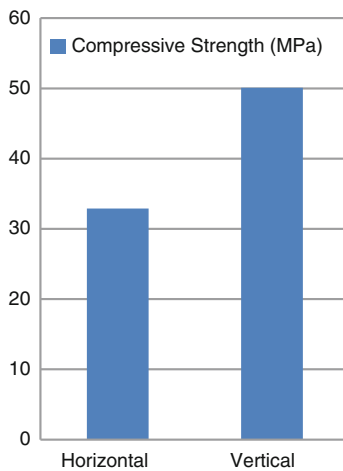
Fig. 9 Comparison of the compressive strength values

infer that the oriented parts made by FDM have lower compressive strengths as compared to bulk ABS. The difference in strengths of the two orientations can be attributed to the slender and long geometries involved in the horizontal samples, which resulted in a higher probability of buckling of individual layers. On the contrary, the layers in the vertical specimens are arranged perpendicular to the applied compressive load, resulting in a higher compressive strength.

Figure 9 shows higher compressive strengths compared to the tensile strengths shown in Fig. 7. Bulk ABS materials and polymers often show a greater compressive strength [24].

The macroscopic view of some of the tested specimens is presented in Fig. 10. It can be noticed that although the X orientation parts have shown near homogenous compression during the test, the Z orientation parts showed barreling and shear compression pattern to a greater extent.

Fig. 10 Failure pattern of the tested samples
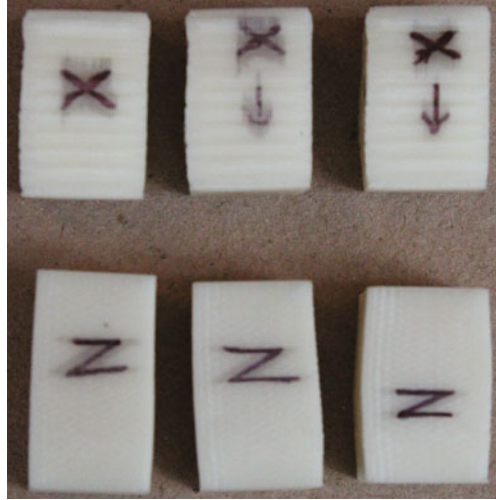
4.3 Izod Impact Test

Unnotched Izod Impact Test is a standard test for determining a material's resistance to impact. A pendulum held at a height is released to hit a sample. On impact, the specimen either breaks or the pendulum rests on the sample. Izod impact is the energy that is required to initiate fracture, and continue the fracture until the sample breaks. A material's impact resistance indicates its ability to absorb applied energy. It can also be inferred that more is a material's impact resistance; more will be its overall toughness. Theoretically, the value of impact energy can be calculated by the Eq. (1) below:

$$E = mg \left(h_i - h_f \right) \tag{1}$$

where E = Absorbed energy, m is the mass of the hitting pendulum bob, g is the acceleration due to gravity, h_0 is the initial height of the pendulum, and h_f is the final height of the pendulum.

The impact resistance in turn is calculated from the Eq. (2) given.

$$S = \frac{E}{t} \tag{2}$$

where S is the Impact resistance in J/m, and t is the thickness of the specimen in meters.

Five specimens were tested for their impact resistance in a Cantilever Beam Impact machine. Failure pattern C (Complete Break) was observed in each experimental run. Tables 6 and 7 show the results of the impact test conducted on X and Z orientation, respectively.

Table 6 Impact test results for the horizontal orientation specimens

| Sample No.	Thickness (mm)	Absorbed energy (J)	Impact resistance (J/m)
X1	6.31	1.19	189
X2	6.38	1.27	199
X3	6.46	1.37	212
X4	6.42	1.32	206
X5	6.37	1.25	196

Avg. impact resistance = 200 J/m
Standard Deviation (s) = 8.9

Table 7 Impact test results for the vertical orientation specimens

Sample No.	Thickness (mm)	Absorbed energy (J)	Impact resistance (J/m)
Z1	6.52	0.69	106
Z2	6.47	0.78	121
Z3	6.32	0.59	93
Z4	6.30	0.63	100
Z5	6.39	0.69	108

Avg. impact resistance = 106 J/m
Standard Deviation (s) = 10

Fig. 11 Comparison of the impact resistance values
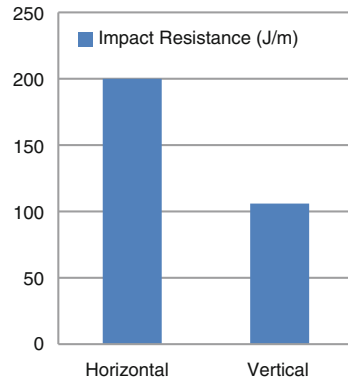
From the results, it can be inferred that the horizontal orientation indicates a higher value of impact resistance and thus absorbs more energy until fracture as compared to the vertical orientation. As impact resistance is a measure of the toughness of the material, we can say that the *X* orientation produces tougher parts than the *Z* orientation. The difference can be observed from the chart in Fig. 11.

The macroscopic view of some of the tested specimens is presented in Fig. 12.

Fractured specimens of both the orientation were studied under the JEOL JSM-5600 SEM. Figure 13 shows the magnified views of the fractured surfaces of the specimens tested for their impact resistance.

Fig. 12 Failure pattern of the fractured test samples

By analyzing the SEM pictures, it can be inferred that the horizontal specimens showed failure of individual fibers resulting in higher impact resistance among the two orientations. The vertical specimens resulted in lower impact resistance because of the weaker bond between individual layers.

4.4 Rockwell Hardness Test

Hardness is basically the resistance of a material to plastic deformation. Rockwell hardness number is a value that is based on the permanent increase in the depth of penetration on a material, when a major load on an indenter is applied and then removed alongside a constant minor load. Hardness numbers have no units and are given in various scales depending upon the material to be tested. This is basically a macroindentation test in which higher numbers in same scale indicate harder materials.

Five samples were tested in the Rockwell hardness testing machine using the *M* scale of hardness. All readings were taken 15 s after the removal of major load. Tables 8 and 9 show the results of the hardness test conducted on *X* and *Z* orientation, respectively.
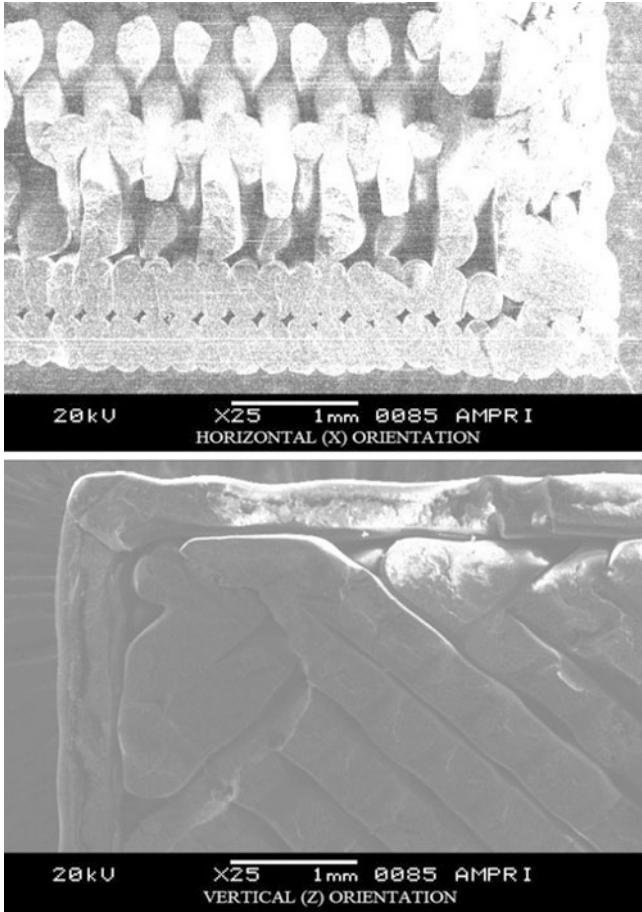
Fig. 13 Scanning electron microscope (SEM) pictures of the fractured horizontal and vertical specimens

Table 8 Hardness test results for the horizontal orientation samples

Sample no.	Hardness no. (M scale)
X1	30
X2	26
X3	32
X4	30
X5	27

Avg. hardness number = 29 HRM
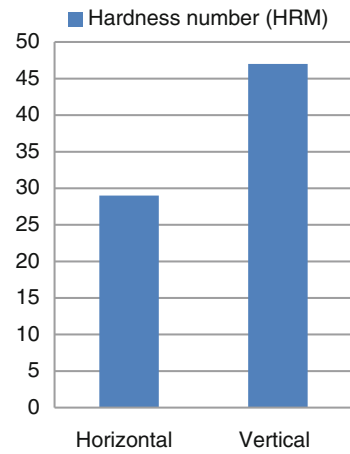Standard Deviation (s) = 2.4

Table 9 Hardness test results for the vertical orientation samples

Sample no.	Hardness no. (M scale)
Z1	52
Z2	42
Z3	48
Z4	50
Z5	45

Avg. hardness number = 47 HRM
Standard Deviation (s) = 4.0

Fig. 14 Comparison of the hardness values

Fig. 15 Failure pattern of an indented Z orientation test sample
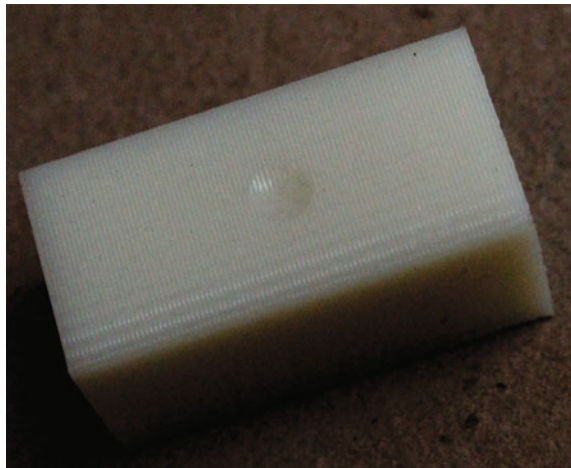
From the results, it can be examined that the vertical orientation indicates a higher value of hardness number as compared to the horizontal orientation. The difference can be observed from the chart in Fig. 14.

The macroscopic view of a tested specimen is presented in Fig. 15.

5   Conclusion and Future Work

The present paper studies in detail the effect of build orientation on the mechanical properties of ABS P400 FDM parts. The following conclusions may be drawn on the basis of this research:

(a) Horizontal (*X*) build orientation produces parts with a greater tensile strength as compared to vertical (*Z*) orientation. However, these strengths are lesser than the tensile strength of injection-molded P400 ABS.
(b) Vertical (*Z*) build orientation produces parts with a greater compressive strength than horizontal orientation. These strengths are lesser than that of bulk ABS material.
(c) Horizontal orientation produces tougher parts with more impact resistance than vertical orientation.
(d) Vertical orientation produces harder parts with more resistance to plastic deformation than vertical orientation.
(e) The manufacturing of an FDM part should be done keeping the working conditions in mind. If the part would be subjected to greater tensile or impact loads, horizontal orientation should be set before giving run command to the machine. On the other hand, if the part is expected to bear more compressive loads or plastic deformation, vertical orientation should be set.
(f) Compressive strength of ABS P400 parts in any build orientation is greater than the tensile strength.

As can be seen in the Fishbone diagram in Fig. 2, there are many other process parameters that affect the properties of an FDM part, for example raster width, fill pattern, deposition speed etc. Opportunities exist to study the variation in mechanical properties with these process parameters. Also there are some mechanical properties like flexural and torsional properties which also play an important role in many operational environments. Experiments quantifying the relation of various process parameters with these properties can also be an area that can be researched.

References

1. Pham DT, Demov SS (2001) Rapid manufacturing: the technologies and applications of rapid prototyping and rapid tooling. Springer-Verlag London Limited
2. Kai CC, Fai LK (2000) Rapid prototyping: principles and applications in manufacturing. World Scientific

3. Tagore GRN, Anjikar SD, Venu Gopal A (2007) Multi objective optimisation of build orientation for rapid prototyping with fused deposition modeling (FDM). In: Seventeenth Solid Freeform Fabrication (SFF) Symposium, Austin, pp 246–255

4. Wright PK (2001) 21st century manufacturing. Prentice Hall

5. Ahn SH, Montero M, Odell D, Roundy S, Wright PK (2002) Anisotropic material properties of fused deposition modeling ABS. Rapid Prototyping J 8(4):248–257

6. Sun Q, Rizvi GM, Bellehumeur CT, Gu P (2008). Effect of processing conditions on the bonding quality of FDM polymer filaments. Rapid Prototyping J 14(2):72–80

7. Swanson WJ, Turley PW, Leavitt PJ, Karwoski PJ, LaBossiere E, Skubic RL (2004) High temperature modeling apparatus. United States Patent. US 6,722,872 B1"

8. Novakova-Marcincinova L, Novak-Marcincin J (2012) Testing of materials for rapid prototyping fused deposition modelling technology. World Academy of Science, Engineering and Technology 70(73)

9. Sood Anoop Kumar, Ohdar RK, Mahapatra SS (2010) Parametric appraisal of mechanical property of fused deposition modeling parts. Mater Des 31:287–295

10. Lee BH, Abdullah J, Khan ZA (2005) Optimization of rapid prototyping parameters for production of flexible ABS object. J Mater Process Technol 169:54–61

11. Hossain MS, Ramos J, Espalin D, Perez M, Wicker R (2013) Improving tensile mechanical properties of FDM-manufactured specimens via modifying build parameters. In: International Solid Freeform Fabrication Symposium, pp 380–392

12. Fatimatuzahraa AW, Farahaina B, Yusoff WAY (2011) The effect of employing different raster orientations on the mechanical properties and microstructure of fused deposition modeling parts. In: IEEE symposium on business, engineering and industrial applications, pp 22–27

13. Anitha R, Arunachalam S, Radhakrishnan P (2001) Critical parameters influencing the quality of prototypes in fused deposition modelling. J Mater Process Technol 118:385–388

14. Reddy BV, Reddy NV, Ghosh A (2007) Fused deposition modelling using direct extrusion. Virtual Phys Prototyping 2:51–60

15. Es-Said OS, Foyos J, Noorani R, Mandelson M, Marloth R, Pregger BA (2000) Effect of layer orientation on mechanical properties of rapid prototyped samples. Mater Manuf Process 15 (1):107–122

16. Thrimurthulu K, Pandey PM, Reddy NV (2004) Optimum part deposition orientation in fused deposition modelling. Int J Mach Tools Manuf 44:585–594

17. Waghchore RK (2012) Determination of build orientation of rapid prototyping (RP) components for optimum builds time. Int J Adv Technol Eng Res 2(2):27–31

18. Masood SH, Rattanawong W, Iovenitti P (2003) A generic algorithm for part orientation system for complex parts in rapid prototyping. J Mater Process Technol 139(1–3):110–116

19. Byun H-S, Lee KH (2006) Determination of the optimal build direction for different rapid prototyping processes using multi-criterion decision making. Robotics Comput-Integr Manuf Elsevier 22:69–80

20. Lee CS, Kim SG, Kim HJ, Ahn SH (2007) Measurement of anisotropic compressive strength of rapid prototyping parts. J Mater Process Technol 187–188:627

21. Agnes B, Volker S (2011) Mechanical properties of fused deposition modelling parts manufactured with ULTEM*9085. ANTEC 2011, Boston

22. Anna B, Guceri S (2003) Mechanical characterization of parts fabricated using fused deposition modelling. Rapid Prototyping J 9(4):252–264

23. Agarwala MK, Jamalabad VR, Langrana NA, Safari A, Whalen PJ, Danforth SC (1996) Structural quality of parts processed by fused deposition. Rapid Prototyping J 2(4):4–19

24. ASM (1988) Engineered materials handbook, engineering plastic, ASM international, vol 2

Estimation of the Effect of Process Parameters on Build Time and Model Material Volume for FDM Process Optimization by Response Surface Methodology and Grey Relational Analysis

Manu Srivastava, Sachin Maheshwari, T.K. Kundra and Sandeep Rathee

Abstract In this study, a hybrid optimization approach is proposed for build time and model material volume in Fused Deposition Modeling (FDM) process on a FDM Maxum Modeler. A combination of response surface methodology (RSM) and grey relational analysis (GRA) is proposed and applied to optimize process parameters of FDM process. The significant input parameters such as contour width, air gap, raster angle, and spatial orientation are considered, and build time and model material have been taken as responses for this study. Thirty experiments were conducted on acrylonitrile butadiene styrene (ABS) P400 for conical primitives using full factorial central composite design. The optimum process parameter conditions were obtained from grey relational grade. The results obtained provide useful information of the method to control responses and ensure minimal build time and model material volume for prototyping requirements. The assessment outcome provided a scientific reference to obtain minimal values of build time and model material volume utilized, and it was found out that these correspond to a contour width of 0.654 mm, air gap of 0.0254 mm, raster angle of 0°, and orientation of 0°.

M. Srivastava (✉) · S. Maheshwari · S. Rathee
Division of Manufacturing Processes and Automation Engineering,
Netaji Subhas Institute of Technology, New Delhi, India
e-mail: manyash@gmail.com

S. Maheshwari
e-mail: ssaacchhiinn@gmail.com

S. Rathee
e-mail: rathee8@gmail.com

T.K. Kundra
Department of Mechanical Engineering, Indian Institute of Technology Delhi,
New Delhi, India
e-mail: tkkundra@gmail.com

1 Introduction

There has been an ever increasing tendency to reduce the design and manufacturing time; hence the development of advanced manufacturing processes including rapid prototyping. Rapid prototyping (RP) has many attractive features like drastically reduced design times, prototyping times, manufacturing times, freedom from jigs and fixtures, and so on. This makes it desirable technology for modern day applications including biomedical, engineering, design authentication, jewelry, intricate objects, and automotive components manufacturing [1].

To meet the challenges in the manufacturing industry, development of appropriate methodologies to support advancements in the field of optimization of RP processes is essential. FDM is one of the most extensively used RP techniques. It has proven strengths in producing high-strength robust prototypes. It offers a wide range of modelers ranging from legacy modelers like FDM Maxum and FDM Titan to present-day commercial Mojo, uPrint SE, uPrint SE plus, Fortus 250mc, Fortus 360mc, Fortus 400mc, and Fortus 900 mc modelers. The choice of model materials is also impressive including ABS plusP430, ABSi, ABS-ESD7, ABS-M30, ABS-M30i, PC-ABS, PC-ISO, PC, Nylon 12, ULTEM-9085, and PPSF PPSU with tensile strength ranging from 5200 psi for ABS M30 to 10,390 psi for ULTEM-9085. Support material is either soluble or Bass and the model material is available in a number of colors. Similarly, a good range of elongation strength, heat deflection, flexural stress, impact strength, and other unique material properties are available for FDM model materials [2–8].

In fused deposition modeling (FDM), it is important to select process parameters for achieving optimal performance [9]. Usually, the desired process parameters are determined based on previous research and the desired response. However, this does not ensure that the selected machining parameters result in optimal or near-optimal machining performance for that particular FDM modeler and environment. In this research, attempt has been made to optimize the FDM process for a FDM Maxum modeler by using response surface methodology for experimental design and single-objective optimization through the settings of the process parameters. These results are used for estimation of grey relational grade for the multiresponse optimization [10]. Surface finish is one of the major limiting factors in the use of FDM prototypes. Layout in FDM process is a key factor that largely determines the quality and quantity of the prototypes produced. Qualitative and quantitative optimization are two aspects of layout optimization. Qualitative aspect refers to selecting layout so as to optimize surface finish, dimensional accuracy, strength, etc. of the prototypes. Quantitative aspect on the other hand refers to optimizing build time, model material, support material, and overall production cost. Though a lot of research has been done to improve the qualitative performance

for process layout yet optimal parameter selection still remains a challenge as far as the quantitative performance is concerned. Models for various quantitative responses with respect to various relevant process parameters are built, evaluated, and validated in this research for FDM process. These results can be utilized for other GM techniques with suitable process-specific modifications.

In the following sections, RSM-based experimentation is first discussed. GRA is then introduced. Then, the experimental results when using RSM and GRA together to optimize the FDM process cost with minimum build time and model material volume are given. Finally, the paper concludes with a summary.

2 RSM-Based Experimentation

Common methods of evaluating the layout performance in the FDM operation are based on the following performance characteristics: Build time required, amount of support structure required, amount of model material used, and production cost incurred. Out of these, first three can be correlated with build parameters such as contour width, raster width, raster angle, air gap etc. Production cost can be easily predicted as a function of three remaining performance characteristics [11–13]. Proper selection of the build parameters can result in reduced build time required, lesser amount of support structure required, amount of model material used, and hence lesser production cost incurred.

Experiments were individually conducted to acknowledge significance of process parameters, i.e., contour width, orientation, raster angle, and air gap on build time and model material volume of the ABS work piece on a FDM Maxum Modeler. A conical primitive was taken of STL Size $X = 20$ mm, $Y = 20$ mm, and $Z = 69.999$ mm. The arrangement to conduct the experiments use a face-centered CCD with four variables, having a total of 30 runs in three blocks [14]. The different factors and their levels are depicted in Table 1. The CAD drawing for conical primitive was made using Solidworks software and then it was converted into .stl format. This .stl was inputted to Insight 6.4 and the different experimental runs and corresponding responses are tabulated in Table 2.

Table 1 Input variables used in the experiments and their levels

S. No.	Parameters	Level 1	Level 2	Level 3
1	Contour width (A)	0.4290	0.5415	0.6540
2	Orientation (D)	0	15	30
3	Raster angle (E)	0	15	30
4	Air gap (F)	−0.0254	0	0.0254

Table 2 CCD and experimental results for four variables in uncoded units

Std	Run order	A: contour width(mm)	B: air gap (mm)	C: raster angle (Degree)	D: orientation (Degree)	Build time (hour)	Model volume (Cubic cm)
18	1	0.654	0	15	15	1.8334	7.5686
20	2	0.5415	0.0254	15	15	1.8268	7.1674
7	3	0.429	0.0254	30	0	1.7534	7.1492
10	4	0.654	−0.0254	0	30	1.9632	8.0034
29	5	0.5415	0	15	15	1.8434	7.5684
16	6	0.654	0.0254	30	30	1.9934	7.1822
3	7	0.429	0.0254	0	0	1.6898	7.1432
15	8	0.429	0.0254	30	30	2.0098	7.155
8	9	0.654	0.0254	30	0	1.7334	7.175
23	10	0.5415	0	15	0	1.7132	7.4752
6	11	0.654	−0.0254	30	0	1.7868	8.0132
11	12	0.429	0.0254	0	30	1.9368	7.1434
12	13	0.654	0.0254	0	30	1.92	7.1718
1	14	0.429	−0.0254	0	0	1.72	8.0366
22	15	0.5415	0	30	15	1.8832	7.5752
9	16	0.429	−0.0254	0	30	1.9874	8.0388
19	17	0.5415	−0.0254	15	15	1.8698	8.0304
21	18	0.5415	0	0	15	1.8266	7.5612
13	19	0.429	−0.0254	30	30	2.0632	8.0486
2	20	0.654	−0.0254	0	0	1.703	8.005
26	21	0.5415	0	15	15	1.8434	7.5684
30	22	0.5415	0	15	15	1.8434	7.5684
24	23	0.5415	0	15	30	1.9766	7.5636
14	24	0.654	−0.0254	30	30	2.0368	8.0162
28	25	0.5415	0	15	15	1.8434	7.5684
5	26	0.429	−0.0254	30	0	1.812	8.0452
25	27	0.5415	0	15	15	1.8466	7.5676
17	28	0.429	0	15	15	1.8502	7.569
4	29	0.654	0.0254	0	0	1.6632	7.1694
27	30	0.5415	0	15	15	1.8434	7.5684

3 Measurement of Responses

The responses were measured using FDM control center after slicing, tessellation, and support material generation time of the .stl file. This is done automatically on Insight software and the corresponding build time, model material volume, and support material volume can be directly calculated.

4 Grey Relational Analysis [10, 15, 16]

GRA is a decision-making approach based on grey system theory (GST) developed originally by Deng [16]. In GST, black implies a system with deficient information whereas a white system is the one with complete information. However, grey relation is the one with incomplete information which is used to characterize the grade of association between two sequences so that the distance of two factors can be measured in discrete manner. When experiments are unclear or if the experimental method is inaccurate, GRA assists to reimburse for the deficiency in statistical regression. GRA is an effective means of relationship analysis between sequences with less data and can analyze many factors which can overcome disadvantages of statistical method.

4.1 Data Preprocessing

Function of factors is neglected when the range of sequences is large or the standard value is large. However, GRA might produce incorrect results if the factor measured unit, goals, and directions are different. Thus, there is a need to preprocess original experimental data to avoid such effects. Data preprocessing is a process of transforming the original sequence to some comparable sequence. For this the experimental data are normalized in the range of 0 and 1, this process is called grey relational generating. Three different kinds of data normalizations which are generally carried out include rendering whether the lower is better (LB), the higher is better (HB), or nominal is better (NB). If the target value of original sequence is the smallest possible, then it has a characteristic of "lower the better." Normalization is taken using following LB equations:

$$X_i * (k) = \frac{\max X_i(k) - X_i(k)}{\max X_i(k) - \min X_i(k)}$$

If expectancy is as-high-as-possible, then original sequence should be normalized by the following HB equations:

$$X_i * (k) = \frac{X_i(k) - \min X_i(k)}{\max X_i(k) - \min X_i(k)}$$

Conversely, if a specific target value needs to be achieved, then the original sequence will be normalized by the following NB equation:

$$X_i * (k) = 1 - \frac{|X_i(k) - X_o b(k)|}{\max X_i(k) - X_o b(k)}$$

where $i = 1, \ldots, n$; $k = 1, 2, \ldots, p$; $X_i^*(k)$ is normalized value of the kth element in the ith sequence, $X_ob(k)$ is desired value of the kth quality characteristic, max $X_i^*(k)$ is the largest value of $X_i(k)$, and min $X_i^*(k)$ is the smallest value of $X_i(k)$, n is the number of experiments, and p is the number of quality characteristics.

4.2 Grey Relational Coefficient and Grey Relational Grade

A grey relational coefficient (GRC) is calculated in order to display the relationship between the optimal and actual normalized experimental results and needs to be expressed as,

$$Z_i * (k) = \frac{\Delta min + \zeta \Delta max}{\Delta 0, i(k) + \zeta \Delta max}$$

where $\Delta 0, i(k) = |X_0(k) - X_i(k)|$ is the difference of the absolute value $X_0(k) - X_i(k)$; and ζ is the distinguishing coefficient or identification coefficient. In general, it is set to 0.5. Δmin is the smallest value and Δmax is the largest value of $\Delta 0, i$, respectively.

Finally, the grey relational grade $0 \leq \zeta \leq 1$ was obtained by calculating the average values of all the grey relational coefficients. The grey relational grade γi can be compounded as

$$\gamma i = \frac{1}{P} + \sum_{k=1}^{p} \zeta i * (k)$$

where n is the number of process responses. Higher GRG value corresponds to intense relational degree between the reference sequence $X_0(k)$ and the given sequence $x_i(k)$. The reference sequence $X_0(k)$ implies best process sequence which means higher GRG reflects that corresponding parameter combination is closer to optimal. The mean response for the GRG with its grand mean and the main effect plot of GRGs have great significance as the optimal process condition can be obtained from this plot. With the above values, influential degree of the factors on the system can be identified.

4.3 Analysis and Discussion of Experimental Results

In this work, the effect of different FDM process parameters such as contour width, raster angle, orientation, and air gap on responses indicating cost of layout such build time and model material volume is investigated. Table 2 lists experimental results obtained corresponding to different parametric conditions. Generally, a

lower value of the layout cost is desirable, which implies that the data sequences have a the-lower-the-better characteristic. In normalized experimental results for each performance characteristic, we need to normalize the original sequence in the experiment in range of 0–1 due to different measurement units. This preprocessing step of data is called as grey relational generating. For reducing cost, the model material volume and build time "the-lower-the-better" characteristics need to be adopted. Table 3 lists normalized experimental results and deviation sequences for these responses. The grey relational coefficients, given in Table 4, for each response

Run order	Normalized values		Deviation sequence	
	BT	MV	BT	MV
1	0.5745	0.5302	0.4255	0.4698
2	0.591	0.9733	0.409	0.0267
3	0.7745	0.9934	0.2255	0.0066
4	0.25	0.0499	0.75	0.9501
5	0.5495	0.5304	0.4505	0.4696
6	0.1745	0.9569	0.8255	0.0431
7	0.9335	1.0000	0.0665	0.0000
8	0.1335	0.9870	0.8665	0.0130
9	0.8245	0.9649	0.1755	0.0351
10	0.875	0.6333	0.125	0.3667
11	0.691	0.0391	0.309	0.9609
12	0.316	0.9998	0.684	0.0002
13	0.358	0.9684	0.642	0.0316
14	0.858	0.0133	0.142	0.9867
15	0.45	0.5229	0.55	0.4771
16	0.1895	0.0108	0.8105	0.9892
17	0.4835	0.0201	0.5165	0.9799
18	0.5915	0.5383	0.4085	0.4617
19	0	0.0000	1	1.0000
20	0.9005	0.0482	0.0995	0.9518
21	0.5495	0.5304	0.4505	0.4696
22	0.5495	0.5304	0.4505	0.4696
23	0.2165	0.5357	0.7835	0.4643
24	0.066	0.0358	0.934	0.9642
25	0.5495	0.5304	0.4505	0.4696
26	0.628	0.0038	0.372	0.9962
27	0.5415	0.5313	0.4585	0.4687
28	0.5325	0.5297	0.4675	0.4703
29	1	0.9711	0	0.0289
30	0.5495	0.5304	0.4505	0.4696

Table 3 Normalized values and deviation sequences of BT and MV

Table 4 Grey relational coefficient, grey relational grade and rank

Run order	Grey relational coefficient		Grey relational grade	Rank
	BT	MV		
1	0.5402	0.5155	0.5279	14
2	0.5501	0.9493	0.7497	5
3	0.6892	0.9869	0.8380	3
4	0.4000	0.3448	0.3724	27
5	0.5260	0.5157	0.5209	16
6	0.3772	0.9207	0.6489	10
7	0.8826	1.0000	0.9413	2
8	0.3659	0.9746	0.6702	9
9	0.7402	0.9344	0.8373	4
10	0.8000	0.5769	0.6885	8
11	0.6180	0.3423	0.4802	23
12	0.4223	0.9996	0.7109	6
13	0.4378	0.9406	0.6892	7
14	0.7788	0.3363	0.5576	12
15	0.4762	0.5117	0.4939	22
16	0.3815	0.3358	0.3586	28
17	0.4919	0.3379	0.4149	26
18	0.5504	0.5199	0.5351	13
19	0.3333	0.3333	0.3333	30
20	0.8340	0.3444	0.5892	11
21	0.5260	0.5157	0.5209	15
22	0.5260	0.5157	0.5209	17
23	0.3896	0.5185	0.4540	24
24	0.3487	0.3415	0.3451	29
25	0.5260	0.5157	0.5209	18
26	0.5734	0.3342	0.4538	25
27	0.5216	0.5161	0.5189	20
28	0.5168	0.5153	0.5161	21
29	1.0000	0.9453	0.9726	1
30	0.5260	0.5157	0.5209	19

have been accumulated to evaluate GRG, which is the overall representative of both the features considered for low cost. Experiment number 29 generated the highest GRG. Thus multicriterion optimization problem has been transformed into single equivalent objective function optimization problem using the combination of RSM and GRA. Higher value of GRG implies that corresponding factor combination is more close to the optimal.

5   Results and Discussion

Statistical analysis was carried out on the experimental data obtained through face-centered central composite design using statistical software Design Expert.

Table 2 tabulates the responses obtained from the experimentation. The detailed analysis of this experiment design was performed by the same authors [17]. Regression analysis is performed to find out the relationship between the input factors and the responses. RSM is used to check the sufficiency of models which includes lack of fit test, test of significance, actual versus predicted plot, Box Cox plot, and normal plot of residuals at a confidence level of 95 %.

Normalized values are calculated and corresponding deviation sequences are estimated for all the experimental runs based on the principles of GRA. Finally, Grey relational coefficients (GRC) for both the responses are calculated. The Grey relational grade (GRG) is calculated as an average of both the individual GRCs. This is used for the ranking the experimental runs in order to predict the optimal process parameter combination for multiresponse optimization. The results are tabulated in Table 4.

6   Conclusions

In this investigation, RSM is coupled with GRA to optimize the process parameters having a significant effect upon the cost (Build Time and Model Material Volume) of FDM process. Based on the recognition of significant process parameters and corresponding development of mathematical model, the multiobjective optimization of responses is attempted [12, 13, 18]. The optimal conditions established by grey analysis approach are as follows: a contour width of 0.654 mm, air gap of 0.0254 mm, raster angle of 0°, and orientation of 0°.

By applying these process parameter values, minimum output responses build time and model material volume were found out to be 1.6632 and 7.1694, respectively.

This may provide the RP personnel (experimenter and practitioner) an effective guideline to pick optimum parameter settings for attaining desired model material volume and build time during processing of FDM parts.

References

1. Tolio T, Ceglarek D, ElMaraghy HA, Fischer A, Hu SJ, Laperrière L, Newman ST, Váncza J (2010) SPECIES-Co-evolution of products, processes and production systems. CIRP Annals-Manuf Technol 59:672–693
2. Stratasys (2013) Material safety data sheet
3. System Documentation (1998) S.I., FDM, FDM®

4. Stratasys, Insight Help/Glossary, Stratasys
5. Stratasys (2014) Stratasys data sheets: the truth about speeds. www.stratasys.com
6. Stratasys (2014) ABS-M30 production-grade thermoplastic for Fortus 3D production systems. http://www.stratasys.com/~/media/Main/Secure/Material%20Specs%20MS/Fortus-Material-Specs/FortusABSM30MaterialSpecSheet-US-09-14-Web.pdf
7. Stratasys (2005) FDM Maxum™ User Guide Version 1.3
8. Stratasys (2015) Compare FDM materials. http://www.stratasys.com/materials/fdm/compare-fdm-materials
9. Srivastava M, Maheshwari S, Kundra TK (2014) Experimental evaluation of FDM process for support material optimization, in international conference on advances in design & manufacturing 2014 (ICAD&M'14) 2014
10. Lin CL, Lin JL, Ko TC (2002) Optimisation of the EDM process based on the orthogonal array with fuzzy logic and grey relational analysis method. Int J Adv Manuf Technol 19:271–277
11. Srivastava M, Maheshwari S, Kundra TK (2014) Experimental evaluation of FDM process for support material optimization. In: International conference on advances in design & manufacturing. NIT Trichy
12. Srivastava M, Maheshwari S, Kundra TK (2014) Experimental evaluation of FDM process for model material volume optimization for cylindrical primitives. IJSER 5(11)
13. Srivastava M, Saktk M, Experimental evaluation of FDM process for production cost optimization. Int J Res Mech Eng Technol 5(spl-1)
14. StatEase (2014) Design expert, F.I.T. package, Editor
15. Chang C, Tsai C, Chen L (2003) Applying grey relational analysis to the decathlon evaluation model. Int J Comput Internet Manage 11(3):54–62
16. Dang JL (1989) Introduction to grey system theory. J Grey Syst 1:1–24
17. Srivastava M, Maheshwari S, Kundra TK (2015) Optimization of build time and model volume for a FDM maxum modeler using response surface methodology. Int J Technol Res Eng
18. Bharti PS (2012) Optimization of process parameters of electric discharge machining based on neural networks and Taguchi's method. Guru Gobind Singh Indraprastha University, New Delhi

Current Trends of Additive Manufacturing in the Aerospace Industry

L. Jyothish Kumar and C.G. Krishnadas Nair

Abstract Additive Manufacturing offers unmatched flexibility in terms of part geometry, material composition and lead-time. It is moving towards revolutionizing the aerospace manufacturing sector through production of highly complex, light-weight parts with reduced material waste. It can also be employed for repair of complex components such as engine blades/vanes, combustion chamber, etc. Complex geometry thin walled aircraft engine components and structures, difficulty in machining of materials are other main factors forcing aerospace sector to adopt the use of additive manufacturing technology. In this paper an attempt has been made to explore the additive manufacturing research and development activities in aerospace industry.

Keywords 3D printing · Additive manufacturing · Free form fabrication · Aerospace application

1 Introduction

Aerospace industry is one of the important adopters of Additive Manufacturing (AM) technology for prototyping, testing and production of end use parts. Laser Metal Deposition, Laser Cusing, Direct Metal Laser Sintering, Laser Melting and Selective Laser Melting are the major AM technologies used to produce aerospace parts.

As per the recent survey, only aerospace applications accounted for 12.3 % in the global Additive Manufacturing field. The survey also predicts that the AM sector is expected to grow from $1.5 billion industry to $100 billion within the next 20 years and much of this growth is accounted from the aerospace sector only [1].

L.J. Kumar (✉)
Jain University, Bangalore, India
e-mail: jyothish@rapitech.co.in

C.G. Krishnadas Nair
Jain University, Governing Council, IIAEM, Bangalore, India

2 Background

2.1 Additive Manufacturing Application for the Aerospace Industry

The aerospace industry demands stronger, lighter and more durable components. Today Additive Manufacturing technology creates new possibilities to meet these challenges. Also the aerospace industry has incorporated AM process from concept design to end use parts and repairs. The areas of applications include rapid prototyping of components in the design phase using plastic and metal followed by making of dies/mould/tools for mass production and direct manufacture of complex shape metal parts, repairing of damaged parts instead of scrapping or replacement of damaged parts.

Laser Metal Deposition (LMD) Technology is the best process to repair aerospace components. In case of LMD for repair the metal powder will be directly fed onto the damaged portion of the part and laser cured, restoring the original strength of the part.

Currently machining, forging and other conventional processes are producing the aerospace parts. There is an extreme waste of highly expensive material in the conventional manufacturing processes and only less than 5 % of the original material is the content in the finished part. In case of Additive Manufacturing there is maximum utilization of material and also produces near net shape parts.

In case of aero engines, the increase in the operating temperature will have direct impact on fuel efficiency. AM has the potential to process higher temperature materials such as nickel alloys and inter metallic materials which are difficult to cast and machine. These materials are also used at higher temperatures. The process has flexibility to produce sophisticated component assemblies, with varying shape, composition, structures and properties, as required by the designer. Replacing the conventional method of forging/machining of several components and assembling them for, e.g. assembled turbine disc with blades, assembled compressor discs with blades, stator and rotor turbine vane assemblies, etc.

2.1.1 GE Aviation—Leap Engine Fuel Nozzle Production Using Additive Manufacturing

GE Aviation has been evaluating Additive Manufacturing for over a decade and now it has successfully produced *Leap* **Engine Fuel Nozzle** in **cobalt chrome** by laser AM melting process as shown in Fig. 1.

The Leap engine fuel nozzle has already cleared ground-based engine testing and has been certified for use on civil aircraft. The AM part has replaced *an assembly of 20 components* with reduced cost, weight, without joints and improved performance.

Fig. 1 Laser sintered leap engine fuel nozzle in cobalt chrome

**Fig. 2** Leap engine (nozzle indicated) *Courtesy* GE aviation
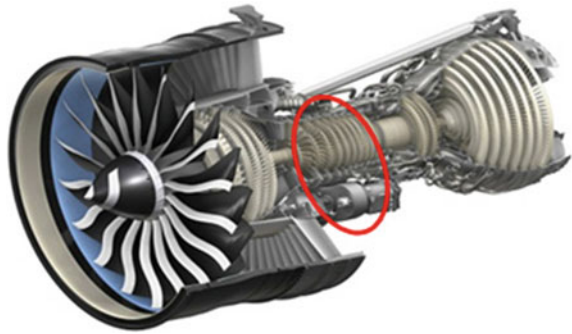
As shown in the Fig. 2 on each LEAP engine there are 19 fuel nozzles. By 2018, it is expected that the production volume increase from 25,000 to 40,000 parts, and by 2020 more than 100,000 parts will be manufactured [2, 3].

2.1.2 SAFRAN R&D Employs Additive Manufacturing for Developing Engine Components and Aircrafts

SAFRAN Group has identified additive manufacturing process as a breakthrough technology for a number of engine components for development of prototype and engine both Turbomeca and Snecma. Turbomeca, which makes helicopter engines and Snecma aircraft engines, extensively used this technology in the design phase. As shown in Fig. 3 Snecma has guide vanes for the silver-crest business jet engine and manifold for Vinci rocket engines, hydrogen turbo pump. Snecma has successfully used the technology for speedy implementation of design changes and also for repair of components. Extensive researches have been under taken to develop complex assemblies as integrated single component by this process. Examples are guide vane assemblies, integrated fuel manifold and combustion chamber and the like [4].

Fig. 3 Engine stator vane aircraft in high temperature alloys
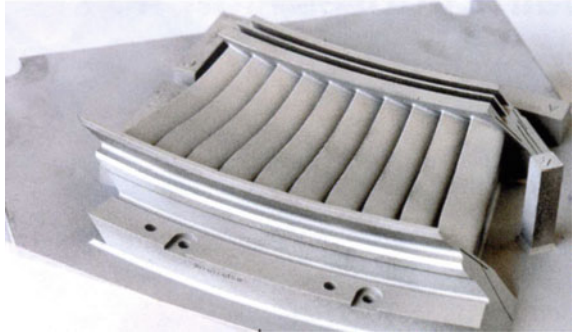
Fig. 4 The first test piece produced on the M2 cusing machine (*Courtesy* NASA/MSFC/Andy Hardin)

2.1.3 NASA Creates Complex Rocket Injector Using Additive Manufacturing

NASA engineers used Additive Manufacturing technology to produce intricate metal rocket injector part (as shown in Fig. 4) for their next-generation Space Launch System (SLS) J-2X engine.

Rocket injector was manufactured from selective laser melting (SLM) additive manufacturing process using nickel–chromium alloy powder. The traditionally manufactured injector had 115 parts and 3D printed injector had only two parts.

Additive Manufacturing process considerably reduced the manufacturing time needed to produce injector part from months to weeks. The part was built into single piece without joints, which was structurally stronger and more reliable leading to the overall safety of the vehicle. It was a significant improvement in saving time and cost for NASA. This part will undergo structural and hot-fire tests and finally will be used in the J-2X engine by 2017 [5].

2.1.4 Additively Manufactured Titanium Component in Airbus A350 XWB

The leading commercial aircraft manufacturer Airbus has been increasingly *gaining the importance* of Laser Melting of Metal Powders in aircraft manufacturing.

The *'Cabin bracket connector'* (shown in the Fig. 5) used in the Airbus A350 XWB. The bracket was additively manufactured using Laser CUSING (Concept Laser GmbH) technology. Earlier this part was milled and machined out of aluminium alloy and now it is a 3D printed part, which is made out of titanium (Ti) powder material with a more than 30 % weight reduction. Milling of aircraft parts leads 95 % waste, which can be recycled where as with Laser Cusing the percentage of waste is only 5 %.

In AM process tools are not required to produce functional sample part thereby eliminating the tool cost. This also helps in identifying early stage design errors and design optimization. Earlier Airbus projected 6 months to develop component and now it has reduced to 1 month [6].

2.1.5 Fused Deposition Modelling Reduces Tooling Cost and Lead-Time to Produce Composite Aerospace Parts

Advanced Composite Structures (ACS), a US-based company produced a camera fairing (as shown in Fig. 7) which is used by the military aircraft in forward looking infrared camera. The Fused Deposition Modelling technology (FDM) machine from Stratasys used to build layup tool directly from a CAD data. FDM tooling can be produced in a single day compared to several weeks for *Computer Numerical Control (CNC) tooling*. The technology helped to reduce cost and time in developing layup tool (shown in Fig. 6). FDM tool cost was $400 compared with USD CNC tool of $2000. Also the lead-time to produce FDM tool was between 2 and 45 days in CNC, which shows a significant reduction in lead-time and cost [7].

Fig. 6 FDM-layup tool

Fig. 7 FDM-layup tool
produced the aircraft camera
fairings

2.1.6 Boeing Using 3D Printing Technology

3D Printing technology is being significantly used by Boeing. According to a news
source (*Geek Wire*), around 300 aircraft production parts are made out of 3D
printing technology, on 10 different aircraft production programs. At present it is
projected that more than *20,000 non-metallic* additive manufactured parts are used
on their vehicles. The company spokesman Nathan Hulings says "The *F/A-18
Super Hornet has approximately 150 parts in the forward fuselage area that have
been produced through selective laser sintering*" [8].

At present the company only uses non-metallic 3D printed parts on production
programs and evaluating other materials like metals and alloys.

2.1.7 Lockheed Martin Space Systems Company Demonstrates Digital Production Innovations

Additive Manufacturing of Titanium Parts

Lockheed Martin Space Systems Company is employing 3D printing technology to
produce satellite parts out of *titanium material* to reduce cost, cycle time and

Fig. 8 3D printed titanium part

material waste. At present, the company is metal 3D printing technology to develop 3D printed satellite parts (as shown in Fig. 8) and plans to increase the process to manufacture complex parts in the future [9].

2.1.8 Rolls-Royce 3D Prints Largest Component for Trent XWB-97 Engine

Rolls-Royce plans to test the largest engine part '*front bearing housing*' as shown in Fig. 9 made by 3D printing technique. The intricate design and large titanium front bearing part which is having a 1.5 m diameter and 0.5 m thick, *holding 48 aero foils was manufactured using 'Electron Beam Melting' additive manufacturing process.* This process builds complex, solid metal parts by melting metal powder using focused electron beam. The front bearing housing holds the bearing for the low and intermediate pressure compressor inside Rolls-Royce Trent XWB-97 engine.

By using this AM process, Rolls-Royce saved 30 % manufacturing time compared to conventional manufacturing methods [10].

2.1.9 Pratt and Whitney Uses 3D Printing for Aero Engine Parts

Aero engine maker Pratt and Whitney use additive manufacturing technology to manufacture compressor stators as shown in Fig. 10 and sync ring brackets for its first *Pure Power PW1500G* engine. Pratt and Whitney delivered its first engine to the world's largest aircraft manufacturer **Bombardier,** for its **CSeries** passenger aircraft. Compressor stators and sync ring brackets components that are produced using AM process have undergone rigorous engine testing before using in the engine assembly.

Fig. 9 The front bearing housing was made using additive layer manufacturing (bearing housing *indicated*)
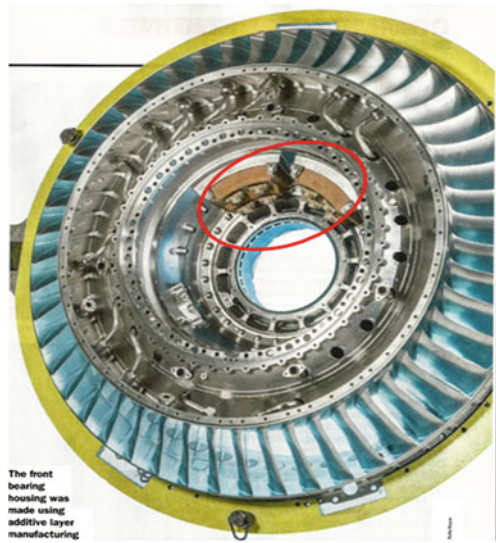
Fig. 10 3D-printed: Pratt Whitney's compressor stators
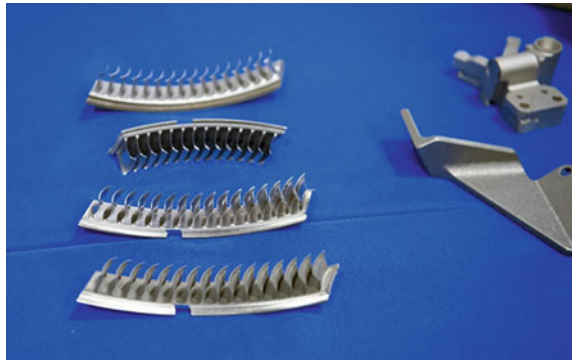
Lynn Gambil, Chief engineer, Manufacturing Engineering at Pratt and Whitney commented "AM offers a number of benefits: It dramatically reduces production time, from design, to prototype, to finished product and it decreases waste and consumption of raw materials. Furthermore it allows precision production of parts with complex geometry with reduced tooling, and permits multiple parts from an assembly to be made in one integrated piece" [11].

By using AM process Pratt and Whitney have saved 15 months lead-time compared conventional manufacturing processes and up to 50 % weight reduction in a single part.

Fig. 11 The robust one-piece 3D-printed titanium brackets (*indicated*) have better thermal conductivity characteristics than conventionally manufactured parts. They are able to withstand the high temperature and external forces in space (*Courtesy* EOS)
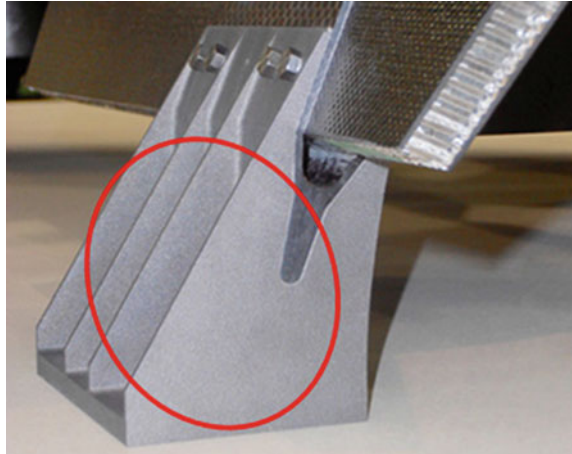
2.1.10 Airbus Defence and Space Used Additive Manufacturing to Reduce Production Time of Satellite Parts

The latest generation of satellites from Airbus Defence and Space contains the special *clamps* as shown in Fig. 11 made by AM. These clamps join the body of the satellite to the feed and sub-reflector assembly at the top end.

Airbus Defence and Space engineers selected additive manufacturing method from EOS GmbH for production of Clamps using titanium metal powder. Laser fuses the metal powder selectively to produce solid part in case of EOS-Direct Metal Laser Sintering process.

These components withstand the range of 330 °C at a force effect of 20 kN without any problems. The Spanish aerospace experts could also reduce the production time of by 5 days, production cost saving over 20 % and significant weight reduction of the component [12].

2.1.11 Hindustan Aeronautics Ltd., Used 3D Printing Technology for Aircraft Engine Model

Hindustan Aeronautics, Ltd. (HAL), India's only military aircraft producer is taking great strides toward making "Made in India" a world-class label. HAL used 3D printing technology to create prototype model for a 25-kN aircraft engine as shown in Fig. 12. The first engine prototype was on display as an operational model at Aero India expo-2015. Following Fig. 12 shows the various engine prototype components produced from Nylon plastic material using Selective Laser Sintering AM process. Bangalore-based company RAPITECH SOLUTIONS INC produced these components in less than 20 days. In this project Additive manufacturing drastically reduced prototype development time and cost compared to conventional manufacturing [13].

Fig. 12 The 25-kN aircraft engine prototype made out of selective laser sintering AM technology during Aero India expo-2015

2.1.12 Research and Development on Laser Metal Deposition Technology at Hindustan Aeronautics Ltd. (HAL)

Hindustan Aeronautics Limited Engine division is evaluating Laser Metal Deposition (LMD) additive manufacturing (from RPM Innovations Inc., & Efesto LLC, USA) for multi alloy deposition and repairing of aero engine parts. The technology is capable of free form fabrication and repairing of intricate aerospace parts using blown powder additive manufacturing technology.

Figure 13 shows the multi alloy (Inconel 625-Haynes 230—Inconel 718) LMD specimen with functional gradient zones with excellent properties for large aerospace user [14].

HAL R&D is also adapting AM technology for development of high pressure HPT Rotor blades, Nozzle guide vanes, Combustion chamber, HPC stator Stage 5 assembly, Vane IGV blades, HPC Stage 5 blades along with gear box assembly and with intricate cooling passages. Another area of application, HAL Foundry and Forge division is considering, is the manufacture of sand mould and cores for
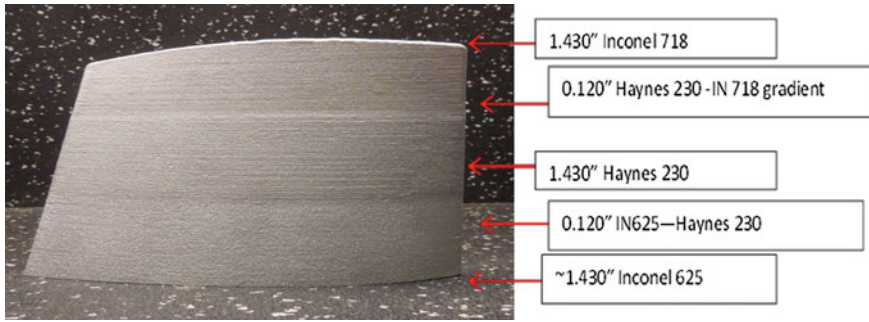
Fig. 13 Aerofoil with multi alloy deposition (Inconel-Haynes-Inconel using LMD technology from RPM Innovations, USA) for testing and evaluation of application of laser metal deposition (LMD)

manufacture of aluminium alloy and magnesium alloy castings as well as tools for investment castings.

2.1.13 Research and Development of Jet Engine at Monash University, Australia

Australian Research Council (ARC) has been promoting Australia's manufacturing industry through high value additive manufacturing technology in collaboration with Monash University. Professor Xinhua Wu is leading this research team. ARC has funded $9 million (AUD) to focus and develop Australia's aerospace industry.

The research group is focusing on Selective Laser Sintering (SLS) additive manufacturing technology to build Titanium alloy components. Professor Wu has printed a prototype of small jet engine (as shown in Fig. 14) using SLS metal AM technology as apart of their research and development [15].

The research team found that using 3D printing technology, engine components could be produced in less time, cost, reduced weight and carbon emissions.

Fig. 14 3D printed small jet engine
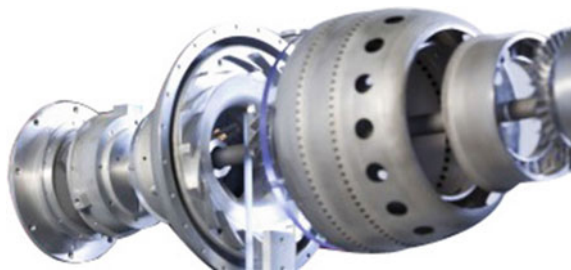
2.1.14 Research on Additive Manufacturing of Ceramics for Direct Digital Investment Casting—Georgia Tech University, USA

The Innovative Large Area Maskless Photopolymerization (LAMP) is an additive manufacturing technology, which was invented and developed by Georgia Tech University with support from the Defense Advanced Research Projects Agency (DARPA)'s Disruptive Manufacturing Technologies program, and the project is titled "Direct Digital Manufacturing of Airfoils".

LAMP technology directly produces complex ceramic cores and integral-cored shell moulds for investment casting directly from CAD data. The high resolution UV light selectively cures ceramic filled photo curable resin layer by layer and solidifies to a physical object. 3D printed moulds are then thermally post-processed which are foundry-ready for casting.

These castings are used for production of single crystal nickel-super alloy airfoils for aero turbine engines. This helps in cost reduction of manufacturing of turbine airfoils [16].

2.1.15 The World's First 3D Printed Aircraft—Southampton University Laser Aircraft

Prof. Jim Scanlan and Andy Keane University of Southampton, Computational Engineering and Design Group University of Southampton, UK designed and 3D printed plastic aircraft model (as shown in Fig. 15) using Selective Laser Sintering

Fig. 15 World's first 3D printed aircraft model
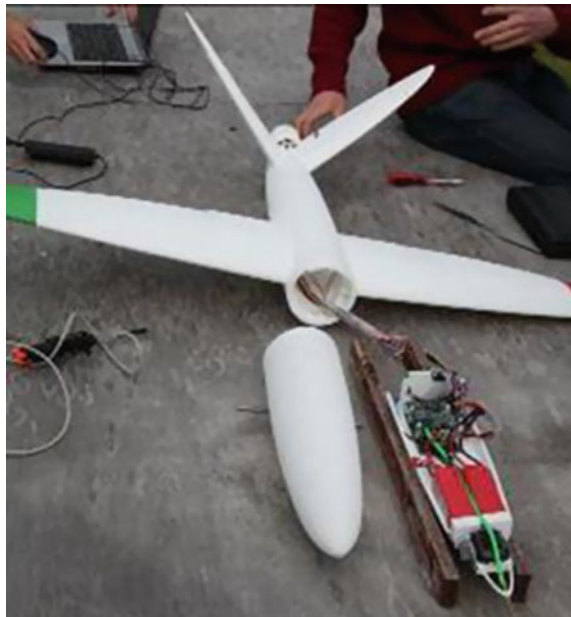
(SLS) technology. The 3D printed aircraft model was assembled with five structural/aerodynamic components and without conventional fasteners.

The purpose of the research was to study the

a. Use of snap fit methods to locate avionics, payload and propulsion items.
b. Use of a complex geodetic internal structure, which is directly 3D, printed to the internal surfaces of the aircraft.
c. Use of a concept optimization process to provide an optimal shape and minimal structural weight

Specification of the 3D printed aircraft

- 0.5 kg payload
- Full Nylon 12 SLS printed structure
- 30 min endurance
- Electric propulsion
- Top speed of 90 mph
- On-board GPS systems
- SMS capable
- Fastener-free assembly [17].

2.1.16 Development of New Material for Additive Manufacturing Aerospace Components—GKN Aerospace, UK

GKN Aerospace supported by Aerospace Technology Institute (ATI, UK) and consortium partners-Phoenix Scientific Industries Ltd., UK, Metalysis and University of Leeds will be investigating titanium alloys and powders characteristics using Additive Manufacturing for the aerospace industry.

The research team says "Today additive manufacturing uses metal alloys and powders which have not been developed for these processes and are not optimized for this environment". The research partners will investigate developing titanium alloys and powders with the characteristics that are specifically suitable to additive manufacturing. Later, they will define the production methods that produce additive manufacturing designed materials to ensure the cost is minimized and at the same to retain the production quality, quantity and rigorous standards required by aerospace industry [18].

2.1.17 Additive Manufacturing Research in China—Aviation and Aerospace Applications

Additive Manufacturing Research in China has commenced recently. The Chinese Government has made major investment in AM technology to develop China's high value manufacturing sector and to focus on production of large aerospace parts using Chinese developed technologies.

Fig. 16 Laser cladding cell at NPU

Northwest Polytechnic University (NPU) has developed the production of large-scale laser cladding cell. The laser-cladding cell can build a part size of $5 \times 2.5 \times 0.6$ m; accuracy of deposition speed is ± 1 mm and an inert atmosphere of 50 ppm (shown in Fig. 16).

Fig. 17 C919 central wing spar

During 2013, Northwest Polytechnic University (NPU) Laser Cladding Cell has developed central wing spar for 'Comac C919' passenger-plane and it is predicted to enter the commercial service in 2016. The length of this central wing spar is 5 m and having mechanical properties equal to forging parts as claimed by the NPU University (shown in Fig. 17).

Airbus Industries has signed an agreement with NPU in 2014 to manufacture titanium test specimens. Later, these specimens will be measured and evaluated by Airbus. The replacement of parts, which are not in the production line, is the future application of this technology [2].

3 Summary

The introduction of latest additive manufacturing processes like Laser Metal Deposition, Laser Cladding, Electron Beam Melting, Direct Metal Laser Sintering, Selective Laser Melting and advanced high temperature super alloys have drastically enhanced the applications of additive manufacturing technology in the aerospace industry. The increased demand for complex and lightweight metal parts such as turbine disc with blades, stator and rotor turbine vane assemblies, combustion chamber, fuel nozzle, etc., from the aerospace industry has made the technology most suitable for aerospace applications. Continuous innovations and growth in additive manufacturing will thus have a significant place in the future of aircraft manufacturing.

References

1. Wohlers Report (2014) 3D Printing and Additive Manufacturing State of the Industry
2. Anderson E (2013) Additive manufacturing in china: aviation and aerospace applications: Part2. In: Wimpenny D, Trepleton R, Jones J (eds) Additive manufacturing in the aerospace industry
3. GE Reports Staff (2015) The FAA cleared the first 3D printed part to fly in a commercial jet engine from GE. GE Reports, April 2015
4. Safran Magazine (2014) Safran at the cutting edge of additive manufacturing, pp 12–13
5. Szondy D (2012) NASA using 3D laser printing to create complex rocket parts, Nov 2012, Gizmag & NASA
6. Concept Laser (2014) A World First: Additively Manufactured Titanium Components Now Onboard the Airbus A350 XWB, Additive Manufacturing Amazing, Oct 2014
7. Stratasys Case Study Additive manufacturing reduces tooling cost and lead time to produce composite aerospace parts. Stratasys Ltd, USA
8. Krassenstein B (2015) 20,000 3D printed parts are currently used on boeing aircraft as patent filing reveals further plans, March 2015
9. Martin L (2014) Lockheed martin space systems company demonstrates digital production innovations during manufacturing day activities, Oct 2014
10. Anderson S (2015) Rolls-Royce to get largest 3D printed component off the ground, flight-testing engine later Year, Feb 2015

11. Peach M (2015) Pratt and Whitney uses 3D printing for aero engine parts, April 2015
12. Electro Optical Systems (Shanghai) (2014) Airbus defence and space cuts production time for satellite parts with additive manufacturing. Electro Optical Systems (Shanghai) Co., Ltd. Sept 2014
13. RAPITECH Solutions Inc., Project Engine Prototype Model. RAPITECH Solutions Inc., India
14. RPM Innovations & Efesto LLC USA Testing Model, Laser Metal Deposition- Multi Alloy Deposition Model. RPM Innovations & Efesto LLC USA
15. Monash University Positioned for take-off in the aerospace industry. Monash University Press Release, Nov 2014
16. Direct Digital Manufacturing Laboratory, Additive manufacturing of ceramics for direct digital investment casting. Georgia Tech University, USA
17. Scanlan J, Keane A The world's first 3D printed aircraft. SULSA—Southampton University Laser Sintered Aircraft
18. GKN Aerospace (2015) 3 year project to develop new titanium powder for AM of aerospace components" Spicer Unmanned Air Vehicle, April 2015

Influence of Oxygen Partial Pressure on Hydroxyapatite Coating of Additive Manufactured Component by Pulsed Laser Deposition

K. Hariharan and G. Arumaikkannu

Abstract Additive manufactured polyamide substrate has a wide range of application in the medical field due to its good mechanical property and biological behaviour. The biocompatibility of this polyamide is further enhanced by coating Hydroxyapatite (HA) over the surface, Pulsed Laser Deposition (PLD) has become widely used technique to deposit HA, because the film obtained by this method will have better crystalline and required surface roughness which facilitates a better osseointegration. This work aims to deposit HA over polyamide substrate using PLD with different oxygen partial pressures of 2×10^{-4}, 2×10^{-3} and 2×10^{-2} Torr. The characterization of coating was performed by Scanning Electron Microscope with Energy Dispersive X-ray spectroscopy (SEM-EDX), Atomic Force Microscope (AFM) and X-Ray Diffraction (XRD). These results suggest that the surface microstructure, crystallinity and surface roughness has significant changes when the oxygen pressure was varied. Therefore, the oxygen pressure plays a key role in the quality HA layer developed using Pulsed Laser Disposition.

Keywords Additive manufacturing · Polyamide · Hydroxyapatite · Oxygen pressure · Pulsed laser deposition

1 Introduction

Medical devices and implants are fabricated in many conventional techniques, but due to advancements in implant manufacturing industry, Additive Manufacturing (AM) takes a wide platform in fabricating these devices with good mechanical property, dimensional stability and customised according to the patient data with

K. Hariharan (✉) · G. Arumaikkannu
Department of Manufacturing Engineering, College of Engineering Guindy,
Anna University, Chennai, India
e-mail: hariharancim28@gmail.com

G. Arumaikkannu
e-mail: arumai@annauniv.edu

variety of biomaterials. Polyamide is a notable biomaterial because of its good mechanical property, broad temperature tolerance, and biological behaviour; hence it is used to fabricating medical devices, dental screws and implants using AM technique [1]. Conventional fabrication of scaffolds and implants suffers, because of its fabrication cost, complex design, difficulties in shaping bone grafts for bone defects, customisation and immune rejection [2]. Recent advancements in the areas of Additive Manufacturing (AM) lead to the emergence in the field of medicine or health care which overcome the difficulties of conventional fabrication [3]. AM fabricates implants and prosthesis directly from 3D CAD data obtained from CT/MRI without any tooling or process planning. Selective laser sintering (SLS) is an Additive Manufacturing technique that has an ability to build parts with variety of polymers, ceramics and metal powders with different properties for obtaining complex parts directly from CAD design. In this process, CO_2 laser sinters selectively thin layers of powder particle spread over a moving platform [4–8]. The biocompatibility of this implant or prosthesis further enhanced by coating Hydroxyapatite (HA) powder over the surface, which will form an intermediate region between the bone and implant [9]. The bulk HA cannot be used as implant to replace bone defects or for load-bearing applications due to its poor mechanical properties. Hence, HA thin film was developed to combine the mechanical performance of implants and the bioactivity of HA [10]. The HA powder coatings on implant are widely used in orthopaedic applications and dentistry. Common techniques like plasma spraying, magnetron sputtering, sol–gel method, biomimetic deposition, electrodeposition, etc., were used for HA coating on implants, [11]. Higher porosity, non-uniform coating thickness, poor crystallinity, phase impurity, and poor adhesion are encountered commonly among these techniques. Pulsed laser deposition (PLD) is a relatively modern technique in depositing a high quality HA coating with preserved stoichiometry of target material, to control the adherence, crystalline and surface roughness [12].

Pulsed Laser Deposition is a three step process: which includes (1) The laser beam and target interaction and forms a plasma plume of target material, (2) Plume transportation in ambient gas, (3) Film growth on a substrate surface [13]. Despite of simplicity of the film deposition, there is need of addressing the influence of some process parameters of PLD. The parameters such as substrate temperature, laser fluence and gas ambient pressure among that ambient oxygen pressure plays a key role in the process parameter of PLD process because this pressure will orient the plume in forward direction towards the substrate [14]. Several author has reported that the existence of oxygen gas has a strong influence on expansion of the plasma plume and modifies the kinetic energy of the ablated species from the target and results in different thin film characteristics such as surface morphology, growth rate, roughness, chemical composition, etc. [15–19]. In the present study, the various characteristics of HA films on Additive manufactured Polyamide by Pulsed Laser Deposition under the range of oxygen partial pressure was studied. It was found that surface microstructure, crystallinity and surface roughness of the film was sensitive to the oxygen pressure.

2 Experimental Details

2.1 Fabrication of Polyamide Substrate

The substrate was fabricated using Selective Laser Sintering (SLS) an AM technique. A 3D CAD model was generated and the data was sliced into layers. The model is loaded on to SLS machine and a computer directed CO_2 laser sinters layers of polyamide powder together where the chamber was maintained at a temperature of 115 °C with nitrogen gas circulation. After each solidification layer, another layer of powder was deposited and again sintering will take place until the part was completed [20, 21].

2.2 Preparation of Hydroxyapatite Target for Deposition

HA powder was prepared by wet chemical precipitation method. In this method, calcium hydroxide and ammonium phosphate (Dibasic) powder were taken as a precursor in the ratio of 10:6. These precursors were made into solution and precipitate was obtained. Then it was calcined at a temperature of 500 °C to obtain HA powder [22]. The prepared HA powder was made into pellets with high pressure hydraulic press with 400 MPa load and sintered at 800 °C for 5 h.

2.3 Pulsed Laser Deposition

Pulsed Laser Deposition of HA on Polyamide was carried out using Nd:YAG laser (Quanta Laser, USA) with a wavelength (λ) of 1064 nm and energy of 200 mJ. The deposition chamber was evacuated with a base pressure of 3×10^{-6} Torr and laser beam was focused towards the rotating target at an incident angle of $\sim 45°$ for deposition. The substrate temperature was maintained 150 °C. The pulsed laser deposition parameters are listed in Table 1, only oxygen pressure was varied and other parameters are kept constant.

Table 1 Pulsed laser deposition (PLD) Parameters

S. No.	Process parameter and its levels
1	Oxygen Pressure—2×10^{-4} Torr, 2×10^{-3} Torr, 2×10^{-2} Torr
2	Laser power—200 mJ
3	Substrate temperature—150 °C
4	Deposition time—30 min
5	Target substrate distance—3.5 cm

2.4 Film Characterization

The microstructure of deposited surface was examined using SEM and EDX analysis was carried out to find the stoichiometry of deposited layer. XRD measurement was performed to observe the crystalline phases in deposited layer. AFM was used to measure the roughness of the films at a randomly chosen area of 3×3 μm^2. Thickness of the film was measured using profilometer at a step grown by putting a mask on a part of substrate during deposition process.

3 Results and Discussion

3.1 Surface Microstructure

Figure 1 shows the surface microstructure of the HA film deposited under various oxygen pressure. At low oxygen pressure of 2×10^{-4} Torr, the film consist of very small, smooth and fine particles which was scattered over the surface. Some large particles were also observed over the surface due to high kinetic energy of particles which was ablated from the target. When the oxygen pressure was increased at 2×10^{-3} and 2×10^{-2} Torr, the grain size varies from smaller to bigger. The microstructure of the surface deposited at high pressure become porous. The oxygen pressure reduces the scattering of plume which results in deposition of larger particles and forms a porous layer [23, 24].

3.2 Surface Roughness

PLD process parameters play a major role in the particle deposition and film roughness but oxygen pressure was most important among them. Figure 2a–c shows AFM images of 3D roughness of the HA film with granular structure. Film grown at lower pressure had smooth surface and the roughness of about 20.58 nm (Fig. 2a) with further increase in the pressure, peaks and valleys like structure was observed. Film grown at very high pressure of 2×10^{-2} Torr shows a homogeneous granular structure (Fig. 2c). After initial free expansion, the mean free path of the ablated particles was reduced largely by the presence of oxygen pressure and at higher pressure more particle collision and scattering occurred and formed a cluster like surface with small, medium and large granular like particles [25]. The average surface roughness (R_a) of the films grown at different oxygen pressure was shown in the Fig. 3.

Fig. 1 Surface morphology
of HA film deposited under
various oxygen pressure
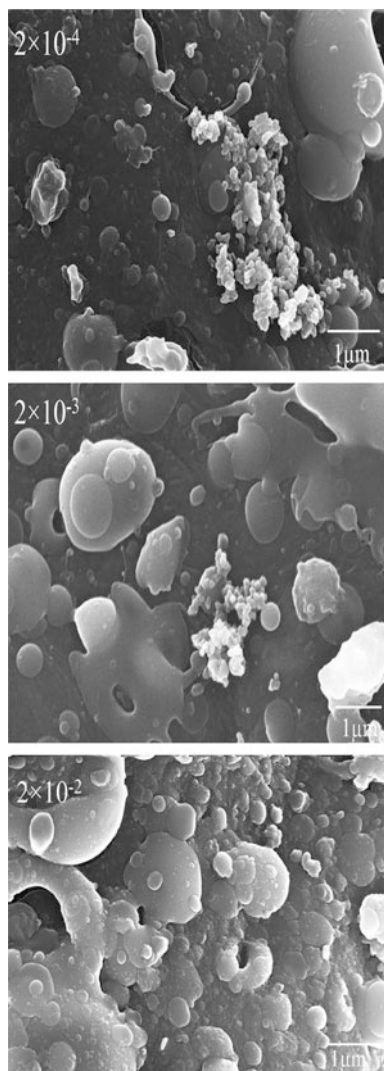
3.3 Crystallinity of HA Film

Figure 4 shows the XRD pattern of HA film grown on Polyamide substrate by PLD
with various oxygen pressure ranges from 2×10^{-4} to 2×10^{-2} Torr. It was
evident that all the peaks correspond to the standard HA peaks with crystalline
phase. It was also noticed that as the oxygen pressure increases, the peak became
narrow and sharper. This results indicate that the oxygen pressure significantly
influence in the crystallinity.

Fig. 2 3D AFM image of HA film. **a** 2×10^{-4}. **b** 2×10^{-3}. **c** 2×10^{-2}
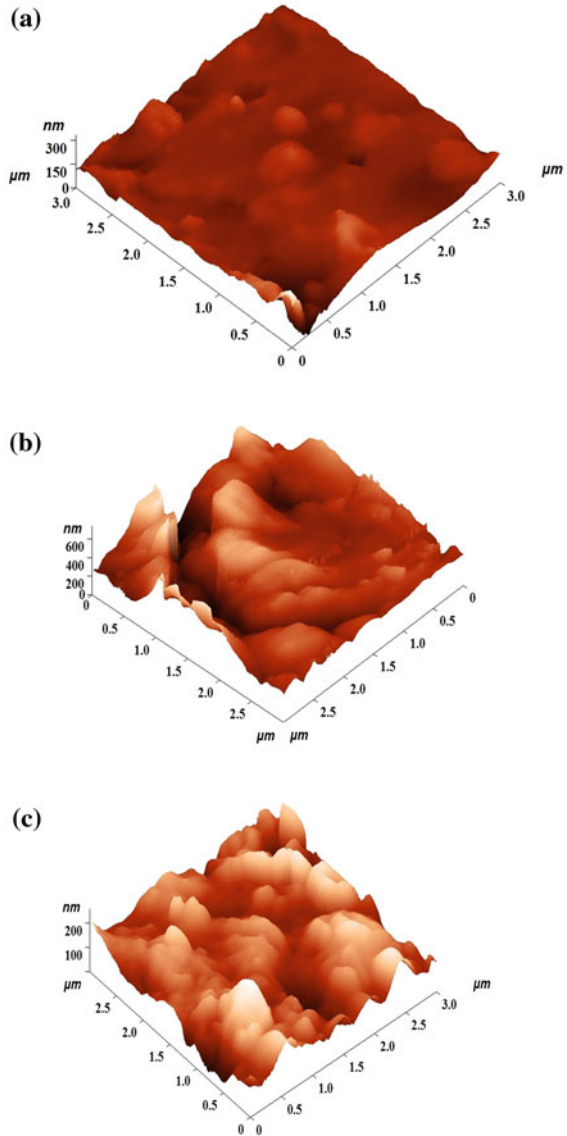
3.4 Growth Rate and Stoichiometry

The film thickness, growth rate and Ca/P ratio were listed in the Table 2. With increase in oxygen pressure, the quantity of oxygen atoms in chamber also increases and leads to more plasma collision and block the atom mobility, hence the growth rate decreases linearly with increase in oxygen pressure as shown in Fig. 5.

Fig. 3 Average Roughness
of HA film grown at different
oxygen pressure
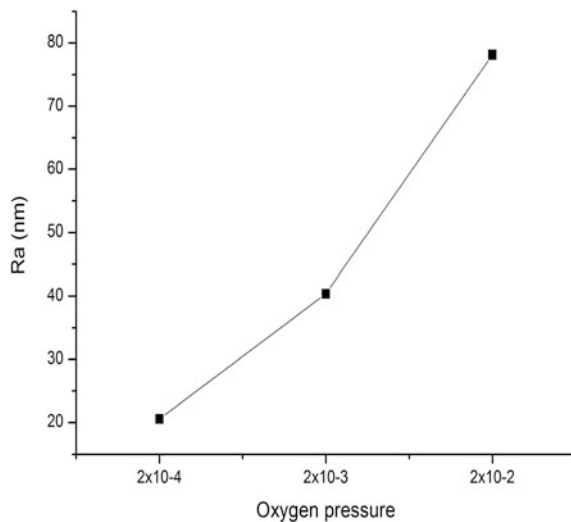
Fig. 4 XRD Pattern of HA
film grown at different oxygen
pressure
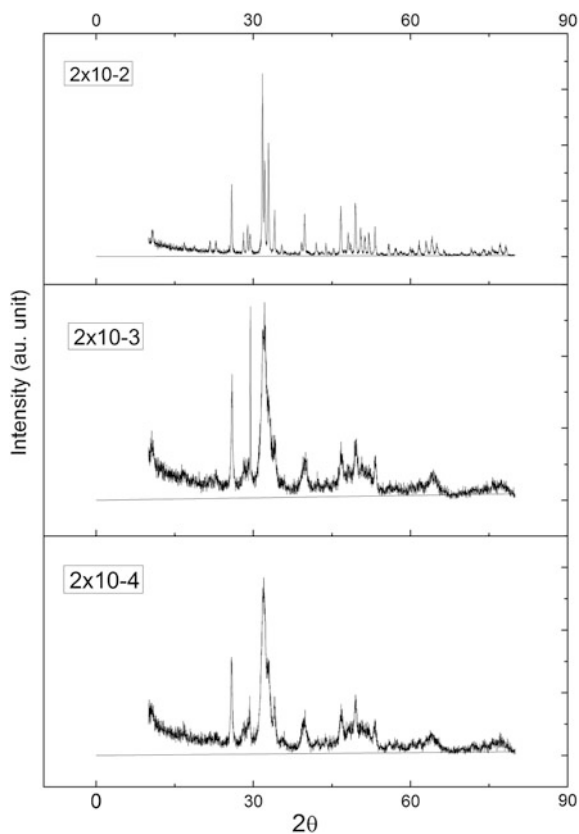
Table 2 Thickness, growth rate and Ca/P ratio of Ha layer deposited at various oxygen Pressure oxygen pressures

Oxygen pressure (Torr)	2×10^{-4}	2×10^{-3}	2×10^{-2}
Film thickness (nm)	800	539	280
Growth rate (nm/min)	28.06	17.96	9.33
Ca/P ratio	1.7	1.65	1.6

Fig. 5 Growth Rate of HA layer
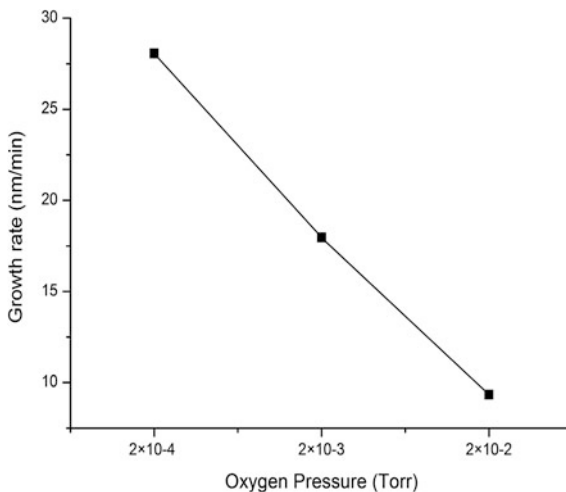
Fig. 6 Ca/P ratio of HA layer
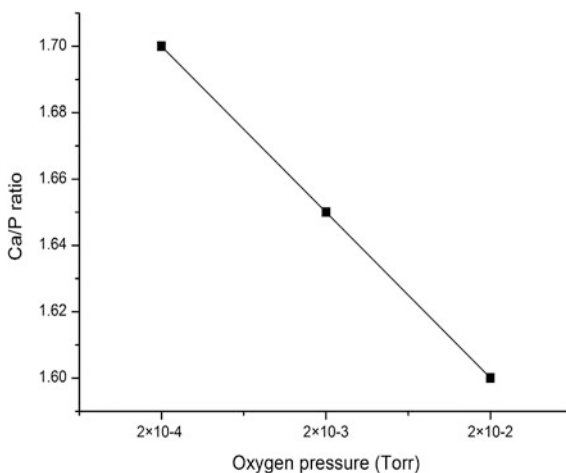
The Ca/P ratio were analysed using EDX which was shown in the Fig. 6. The Ca/P ratio gradually decreases with increase in the oxygen pressure. The amount of phosphorus deposited over the film was increased due to increase in the oxygen pressure because the ablated calcium will react with the oxygen and forms calcium oxide which reduces the deposition of calcium.

4 Conclusion

In this work, synthesised HA powder was successfully deposited over additive manufactured polyamide substrate using Pulsed Laser Deposition technique with various oxygen pressure. With increase in the oxygen pressure the particles become bigger and surface become rougher. The crystallinity was improved with increase in the pressure, whereas the Ca/P ratio decreased with increase in the pressure. Since the oxygen pressure influences the kinetic energy of ablated particle, there was a major influence in the growth rate and thickness of the film due to the pressure. The growth rate and thickness decreased due to the increase in the oxygen pressure since it influences the ablated particle to reach the substrate. This surface characterisation was important for the application of orthopaedic and dental application for fixing fractures, spinal reconstruction, and soft tissue anchorage, etc., which facilitates a better osseointegration.

References

1. EOSINT, Plastic laser-sintering for direct manufacturing. EOS GmgH, Technical Data. Bimingham—UK, 2002. Fine Polyamide PA 2200 for EOSINT P., Material Data Sheet
2. Tyndyk M, Lohfeld S, Barron V, McHugh E (2006) Assessment of SLS fabricated scaffolds for skeletal reconstruction in the spine. J Biomech 39 (Suppl 1)
3. Gibson I, Cheung LK, Chow SP, Cheung WL, Beh SL, Savalani M, Lee SH (2004) The use of Rapid Prototyping to assist medical applications", 10èmes Assises Européennes de Prototypage Rapide—14 and 15 Sept 2004
4. Salmoria GV, Leite JL, Ahrens CH, Lago A, Pires ATN (2007) Rapid manufacturing of PA/HDPE blend specimens by selective laser sintering: microstructural characterization. Polym Test 26(3):361–368
5. Salmoria GV, Leite JL, Paggi RA, Lago A, Pires ATN (2008) Selective laser sintering of PA12/HDPE blends: Effect of components on elastic/plastic behavior. Polym Test 27(6):654–659
6. Salmoria GV, Ahrens CH, Klauss P, Paggi RA, Oliveira RG, Lago A (2007) Rapid manufacturing of polyethylene parts with controlled pore size gradients using selective laser sintering. Mater Res 10(2):211–214
7. Salmoria GV, Leite JL, Lopes C, Machado RAF, Lago A (2007) Advanced research in virtual and rapid prototyping. Taylor & Francis, London, pp 305–311
8. Salmoria GV, Leite JL, Lopes CH, Paggi RA, Lago A (2007) Advanced research in virtual and rapid prototyping. Taylor & Francis, London, pp 313–317
9. Bao Q, Chen C, Wang D, Ji Q, Lei T (2005) Pulsed laser deposition and its current research status in preparing hydroxyapatite thin films. Appl Surf Sci 252:1538–1544
10. Yan W-Q, Nakamura T, Kawanabe K, Nishigochi S, Oka M, Kokuba T (1997) Apatite layer–coated titanium for use as bone bonding implants. J Biomater 18:1185–1190
11. Koch CF, Johnson S, Kumar D, Jelinek M, Chrisey DB, Doraiswamy A et al (2007) Pulsed laser deposition of hydroxyapatite thin films. Mater Sci Eng C 27:484–494
12. Bao Q, Chen C, Wang D, Ji Q, Lei T (2005) Pulsed laser deposition and its current research status in preparing hydroxyapatite thin films. Appl Surf Sci 252:1538–1544
13. Chen XY, Liu ZG (1999) Interaction between laser beam and target in pulsed laser deposition: laser fluence and ambient gas effects. Appl Phys A 69(Suppl):S523–S525

14. Bassim ND, Schenck PK, Donev EU, Heilweil EJ, Cockayne E, Green ML, Feldman LC (2007) Effects of temperature and oxygen pressure on binary oxide growth using aperture-controlled combinatorial pulsed-laser deposition. Appl Surf Sci 254(3):785–788

15. Nakata Y, Soumagne G, Okada T, Maeda M (1998) Pulsed-laser deposition of barium titanate films and plume dynamics. Appl Surf Sci 127:650–654

16. Gonzalo J, Roman RGS, Perriere J, Afonso CN, Casero RP (1998) Pressure effects during pulsed-laser deposition of barium titanate thin films. Appl Phys A 66(5):487–491

17. Tyunina M, Levoska J, Leppavuori S (1998) Experimental studies and modeling of Pb–Zr–Ti–O film growth in pulsed laser deposition. J Appl Phys 83(10):5489–5496

18. Zhang J, Cui D, Zhou Y, Li L, Chen Z, Szabadi M, Hess P (1996) Effect of oxygen pressure on the orientation, lattice parameters and surface morphology of laser ablated BaTiO 3 thin films. Thin Solid Films 287(1):101–103

19. Zhao T, Chen F, Lu H, Yang G, Chen Z (2000) Thickness and oxygen pressure dependent structural characteristics of BaTiO3 thin films grown by laser molecular beam epitaxy. J Appl Phys 87:7442–7447

20. Salmoria GV, Leite JL, Paggi RA (2009) The microstructural characterization of PA6/PA12 blend specimens fabricated by selective laser sintering. J Polym Test 28:746–751

21. Van Hooreweder B, Moens D, Boonen R, Kruth J-P (2013) Paul Sas "On the difference in material structure and fatigue properties of nylon specimens produced by injection molding and selective laser sintering". Polym Test 32:972–981

22. Liu Y, Hou D, Wang G (2004) A simple wet chemical synthesis and characterization of hydroxyapatite nanorods. Mater Chem Phys 86:69–73

23. Lee W-J, Lee S-W, Kim H-L, Kim D-J, Han J-S (2005) Characteristics of calcium phosphate films prepared by pulsed laser deposition under various water vapor pressures

24. Jo JH, Tae-Bong HVR, Kwak JS, Kwon DY, Hwang YH, Kim HK (2005) "Effects of oxygen pressure on the crystalline of ZnO films grown on sapphire by PLD method." J Korean Phys Soc 47:S300–S303

25. Haider AJ (2009) "An interesting experimental observation of O_2 pressure effect on the surface roughness of ZnO thin films prepared by PLD technique". Iraqi J Appl Phys Lett 2(4):3, 4

Electro Discharge Machining of Ti-Alloy (Ti6Al4V) and 316L Stainless Steel and Optimization of Process Parameters by Grey Relational Analysis (GRA) Method

Anshuman Kumar Sahu, Pragyan Paramita Mohanty and Sarat Kumar Sahoo

Abstract Increasing demand on micro-product leads to the development of innovative manufacturing process in nonconventional machining process to these micro-scale applications. In the medical field a huge variety of products can be found in prosthesis, surgery devices and tissue engineering, which required the application of the EDM process to manufacture micro cavities. Now-a-days the materials like Ti-alloy (Ti6Al4V) and 316L Stainless Steel are widely used in biomedical fields, which are very difficult to machine. These materials are also used in additive manufacturing process. Here it presents an experimental study of electro-discharge machining (EDM) of titanium alloy (Ti6Al4V) and 316L Stainless Steel. The objective of this work is to study the effect and optimization of machining process parameters like pulse-on-time, discharge current and duty cycle on process performance parameters such as material removal rate (MRR), tool wear rate (TWR) and Radial over cut (ROC). A Taguchi L9 design of experiment (DOE) has been applied and three levels of process parameters have been taken. The optimization method Grey relational analysis (GRA) method was used to optimize the parameters. The Analysis of Variance (ANOVA) also indicated the percentage contribution of machining parameters that influence response performance parameters. By the GRA method it was found that for Ti-alloy the machining parameter duty cycle (DC) has maximum percentage contribution on the output responses followed by discharge current (I_p) and pulse on time (T_{ON}). Similarly for 316L Stainless Steel the

A.K. Sahu (✉) · P.P. Mohanty · S.K. Sahoo
Department of Mechanical Engineering, Veer Surendra Sai University of Technology,
Burla 768018, Odisha, India
e-mail: anshuman.sahu123@gmail.com

P.P. Mohanty
e-mail: pragyanmohanty.design@gmail.com

S.K. Sahoo
e-mail: saratkumar222@gmail.com

machining parameter discharge current (I_p) has maximum percentage contribution on the output responses followed by pulse-on-time (T_{ON}) and duty cycle (DC).

Keywords EDM · Taguchi design · Multi-response optimization method · Grey relational analysis method · ANOVA

1 Introduction

Electro discharge machining (EDM) is a non-traditional machining process, which is very widely used in recent days. In EDM both the work piece and tool are immersed inside a dielectric medium. When a voltage is applied to the work piece and tool circuit, there is a generation of spark in between the electrodes (tool and work piece). Therefore, very high temperature is generated in the spark gap region. Due to the high temperature, the material removal occurs from the work piece by the process of melting and evaporation. In EDM both tool and work piece are electrically conducting [1, 2].

Titanium is a metal with high corrosion resistance, temperature resistance and high strength to weight ratio [3]. Similarly 316L Stainless Steel have also high corrosion resistance properties. Therefore, Titanium, Ti-alloys and 316L Stainless Steel are widely used in aerospace, automobile, biomedical, electronics and chemical industries. Titanium is very strong, light weight, highly durable and long lasting metal. Ti rods, plates and pins are easily works inside the humane body for many years. Due to the non-ferrous properties of titanium implants, it can be safely examined with MRIs and NMRIs [3]. Recently Titanium is widely used in biomedical and medical field because it is easily jointed with bone and body tissue. Irrespective of this, there are certain limitations for the use of Titanium because of its initial cost is high, its availability and manufacturability, but 316L Stainless Steel is less cost as compare to Titanium and it's alloys. These two materials are also required additive manufacturing for use in aerospace and automobile application. The machining of Titanium and it's alloys by traditional machining method is very difficult due to high temperature generation and high tool wear ratio. Also to produce complex shape and micro cavities on these materials for biomedical use is difficult by the conventional machining process. Therefore, non-traditional machining processes are applied in manufacturing industries for machining of titanium, it's alloys and 316L stainless steel [4, 3]. For non-traditional machining the tool also can be made by additive manufacturing process. Recently composite tool as well as composite work piece material were made by different methods like additive manufacturing, powder metallurgy method etc. and the EDM performance were studied by the composite materials [5–13]. Some thermalstructural model of EDM also performed [14]. Here in this paper we have studied Electro discharge machining (EDM) for machining of TI-alloy (Ti6Al4 V) and 316L Stainless Steel by taking cylindrical Copper tool and optimize the process parameters that gives the

Table 1 Chemical composition (weight %) of Ti-alloy

C	Fe	Al	O	N	V	H	Ti
0.018	0.22	6.08	0.18	0.05	4.02	0–0.15	Balance

Table 2 Chemical composition (weight %) of 316L stainless steel

C	Mn	P	S	Si	Cr	Ni	Mo	N	Fe
0.03	2.0	0.045	0.03	0.75	16–18	10–14	2–3	0.1	Balance

maximum benefit to the manufacturing industries. The chemical composition of Ti-alloy and 316L Stainless Steel were presented in Tables 1 and 2 respectively.

2 Experiment

For this experimental study the work can be done by Electric Discharge Machine, model ELECTRONICA-EMS-5535/PS 50 (die sinking type) with servo-head (constant gap) and positive polarity was taken to conduct the experiments. The specification of the machine was given in Table 3. EDM oil (water:kerosene = 60:40) as used as dielectric fluid. Cylinder-shaped Cu tools (diameter 8 mm) were used with EDM oil as dielectric medium [1]. The pulse discharge current was supplied in various steps with positive mode. The EDM machine and Tool and Workpiece during machining were given in Figs. 1 and 2 respectively.

2.1 Work Piece

Work pieces of rectangular block were taken and cut into suitable pieces. These pieces were grinded properly with the help of surface grinding machine and then polished using automatic polishing machine. The final dimensions of the work pieces are 102 mm × 52 mm × 8 mm. Copper tool (stepped cylindrical size of

Table 3 Machine specification

Description	Details
Machine	ELECTRONICA
Model	EMS 5535/PS 50
Supply voltage	75 V
Discharge current	30 A
Servo system	Electromechanical
Power consumption	2 kW
Specification	X = 300 × Y = 200 × Z = 250

Fig. 1 ELEKTRA EMS
5535

Fig. 2 Tool holder with
work piece and tool

diameter 8 and 5 mm having total length of 35 mm) were taken separately for each experiment. The Figures Work pieces after machining were given in Fig. 3.

2.2 Responses and Design of Experiment

In this paper we discuss about the experimental work of EDM process which is consists of design of the L-9 orthogonal array according to Taguchi design [4, 15, 16]. Orthogonal array decrease the total number of experiments, in this experiment total 9 runs have taken. Input parameters current (I_p), Pulse on time (T_{on}), Duty

Fig. 3 Work piece material.
a 316L stainless steel,
b Ti-alloy (Ti6Al4V)
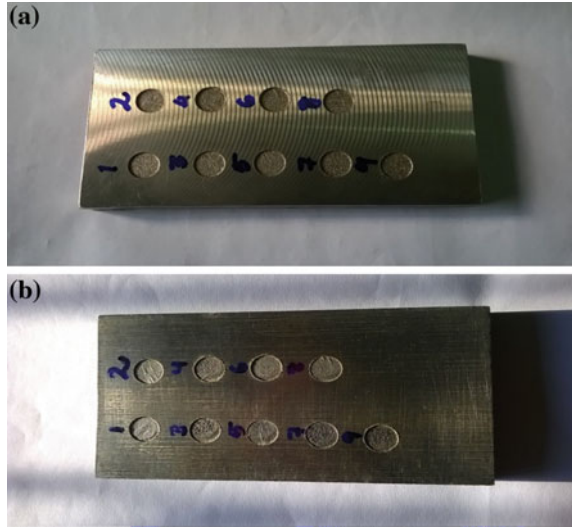
factor (ʈ) or Duty cycle (DC), were taken and for different values of these the material removal rate (MRR), tool wear rate (TWR) and radial over cut (ROC) were calculated for respective 9 experiments [1, 17]. Cylindrical shaped copper tools were taken as electrodes which were diameter of 8 mm [1]. A rectangular block each of Ti-alloy (Ti6Al4 V) and 316L Stainless Steel were taken as work piece and using these copper electrodes holes were made on the work pieces [4, 3, 16]. Varying different input parameters a total 9 numbers of experiments were conducted for each work piece material. For each experiment MRR, TWR and ROC were calculated.

$$\text{MRR} = \frac{W_{ji} - W_{jf}}{\rho t} \tag{1}$$

whereas
W_{ji} Initial weight of work piece before machining
W_{jf} Final weight of work piece after machining
t Machining time
ρ Density of material, For Ti-alloy ρ = 4420 kg/m^3,
      for 316L Stainless Steel ρ = 8027 kg/m^3

$$\text{TWR} = \frac{W_{ti} - W_{tf}}{\rho t} \tag{2}$$

whereas
W_{ti} Initial weight of the tool before machining
W_{tf} Final weight of the tool after machining
t Machining time
ρ Density of tool

Table 4 Machining parameters and their level

Machining parameters	Symbol	Unit	Level 1	Level 2	Level 3
Pulse on time (A)	T_{on}	μs	100	150	200
Discharge current (B)	I_p	Ampere	40	45	50
Duty factor (C)	DC (τ)	%	70	80	90

Table 5 Taguchi L9 experiment layout and output responses

Sl. No.	Input parameters			Responses (Ti-alloy)			Responses (316L S.S)		
	$(mm^3/$ min$)$	$(mm^3/$ min$)$	DC	MRR $(mm^3/$ min$)$	TWR $(mm^3/$ min$)$	ROC (mm)	MRR $(mm^3/$ min$)$	TWR $(mm^3/$ min$)$	ROC (mm)
1	1	1	1	0.4039	0.153	0.035	3.0913	0.328	0.030
2	1	2	2	0.5049	0.216	0.015	4.6312	0.595	0.025
3	1	3	3	0.3685	0.411	0.075	4.1946	0.670	0.015
4	2	1	2	0.3271	0.378	0.055	3.1699	0.817	0.025
5	2	2	3	0.3448	0.248	0.065	3.7468	0.582	0.050
6	2	3	1	0.3007	0.116	0.025	3.4896	0.210	0.070
7	3	1	3	0.2957	0.236	0.085	3.7558	0.583	0.025
8	3	2	1	0.2974	0.116	0.020	4.6424	0.280	0.045
9	3	3	2	0.3886	0.351	0.065	3.5594	0.438	0.080

For Copper ρ = 8940 kg/m^3

$$ROC = \frac{D_f - D_i}{2} \tag{3}$$

where

D_f Final diameter of hole on the work piece,

D_i Initial diameter of tool.

In this process, the effects of different control parameters were studied. These machining parameters with their three levels are listed in Table 4. The Taguchi L9 experiment layout and output responses were given in Table 5.

Here the MRR, TWR and ROC were calculated using relations (1), (2) and (3).

3 Result and Discussion

3.1 Optimization Method

Ultimate aim of any manufacturer is to maximize the efficiency process by minimize the cost input which is maximizing the product quality and quantity. To achieve this goal optimization is the one of the most successful techniques applied

for manufacturing processes. Optimization is the process of finding the best result with the given working parameters. It maximizes the desired benefits and minimizes the effort required.

Taguchi taken the response parameters (variables) by three different types, i.e., smaller is the better, larger is the better and nominal is the best [4, 16]. Considering that there are m experimental trials and for each trial, quality losses of a set of p response variables are calculated. Quality loss (L_{ij}) for jth response with respect to ith trial ($i = 1, 2,..., m; j = 1, 2, ...,p$) for different types of response variables are given as follows [18]:

For smaller the better,

$$L_{ij} = \left(\frac{1}{n} \sum_{k=1}^{n} y_{ijk}^2 \right) \tag{4}$$

For larger the better,

$$L_{ij} = \left(\frac{1}{n} \sum_{k=1}^{n} \frac{1}{y_{ijk}^2} \right) \tag{5}$$

For nominal the best,

$$L_{ij} = \left(\frac{s_{ij}^2}{\bar{y}_{ij}^2} \right) \tag{6}$$

where, $\bar{y}_{ij} = \frac{1}{n} \sum_{k=1}^{n} y_{ijk}$, $s_{ij}^2 = \frac{1}{n-1} \sum_{k=1}^{n} \left(y_{ijk} - \bar{y}_{ij} \right)^2$.

n is the numbers of repetitive experiments, y_{ijk} is the experimental value of jth response variable in ith trial at kth replication and L_{ij} is the calculated quality loss for jth response in ith trial.

The Signal-to-Noise ratio value $\left(\eta_{ij} \right)$ (Table 7) is obtained by putting the value of L_{ij} for the jth response in the ith trial in the equation:

$$\eta_{ij} = -10 \log 10 \, L_{ij} \tag{7}$$

The quality loss (L_{ij}) (Table 6) is normalized to decrease the variability among different responses. The normalized quality loss (S_{ij}) is given as:

$$S_{ij} = L_{ij} / \bar{L}_i \tag{8}$$

where $\bar{L}_i = \frac{1}{m} \sum_{i=1}^{m} L_{ij}$ is the average quality loss for the jth response.

Sometimes, Signal-to-noise ratio is normalized instead of quality loss and is scaled between 0 and 1.

Table 6 Quality loss

Sl. No.	Quality loss (L_{ij}), Ti-alloy			Quality loss (L_{ij}), stainless steel		
	MRR	TWR	ROC	MRR	TWR	ROC
1	6.130	0.023	0.001,225	0.105	0.108	0.000900
2	3.923	0.047	0.000225	0.047	0.354	0.000625
3	7.364	0.169	0.005625	0.057	0.449	0.000225
4	9.346	0.143	0.003025	0.100	0.667	0.000625
5	8.411	0.062	0.004225	0.071	0.339	0.002500
6	11.059	0.013	0.000625	0.082	0.044	0.004900
7	11.436	0.056	0.007225	0.071	0.340	0.000625
8	11.306	0.013	0.000400	0.046	0.078	0.002025
9	6.622	0.123	0.004225	0.079	0.192	0.006400

Table 7 Calculation of S/N ratio

Sl. No.	S/N ratio (η_{ij}), Ti-alloy			S/N ratio (η_{ij}), stainless steel		
	MRR	TWR	ROC	MRR	TWR	ROC
1	−7.875	16.383	29.119	9.788	9.666	30.458
2	−5.936	13.279	36.478	13.279	4.510	32.041
3	−8.671	7.721	22.499	12.441	3.478	36.478
4	−9.706	8.447	25.193	10.000	1.759	32.041
5	−9.248	12.076	23.742	11.487	4.698	26.021
6	−10.437	18.861	32.041	10.862	13.565	23.098
7	−10.583	12.518	21.412	11.487	4.685	32.041
8	−10.533	18.861	33.979	13.372	11.079	26.936
9	−8.210	9.101	23.742	11.024	7.167	21.938

$$Y_{ij} = \frac{(\eta_{ij} - \eta_j^{\min})}{(\eta_j^{\max} - \eta_j^{\min})} \tag{9}$$

where Y_{ij} = scaled signal-to-noise ratio value (Table 8) for the jth response in the ith trial, $\eta_j^{\min} = \min\{\eta_{1j}, \eta_{2j}, \ldots \eta_{mj}\}$. and $\eta_j^{\max} = \max\{\eta_{1j}, \eta_{2j} \ldots \eta_{mj}\}$

3.2 Grey Relational Analysis (GRA) Method

In this method, Grey Relational Grade (GRG) value is taken as the process performance index (PPI) [19]. The steps for obtaining PPI are as follows [19, 18]:

Step 1: Calculation of the Signal-to-Noise ratio (η_{ij}) values for each response for each trial using Eq. (7).

Table 8 Scaled S/N ratio

Sl. No.	Scaled S/N ratio (Y_{ij}), Ti-alloy			Scaled S/N ratio (Y_{ij}), stainless steel		
	MRR	TWR	ROC	MRR	TWR	ROC
1	0.583	0.778	0.512	0.000	0.670	0.586
2	1.000	0.499	1.000	0.974	0.233	0.695
3	0.411	0.000	0.072	0.740	0.146	1.000
4	0.189	0.065	0.251	0.059	0.000	0.695
5	0.287	0.391	0.155	0.474	0.249	0.281
6	0.031	1.000	0.705	0.300	1.000	0.080
7	0.000	0.431	0.000	0.474	0.248	0.695
8	0.011	1.000	0.834	1.000	0.789	0.344
9	0.511	0.124	0.155	0.345	0.458	0.000

Step 2: Obtaining the scaled Signal-to-Noise ratio (Y_{ij}) (Table 8) values for each response for each trial using Eq. (9).

Step 3: Computation of the grey relational coefficients.
Grey relational coefficient (γ_{ij}) for the jth response in the ith trial is calculated as follows:

$$\gamma_{ij} = \left(\Delta_{j\min} + \xi\Delta_{j\max}\right)/\left(\Delta_{ij} + \xi\Delta_{j\max}\right) \qquad (10)$$

where $\Delta_{ij} = \left|1 - Y_{ij}\right|$, $\Delta_{j\min} = \min\left\{\Delta_{1j}, \Delta_{2j}, \ldots, \Delta_{mj}\right\}$,

$$\Delta_{j\max} = \max\left\{\Delta_{1j}, \Delta_{2j}, \ldots, \Delta_{mj}\right\}$$

and ξ = distinguishing coefficient ($\xi \in [0,1]$).
The distinguishing coefficient (ξ) is used to increase or decrease the range of grey relational coefficient and is mostly taken as 0.5 [18].

Step 4: Calculating the grey relational grade (GRG_i) corresponding to ith trial as follows:

$$GRG_i = \sum_{j=1}^{P} W_j \gamma_{ij} \qquad (11)$$

where W_j is the weight for jth response and $\sum_{j=1}^{P} W_j = 1$.

3.3 Calculation of Quality Loss, S/N Ratio and Scaled S/N Ratio

The expressions for quality loss, S/N ratio and Scaled S/N ratio have been discussed in the Sect. 3.1 and calculated values are shown in Tables 6, 7 and 8 respectively.

3.4 Determination of Process Performance Index (PPI) Values and Analysis of Variance (ANOVA)

3.4.1 Grey Relational Analysis (GRA) Method

Here in the GRA method, Grey relational grade (GRG) value is taken as the process performance index value.

The GRG value calculated are shown in Table 9. The higher value of GRG gives the optimum level of input machining parameters.

3.4.2 Analysis of Variance (ANOVA)

The percentage contribution of each input parameters on the output responses can be calculated by performing ANOVA. From the ANOVA table (Tables 12 and 13) effect of the input parameters on the output responses can be calculated and the more significant parameter was obtained.

From the level average values (Tables 10 and 11) and level average values graphs (Fig. 4) for both work pieces and for all the four methods, following results

Table 9 Grey relational coefficient and grey relational grade

Sl. No.	Grey relational coefficient (γ_{ij}) Ti-alloy			Grey relational coefficient (γ_{ij}) 316L SS			GRG_i (Ti-alloy)	GRG_i (316L SS)
	MRR	TWR	ROC	MRR	TWR	ROC		
1	0.545	0.693	0.506	0.333	0.602	0.547	0.581	0.494
2	1.000	0.500	1.000	0.951	0.395	0.621	0.833	0.656
3	0.459	0.333	0.350	0.658	0.369	1.000	0.381	0.676
4	0.381	0.348	0.400	0.347	0.333	0.621	0.376	0.434
5	0.412	0.451	0.372	0.487	0.400	0.410	0.412	0.432
6	0.340	1.000	0.629	0.417	1.000	0.352	0.656	0.590
7	0.333	0.468	0.333	0.487	0.399	0.621	0.378	0.502
8	0.336	1.000	0.751	1.000	0.703	0.433	0.696	0.712
9	0.506	0.363	0.372	0.433	0.480	0.333	0.414	0.415

Mean GRG_i(Ti-alloy) = 0.525, Mean GRG_i(316L SS) = 0.546

Table 10 Level average of GRG values (Ti-alloy)

Machining parameters	Level-1	Level-2	Level-3	Δ	Rank	Optimal level
T_{on} (A)	0.598	0.481	0.496	0.117	3	L-1
I_p (B)	0.445	0.647	0.484	0202	2	L-2
DC (C)	0.644	0.541	0.390	0.254	1	L-1

Table 11 Level average of GRG values (316L SS)

Machining parameters	Level-1	Level-2	Level-3	Δ	Rank	Optimal level
T_{on} (A)	0.609	0.485	0.543	0.124	2	L-1
I_p (B)	0.476	0.600	0.560	0.124	1	L-2
DC (C)	0.599	0.502	0.537	0.093	3	L-1
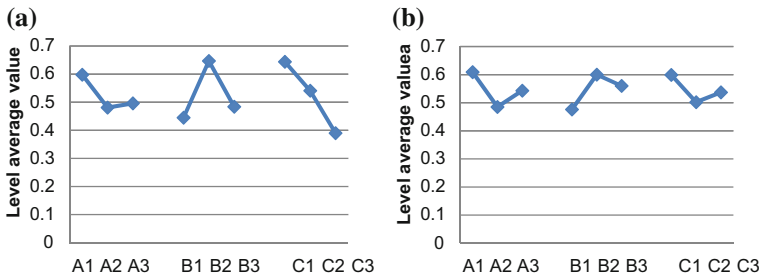
Fig. 4 Graph of level average of GRA values. **a** GRA values of Ti-alloy, **b** GRA values of 316L SS

have obtained. In GRA method, greater value of level average means better quality. So, optimal condition using GRA method for Ti-alloy and 316L SS are A1, B2, C1 and A1, B2, C1 respectively.

The contribution of each input parameters i.e. Pulse-on-time (A), Discharge current (B) and Duty cycle (C), on the performance parameters i.e. material removal rate (MRR), tool wear rate (TWR) and radial over cut (ROC) has been calculated by using Analysis of Variance (ANOVA).

In GRA method, (from Table 12 and also from Fig. 5a), for Ti-alloy it is found that duty cycle (C) has the highest contribution of 41.84 % followed by discharge current (B) and pulse-on-time (A) having contribution of 29.44 and 10.38 %

Table 12 ANOVA table for GRG values (Ti-alloy)

Machining parameters	SS	DF	MS	F	% contribution
T_{on}	0.0243	2	0.01215	0.5664	10.38
I_p	0.0689	2	0.03445	1.6061	29.44
DC	0.0979	2	0.04895	2.2821	41.84
Error	0.0429	2	0.02145	–	18.34
Total	0.2340	8	0.117	–	100

Table 13 ANOVA table for GRG values (316L SS)

Machining parameters	SS	DF	MS	F	% contribution
T_{on}	0.0231	2	0.01155	0.5179	21.83
I_p	0.0236	2	0.0118	0.5291	22.31
DC	0.0145	2	0.00725	0.3251	13.71
Error	0.0446	2	0.0223	–	42.15
Total	0.1058	8	0.0529	–	100
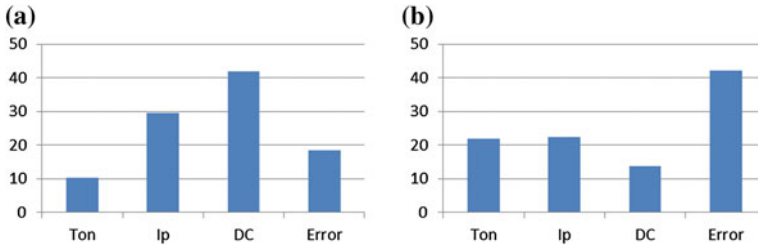
Fig. 5 Percentage contribution of input parameters for GRA method. **a** Ti-alloy, **b** 316L stainless steel

respectively. Similarly, (from Table 13 and also from Fig. 5b), for 316L Stainless Steel it is obtained that discharge current (B) has the highest contribution of 22.31 % followed by pulse-on-time (A) and duty cycle (C) having contribution of 21.83 and 13.71 % respectively.

4 Conclusion

The present study describes a solution towards improvement of quality and productivity of complex parts produced, which is allied with the accurate application of the specified performance.

The model proposed here not only explains the complex build mechanism but also present in detail the processing parameter effect on performance measure. The comparisons of EDM performances with Ti-alloy and 316L Stainless Steel as work piece materials and copper as tool have been taken. The development of multi response optimization techniques are used to optimize process parameters for better performance. The optimization of the process parameters for MRR, TWR, and Radial Overcut has been performed individually for both Ti-alloy and 316L Stainless Steel.

Using the above method in EDM process, it is found that duty cycle having maximum significant effect on the output parameters in case of Ti-alloy work piece. For 316L Stainless Steel, discharge current became more influential factor affecting response parameters.

Owing greater value of level average towards better quality in GRA method, optimal condition for Ti-alloy has been derived as A-1, B-2, C-1 and optimal GRG value is 0.644. Similarly for 316L Stainless Steel the same is A-1, B-2, C-1 with GRG value is 0.600.

References

1. Assarzadeh S, Ghoreishi M (2013) Statistical modeling and optimization of process parameters in electro-discharge machining of cobalt-bonded tungsten carbide composite (WC/6 %Co). In: The Seventeenth CIRP conference on electro physical and chemical machining (ISEM), Procedia CIRP 6 (2013), pp 463–468
2. Mishra PK (2012) Nonconventional machining. Narosa Publishing House, New Delhi
3. Nourbakhsha F, Rajurkarb KP, Malshec AP, Caod J (2013) Wire electro-discharge machining of titanium alloy. Proc CIRP 5:13–18
4. Rajmohan T, Prabhu R, Subba Rao G, Palanikumar K (2012) Optimisation of machining parameters in EDM of 304 stainless steel. In: ICMOC, pp 1030–1036
5. Karthikeyan R, Lakshmi Narayanan PR, Naagarazan RS (1999) Mathematical modeling for electric discharge machining of aluminium-silicon carbide particulate composites. J Mater Process Technol 87(1–3):59–63
6. El-Taweel TA (2009) Multi-response optimization of EDM with Al-Cu-Si-tic P/M composite electrode. Int J Adv Manuf Technol 44(1–2):100–113
7. Mohan B, Rajadurai A, Satyanarayana KG (2002) Effect of sic and rotation of electrode on electric discharge machining of Al-sic composite. J Mater Process Technol 124(3):297–304
8. Simao J, Lee HG, Aspinwall DK, Dewes RC, Aspinwall EM (2003) Workpiece surface modification using electrical discharge machining 43(2003):121–128
9. Singh PN, Raghukandan K, Rathinasabapathi M, Pai BC (2004) Electric discharge machining of Al-10 %sicp as-cast metal matrix composites. J Mater Process Technol 155–156(1–3):1653–1657
10. Lee SH, Li XP (2001) Study of the effect of machining parameters on the machining characteristics in electrical discharge machining of tungsten carbide. J Mater Process Technol 115(3):344–358
11. Wang C, Lin YC (2009) Feasibility study of electrical discharge machining for W/Cu composite. Int J Refract Metal Hard Mater 27(5):872–882
12. Tsai HC, Yan BH, Huang FY (2003) EDM performance of Cr/Cu-based composite electrodes. Int J Mach Tools Manuf 43(3):245–252
13. Puertas I, Luis CJ (2004) A study of optimization of machining parameters for electrical discharge machining of boron carbide. Mater Manuf Processes 19(6):1041–1070
14. Mohanty CP, Sahu J, Mahapatra SS (2013) Thermal-structural analysis of electrical discharge machining process. Proc Eng 51:508–513
15. Tilekar S, Das SS, Patowari PK (2014) Process parameter optimisation of wire EDM on aluminum and mild steel by using Taguchi method. In: AMME 2014, Procedia Materials Science, vol 5, pp 2577–2584
16. Lodhia BK, Agarwal S (2014) Optimization of machining parameters in WEDM of AISI D3 steel using Taguchi technique. In: 6th CIRP international conference on high performance cutting, HPC2014. In: Procedia CIRP 14, pp 194–199

17. Dhar S, Purohit R, Saini N, Sharma A, Kumar GH (2007) Mathematical modeling of electric discharge machining of cast Al-4Cu-6Si alloy-10 wt.% sicp composites. J Mater Process Technol 193(1–3):24–29
18. Gauri SK, Pal S (2010) Comparison of performances of five prospective approaches for the multi-response optimization. Int J Adv Manuf Technol 1205–1220
19. Chenthil Jagan TM, Dev Anand M, Ravindran D (2012) Determination of EDM parameters in AISI202 stainless steel using grey relational analysis. ICMOC, Proc Eng 38:4005–4012

Multi-objective Optimization of Mechanical Properties of Aluminium 7075-Based Hybrid Metal Matrix Composite Using Genetic Algorithm

V. Durga Prasada Rao, V. Navya Geethika and P.S. Krishnaveni

Abstract The present paper involves experimental study and multi-objective optimization of mechanical properties of Aluminium 7075-based hybrid metal matrix composite fabricated by stir-casting process. The composite is reinforced with Silicon carbide (SiC) and Titanium dioxide (TiO$_2$) particulates. The mechanical properties that were considered in this work are impact strength, hardness and tensile strength. These properties of 7075 Al hybrid metal matrix composite are studied by performing Charpy impact test, Rockwell hardness test and tensile test, respectively. The experiments are conducted on specimens prepared by mixing the particulates in different percentage combinations such as (0, 10), (2.5, 7.5), (5, 5), (7.5, 2.5) and (10, 0) of SiC and TiO$_2$, respectively by maintaining the percentage of 7075 Al constant at 90 %. Based on the experimental values, second-order regression equations are fitted between each of the response parameters and the casting parameters (fraction of SiC and fraction of TiO$_2$) using Minitab 17 software. The equations are then optimized by defining them as the objectives of a multi-objective optimization problem (MOOP). A non-dominated sorting genetic algorithm (NSGA-II) is used to solve the MOOP. A single best compromise solution is also found from the Pareto optimal solutions obtained by NSGA II.

Keywords Multi-objective · Optimization · Hybrid · MMC · NSGA

1 Introduction

There are many metals available on metal Additive Manufacturing systems. Titanium and Aluminium alloys are most popularly used in medical and aerospace applications. Aerospace-grade aluminium and other metals are in development.

V. Durga Prasada Rao (✉) · V. Navya Geethika · P.S. Krishnaveni
Mechanical Engineering Department, SRKR Engineering College,
Bhimavaram 534204, Andhra Pradesh, India
e-mail: vdp009@gmail.com

Aluminium alloys are currently produced by direct metal laser sintering (DMLS), in particular with compositions suitable for casting. Also DMLS provides an opportunity to form novel metal matrix composites (MMCs) with metal powders. Recently, some research groups investigated to obtain Al-based MMCs by employing DMLS. They analyzed the behaviour of the composite by varying the size and volume fraction of SiC particles, and identified cracks on these composites while preparing them by DMLS.

Aluminium Metal Matrix Composites (AMMCs) are widely used in the fields of automotive, aerospace and marine applications. Mohd Azil [16] studied Al–Cu–SiC MMC through stir casting method with sand mould and found that, the density characteristic and compressive properties are influenced by particle sizes of SiC, while the hardness and wear resistance characteristics are influenced by weight percentage of SiC. Jin-Feng et al. [11] studied the tensile properties, inter granular and exfoliation corrosion behaviours, and microstructure of 7075 Al alloy under the influence of two different aging treatments, T6I6 and high-temperature pre-precipitation (HTPP) aging. The results were compared with the T6, T73 and RRA treatments. Manoj et al. [14] prepared aluminium-based silicon carbide MMCs and observed that, there is an increase in hardness and impact strength with increase in weight percentage of SiC. Veeresh Kumar et al. [19] studied tensile strength, hardness and wear resistance of Al6061-SiC and Al7075-Al$_2$O$_3$ composites, and concluded that the hardness and density of the composites are improved due to SiC and Al$_2$O$_3$ added to them. Chao et al. [5] fabricated SiC particle-reinforced pure aluminium composites by powder metallurgy method, and tested the effects of particle size and extrusion on their microstructures and mechanical properties. Asif et al. [2] prepared a hybrid composite of aluminium alloy reinforced with silicon carbide particles and solid lubricants such as graphite/antimony tri sulphide (Sb$_2$S$_3$ and reported that the hybrid composite has good tribological characteristics. Aigbodion et al. [1] produced Al–Cu–Mg/Bagasse ash particulate composites with 2–10 % of bagasse by double stir-casting method, and concluded that the enhanced age-hardening of the composites is due to the accelerated precipitation of S′ phases. Bharath et al. [4] made Al6061-Al$_2$O$_3$ particulate metal matrix composites by liquid metallurgy method and found that, there is an increase in the tensile strength and micro-Vickers hardness of the composite due to increase in filler content in the composite. Silva et al. [18] conducted single-step aging of 7075 thick plates by varying the aging times, and concluded that the single-step aging performed in the laboratory can produce acceptable tensile and stress corrosion cracking (SCC) properties when compared with the T7X conditions.

Kataiah et al. [12] considered cast aluminium alloy composites with TiO$_2$ particles of size 30–50 pm and weight ranging from 0 to 20 %, and found that there was significant increase in the ultimate tensile strength and hardness values and a reduction in its ductility as TiO$_2$ composition increases. Lakhan and Purohit [13] investigated the behaviour of Aluminium Cast Alloy (LM6)-Al$_2$O$_3$ composite produced by stir casting technique, and combined the desirable attributes of metals and Ceramics. Elango et al. [9] studied the wear resistance and frictional properties of aluminium alloy (LM25) hybrid metal matrix composite reinforced with SiC and

TiO_2 particulates by conducting dry sliding wear test. Murali et al. [17] fabricated AA7075/TiO_2 in situ composites with different mass fractions of reinforcement by stir casting method, and the phase analysis and morphological characterization of composites were studied using x-ray diffraction techniques and scanning electron microscope.

It is observed that, there is less emphasis in the literature on the study and optimization of MMC's with more than one particulate. Also, Aluminium-based hybrid MMCs would be the future materials for AM research. So in the present work, an attempt is made to formulate and optimize a multi-objective optimization problem in order to optimize the mechanical properties of Aluminium 7075 hybrid MMC using the modified non-dominated sorting genetic algorithm.

2 Methodology

As the present study involves production of Al 7075 MMC by stir casting method and optimization of parameters (fractions of SiC and TiO_2) of MMC, the prediction strategies of impact strength (I_s), hardness (H), and tensile strength (T) have been developed for correlating them to the parameters using regression technique. The purpose of developing mathematical equations relating each of the response variables (I_s, H and T_s) and their parameters is to facilitate the optimization of the response variables. These equations are then considered as three non-conflicting objectives and the optimization of the parameters is done NSGA-II. Finally confirmation tests were conducted to analyze the closeness to GA results. Figure 1 illustrates the flow chart of this procedure.

2.1 Mathematical Modelling

Regression analysis is useful for modelling and analyzing problems involving several independent factors/variables which influence a response parameter. The mathematical model is represented by:

$$V = h\,(S, T) + e \tag{1}$$

where V is the response parameter, h is the response function, S and T are stir casting variables and e is the error which is distributed normally with respect to the response parameter V with zero mean. The relation between V (impact strength/tensile strength/hardness) and the variables S and T can be represented as given below:

Fig. 1 Flowchart of
modelling and optimization
procedure
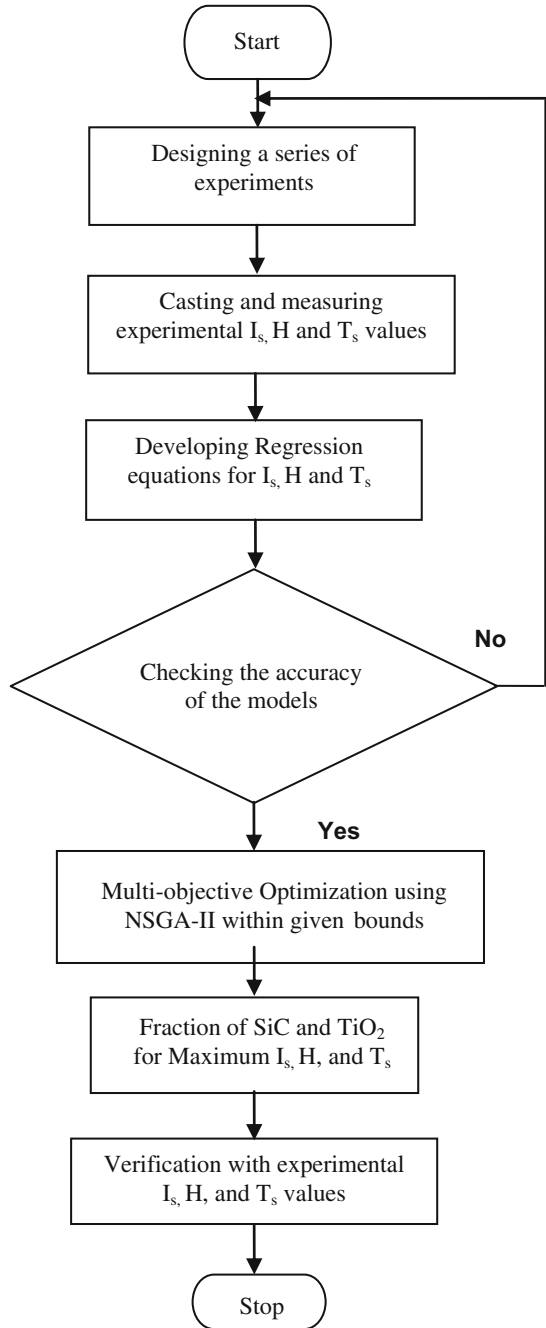
$$V = K\,S^{\alpha}T^{\beta} \tag{2}$$

where K is a constant and α, β are exponents.

The mathematical model is to be changed to linear form by using a logarithmic transformation as given below. It facilitates the determination of constants and exponents.

$$\ln V = \ln K + \alpha \ln S + \beta \ln T \tag{3}$$

The method of least squares can be used to determine the constant and exponents K, α and β. Then the first-order linear model can be obtained as follows:

$$V_1 = V - e = a_0 x_0 + a_1 x_1 + a_2 x_2 \tag{4}$$

where V_1 and V are the estimated and measured values of response variable (impact strength/hardness/tensile strength) on a logarithmic scale, $x_0 = 1$, x_1 and x_2 are logarithmic transformations of fractions of SiC and Tio_2, e and a values represent, respectively the experimental error and the estimates of corresponding parameters. The second-order polynomial model of response is as follows:

$$V_2 = V - e = a_0 x_0 + a_1 x_1 + a_2 x_2 + a_{12} x_1 x_2 + a_{11} x_1^2 + a_{22} x_2^2 \tag{5}$$

where V_2 and V are the estimated and measured values of response variable, and e is the experimental error. The method of least squares can be used to estimate the polynomial parameters $a_1, a_2, a_{12}, a_{11}, a_{22}$.

3 Experimental Details

In this section, the details of experimental conditions, measurements and the procedure used for the study are described.

3.1 Design of Experiments

In the present study, the percentage weight of Al 7075 is fixed at 90 % and the percentage weight of Silicon Carbide (SiC) and Titanium Dioxide (TiO$_2$) are considered as the variable parameters. The Al 7075 in the form of small rods and SiC and TiO$_2$ in the form of powders of 50 μm particle size are used during the stir casting process.

A design of five experiments as shown in Table 1 is considered so that the interactions between each of the response variables (Impact strength and Tensile strength) and the variable parameters can be investigated.

Table 1 Weight percentages of variables used in experimentation

Experiment No.	Weight percentage		
	Al 7075	SiC	TiO$_2$
1	90	0	10.0
2	90	2.5	7.5
3	90	5.0	5.0
4	90	7.5	2.5
5	90	10.0	0

3.2 Furnace and Moulds Used in Experimentation

An electric muffle furnace is used in the present study for melting purpose. The mould used for casting purpose is prepared with the help of mild steel rectangular blocks and square rods. The muffle furnace, the mould used for preparing the test specimens and the casting process are shown in Fig. 2. In the muffle furnace, hand stirring method is employed to mix the constituents of the MMC. The crucible is made up of silicon carbide and is inserted into the muffle furnace. At first the furnace is allowed to attain a temperature of 700 °C before aluminium 7075 is placed in the crucible. Further it is heated to a temperature of 1100 °C so that Al 7075 is melted. The stirring operation is performed with the help of a stirrer made up of graphite. Simultaneously the silicon carbide and titanium dioxide particulates are pre-heated to a temperature of 500 °C and are poured during stirring operation in required proportions at equal intervals of time into the crucible. The mould is pre-heated to a temperature of 500 °C to avoid casting defects. The molten metal is then poured into the mould and it is allowed to solidify.

Fig. 2 Electric muffle furnace, Mould, and Casting process

3.3 Specimens Used in Impact Test, Hardness Test and Tensile Test

In the present work round-shaped specimens are used for tensile test (Fig. 3). The specimens used for hardness test (Fig. 4) and charpy test (Fig. 5) are of square cross section with and without a V-notch, respectively. Figure 6 depicts the test specimens used in Universal testing machine (UTM), Rockwell hardness and impact testing machines respectively.

3.4 Experimental Data

Experimental data of tensile strength, hardness and impact strength corresponding to five sets of tests conducted on UTM, Rockwell hardness testing machine and impact testing machine have been tabulated and given in Tables 2, 3 and 4.

Fig. 3 Tensile test specimen
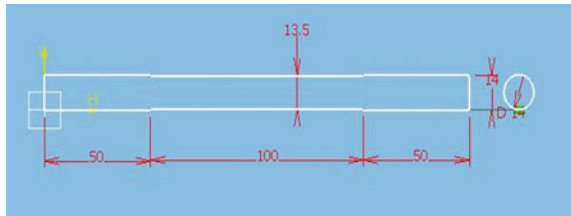
Fig. 4 Hardness test specimen
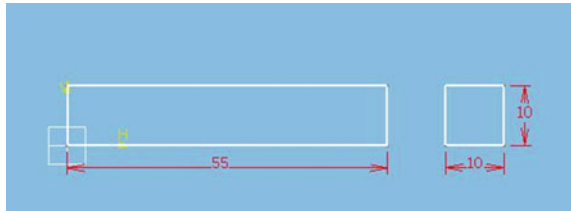
Fig. 5 Charpy test specimen
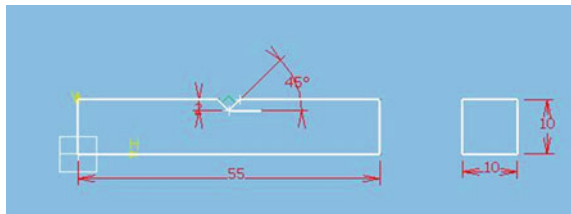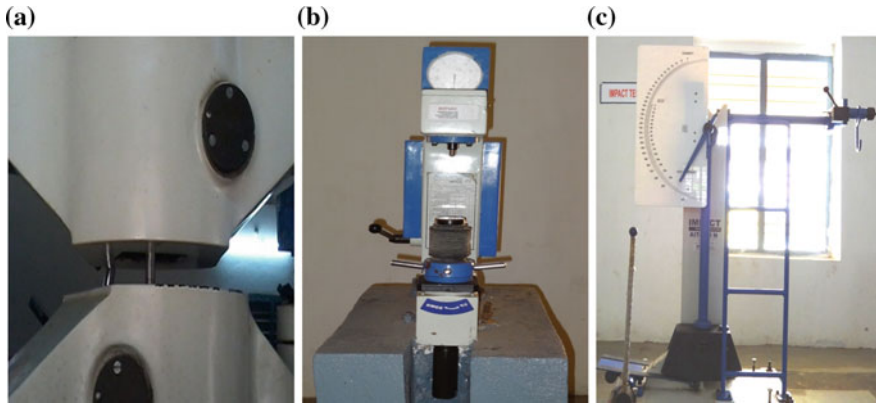
Fig. 6 a Tensile test specimen in UTM. **b** Specimen in Rockwell hardness testing machine. **c** Charpy test specimen in impact testing machine

Table 2 Tensile test results

Comp. No.	1	2	3	4	5
Al/SiC/TiO$_2$	90/0/10	90/2.5/7.5	90/5/5	90/7.5/2.5	90/10/0
Initial diameter(mm)	13.5	13.5	13.5	13.5	13.5
Final diameter(mm)	13.4	13.38	13.32	13.24	13.2
Initial gauge length(mm)	68	68	68	68	68
Final gauge length(mm)	70	71	73	75	76
Yield strength (MPa)	66.001	102.80	143.21	114.15	73.33
Tensile strength (MPa)	97.052	141.96	179.40	164.73	133.39
% reduction in area	1.47	1.77	2.64	3.81	4.4
% elongation	2.94	4.41	7.35	10.29	11.76

Table 3 Rockwell hardness test results

Comp. No.	Al/SiC/TiO$_2$	Hardness (Applied load = 1 KN)—scale B			
		Trial-1	Trial-2	Trial-3	Average hardness number
1	90/0/10	144	164	178	162
2	90/2.5/7.5	161	156	149	155.33
3	90/5/5	155	175	158	162.66
4	90/7.5/2.5	155	176	164	165
5	90/10/0	156	180	190	175.33

Table 4 Charpy impact test results

Comp. No.	Al/SiC/TiO$_2$	Energy (E) required to break the specimen (KJ)				Impact strength E/A (kJ/m^2)
		Trial-1	Trial-2	Trial-3	Average E	
1	90/0/10	0.092	0.064	0.068	0.07466	746.6
2	90/2.5/7.5	0.084	0.084	0.1	0.08933	893.3
3	90/5/5	0.068	0.064	0.1	0.0773	773.3
4	90/7.5/2.5	0.068	0.096	0.064	0.0760	760.0
5	90/10/0	0.064	0.066	0.068	0.0660	660.0

A = Area of cross section = 0.0001 m^2

3.5 Variation of Response Parameters with Respect to Variable Parameters

Figure 7 shows a bar graph on which the variation of impact strength, hardness and tensile strength with respect to the fractions of SiC and TiO$_2$ are represented simultaneously. It is observed from the experimental results that, the impact strength increases as the weight percentage of SiC increase from 0 to 2.5 % and the weight percentage of TiO$_2$ decreases from 10 to 7.5 %, and then decreases as the weight percentage of SiC increases from 2.5 to 10 % and the weight percentage of TiO$_2$ decreases from 7.5 to 0 %. That is, there is an increasing trend for impact strength up to the second combination (Al/SiC/TiO2: 90/2.5/7.5) followed by a slight decreasing trend up to the last combination (Al/SiC/TiO2: 90/10/0) under this study.

The hardness is showing almost an increasing trend as the weight percentage of SiC increases from 0 to 10 % and the weight percentage of TiO$_2$ decreases from 10 to 0 %. The tensile strength increases as the weight percentage of SiC increases from 0 to 5 % and the weight percentage of TiO$_2$ decreases from 10 to 5 %, and then decreases as the weight percentage of SiC increases from 5 to 10 % and the weight percentage of TiO$_2$ decreases from 5 to 0 %. That is, there is an increasing

Fig. 7 Variation of impact strength, hardness, and tensile strength
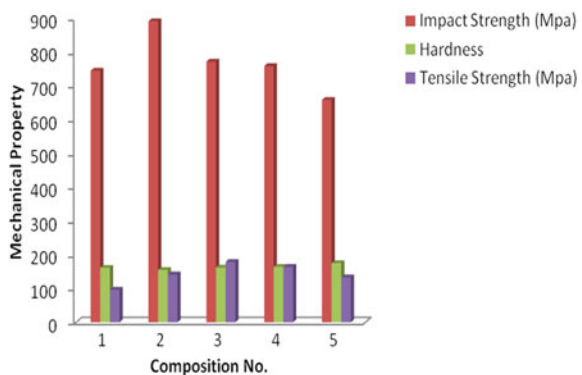
trend for tensile strength up to the third combination (Al/SiC/TiO2: 90/5/5) followed by a slight decreasing trend up to the last combination (Al/SiC/TiO2: 90/10/0) under this study.

4 Formulation of Objective Functions of MOOP

Using the experimental results the empirical equations have been derived to estimate impact strength, hardness and tensile strength in terms of fraction of SiC and fraction of TiO_2. The second-order response equations have been fitted using Minitab 17 software [15] for the response variables, viz., impact strength, hardness and tensile strength and the accuracy of the fit has been tested.

The second-order equations have been considered for optimization process as the first-order model has low predictability. The three regression equations fitted in terms of casting variables are given by:

$$I_s = 772.7 - 1226 X_1 + 44194 X_1 X_2 \tag{6}$$

$$H = 160.94 + 145.3 X_1 - 3315 X_1 X_2 \tag{7}$$

$$T_s = 94.99 + 381.8 X_1 + 23386 X_1 X_2 \tag{8}$$

where I_s Impact strength of MMC in Mpa
H Hardness of MMCMMC
T_s Tensile strength of MMC in Mpa
X_1, X_2 Fractions of SiC and TiO_2 respectively

Thus, the predicted values of impact strength, hardness and tensile strength for the five experiments were calculated by using the second-order equations and compared with those obtained by experimentation. The average percentage error for the five experiments is found to be 3.88 % for impact strength, 0.948 % for hardness and 2.45 % for tensile strength, respectively. As the average percentage errors are well within minimum limit (5 %), the three models, i.e. Eqs. (6)–(8) under the following restriction and the bounds would be considered as the objectives of a multi-objective optimization problem (MOOP). It is then optimized (maximized) by using the NSGA-II.

$$\text{Restriction}: \quad X_1 + X_2 \leq 0.1 \tag{9}$$

$$\text{Bounds}: \quad 0 \leq X_1 \leq 0.1 \quad \text{and} \quad 0 \leq X_2 \leq 0.1 \tag{10}$$

5   Optimization of MOOP by NSGA-II

In NSGA II, after the population is initialized, the non-dominated solutions are extracted and kept as a set, called the first front, F_1. Then, the second front F_2, which is being dominated by the individuals of the first front only, is formed and the front continues. Thus, the initialized population is sorted based on non-domination. An individual is said to dominate another if all or any one of its objective functions is no worse than the other. Latter an individual, depending on the front in which it lies, is assigned a rank along with its fitness value. Also, for each individual a new parameter called crowding distance is calculated. The crowding distance of a particular solution in a population is the quantity, which serves as an estimate of the perimeter of a cuboid formed by using the nearest neighbours as the vertices.

In the next step, a crowded tournament selection operator [10] is used to select parents from the population. The offspring are generated from the selected population by using the simulated binary crossover (SBX) operator and polynomial mutation operator [7, 8], respectively. The individuals of the next generation are set by combining the offspring population with the current generation population, so that elitism is ensured. The new population is sorted again based on non-domination until the best N individuals are selected, so that N is the population size. If the population exceeds N, then, the individuals in a front F_i are selected based on their crowding distance so that the population size becomes N. The process repeats to generate the subsequent generations. The procedure of NSGA-II [6] is outlined in the flow chart shown in Fig. 8.

6   Results and Discussion

The Pareto optimal solutions for the MOOP of 7075 Aluminium MMC are obtained by NSGA-II, the surface plot and the corresponding contour plot of which are shown, respectively in Figs. 9 and 10. It is to be observed that, each of the solutions of Pareto optimal front of MOOP is important with respect to some trade-off relationship among the objectives. However, a user may not be able to identify an exact trade-off relationship among objectives. Thus, it is always necessary, from a practical point of view, to select one best solution among the set by applying suitable qualitative or quantitative information or criteria.

6.1   Single Best Compromise Pareto Solution

One can select a single best compromise Pareto solution by using a quantitative criterion. The min–max method [3] is the most popular one among different

Fig. 8 Flow chart of
NSGA-II
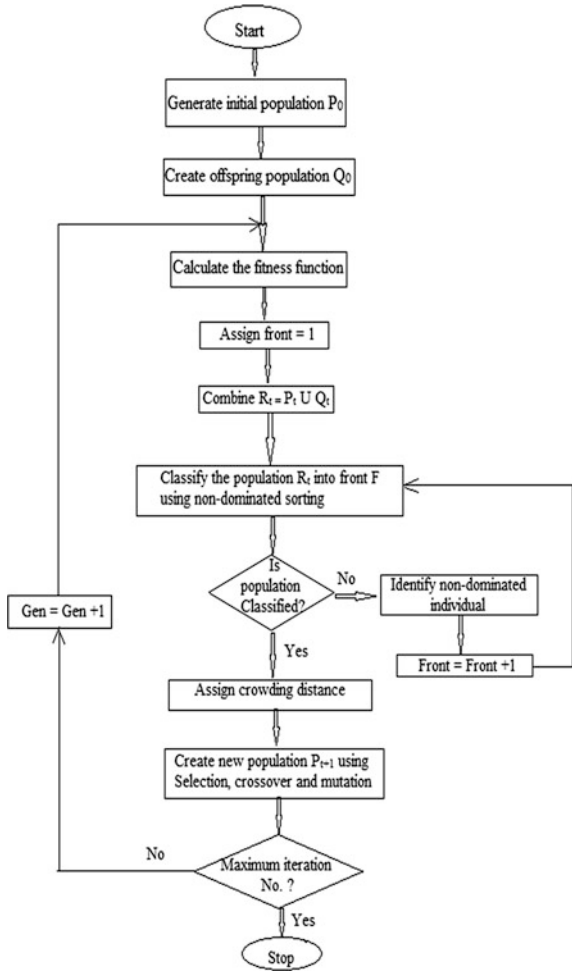
Fig. 9 Surface plot of Pareto
Optimal solutions

Contour Plot of Tensile Strength vs Hardness,Impact Strength
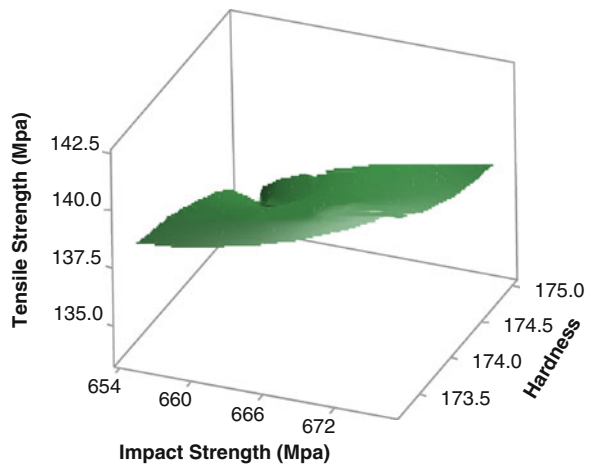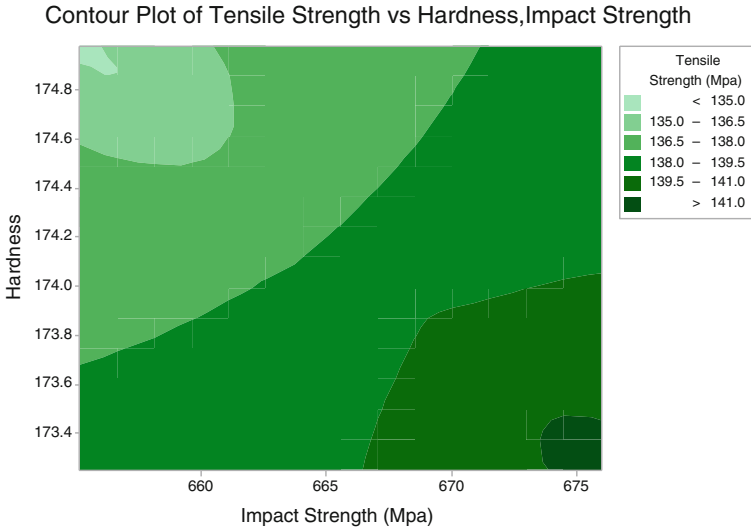
Fig. 10 Contour plot of Pareto optimal solutions

available criteria. As per this approach, the single compromise solution is found by minimizing the maximum deviation from best value. That is, when there are m objectives, the problem is to find the optimal point by

$$\text{Minimize} : [\max\{Z_1, Z_2, \ldots, Z_m\}],$$
$$\text{where } Z_i = f_i(X) - f_i^{\min}(X)$$

$$\text{It is usual to normalize the deviations} : Z_i = \frac{\left|f_i - f_i^{\min}\right|}{f_i^{\min}}$$

In this paper, the best solution among the available multiple solutions is found by slightly modifying the above criterion. The modified criterion is to minimize the sum of maximum deviations of m objectives from their best values subject to the constraints under consideration:

$$\text{Minimize} : \left\{\sum_{i=1}^{m} \frac{\left|f_i - f_i^{\min}\right|}{f_i^{\min}}\right\} \text{ subject to the given constraints.}$$

This problem is solved by the real coded GA with the parameters: Population size $(s_p) = 100$, Number of generations $(n_g) = 250$, Probability of cross-over $(p_c) = 0.9$ and probability of mutation $(p_m) = 0.09$. The convergence graph of GA is shown in Fig. 11. The best compromise solution as per the above criterion is found to be:

Fig. 11 Convergence graph
of compromise solution
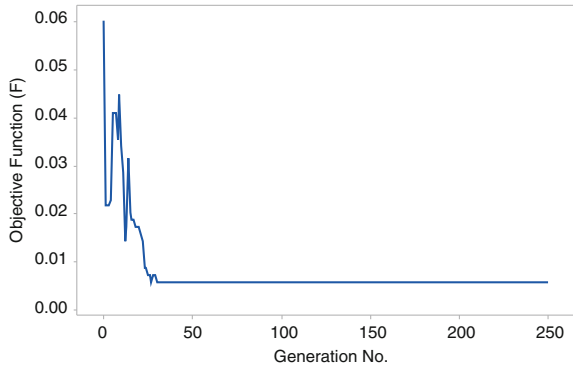
SiC* = 0.095103 or 9.51 %
TiO_2^* = 0.004878 or 0.48 % and
Optimum impact strength, I_s^* = 676.60586 MPa
Optimum hardness, H^* = 173.22059
Optimum tensile strength, T_s^* = 142.149381 MPa.

7   Conclusions

This paper presented multi-objective optimization of mechanical properties of 7075 Aluminium hybrid MMC prepared with SiC and TiO_2 as particulates. The mechanical properties considered under this work are impact strength, hardness and tensile strength.

In this work, the three regression equations obtained for impact strength, hardness and tensile strength in terms of fraction of SiC and fraction of TiO_2 are optimized (maximized) by NSGA II, which has produced better Pareto optimal solutions. Latter the criterion of minimizing the sum of maximum deviations of the objective values from their corresponding best values is used to determine the best compromise solution.

The optimum value of parameters (SiC and TiO_2) obtained under the best compromise solution approach is found to be 9.51 and 0.487 %, respectively. It is close to the 85th Pareto optimal solution (9.47 % of SiC and 0.465 % of TiO_2). It can be concluded from the results that, the SiC is the most influencing parameter in order to have maximum possible values of all the three properties under consideration. This study can be extended to other manufacturing systems such as DMLS and by considering different other cutting parameters, tool geometries for different combinations of cutting tool-work piece materials.

References

1. AigbodionVS, Hassan SB, Dauda ET, Mohammed RA (2011) Experimental study of ageing behaviour of Al–Cu–Mg/Bagasse ash particulate composites. Tribol Ind 33(1):28–35
2. Asif M, Chandra K, Misra PS (2011) Development of aluminium based metal matrix composites for heavy duty applications. J Miner Mater Charact Eng 10(14):1337–1344
3. Belegundu AD, Chandrupatla TR (2002) Concepts and application in Engineering, Pearson Education Asia, pp 379–380, First Indian Reprint 2002
4. Bharath V, Mahadev N, Auradi V (2012) Preparation, Characterization and Mechanical Properties of Al_2O_3 Reinforced 6061Al Particulate's. Int J Eng Res Tech (IJERT) 1(6)
5. Chao S, Min S, Zhangwei W, Yuehui H, Effect of particle size on the microstructures and mechanical properties of SiC-Reinforced pure aluminum composites. ASM Int JMEPEG 20:1606–1612. doi:10.1007/s11665-010-9801-3
6. Deb K (2002) A fast and elitist multi-objective genetic algorithm–II. Evol Comput, IEEE Trans 6(2):182–196
7. Deb K, Agrawal RB (1995) Simulated binary crossover for continuous search space. Complex Syst 9(2):115–148
8. Deb K, Goyal M (1996) A combined genetic adaptive search (Gene AS) for engineering design. Comput Sci Inf 26(4):30–45
9. Elango G, Raghunath BK (2013) Tribological behavior of (LM25Al + SiC + TiO2) Metal matrix composites. Procedia Eng 64:671–680
10. Goldberg DE, DebK (1991) A comparison of selection schemes used in genetic algorithms. In: Foundations of genetic algorithms (FOGA-1), pp 69–93
11. Jin-feng LI, Zhuo-wei PENG, Chao-xing LI, Zhi-qiang JIA, Wen-jing CHEN, Zi-qiao ZHENG (2007) Mechanical properties, corrosion behaviors and microstructures of 7075 aluminium alloy with various aging treatments. School of Materials Science and Engineering, Central South University, Changsha 410083, China
12. Kataiah GS, Girish DP (2010) Int J Pharm Stud Res I(1):17–25
13. Lakhan R, Purohit GK (2013) A study of microstructure and mechanical property of Aluminium–Alumina metal matrix. Int J Eng Res Technol (IJERT) 2(9)
14. Manoj S, Deepak Dwivedi D, Lakhvir S, Vikas C (2009) Development of aluminium based silicon carbide particulate metal matrix composite. J Miner Mater Charact Eng 8(6), 455–467
15. Minitab Inc (2014) Meet MINITAB Release, Ver. 17
16. Mohd Azil Sani Bin Md J (2005) Development of Al–Cu–SiCp metal matrix composite for automotive applications development of Al–Cu–SiCp metal matrix composite for automotive applications. University of Malaya, Kualalumpur
17. Murali M, Sambathkumar M, Senthil Saravanan MS (2014) Micro structural and mechanical properties of AA 7075/Tio2 in situ composites. Univers J Mater Sci 2(3):49–53
18. Silva G, Rivolta B, Gerosa R, Derudi U (2012) Study of the SCC behavior of 7075 Aluminum Alloy after one-step aging at 163 °C. JMEPEG _ASM Int 1059–9495. doi:10.1007/s11665-012-0221-4
19. Veeresh Kumar GB, Rao CSP, Selvaraj N, Bhagyashekar MS (2011) Studies on Al6061-SiC and Al7075-Al2O3 Metal Matrix Composites. J Miner Mater Charact Eng 9(1):43–55

A Review on Status of Research in Metal Additive Manufacturing

Ganesa Balamurugan Kannan and Dinesh Kumar Rajendran

Abstract Additive manufacturing is the essential technology in present near net shape manufacturing scenario in the field of aerospace, automobiles, electronics, medical implants, robotics, biomedical, etc., where near net shape manufacturing plays a prominent role in dimensional accuracy. Additive manufacturing has undergone drastic changes from plastics, polymers to metals. Additive manufacturing plays a key role in manufacturing of required components in short span of time without any defect. In this paper, the different research aspects of additive manufacturing are discussed on basis of two broad areas like design for manufacturing and process parameter control. The field of additive manufacturing has brought the manufacturing to next level were it made production and product development easier. An analysis is made on the published research articles and the research gaps were found and finally the future scope in the field of metal additive manufacturing is provided.

1 Introduction

Fabrication of near net shape metallic components is the attractive manufacturing route for recent aeronautical, aerospace and automotive industries. The additive manufacturing technology through additive manufacturing, 3D models can be printed or fabricated directly using a laser source or electron beam source. The metal additive manufacturing follows the principle of layer by layer printing of 3D

G.B. Kannan (✉) · D.K. Rajendran
Adhoc Faculties, Department of Production Engineering, NIT,
Tiruchirappalli 600015, India
e-mail: gbmpondy@gmail.com

D.K. Rajendran
e-mail: dineshrd453@gmail.com

Fig. 1 Schematic representation of additive manufacturing process
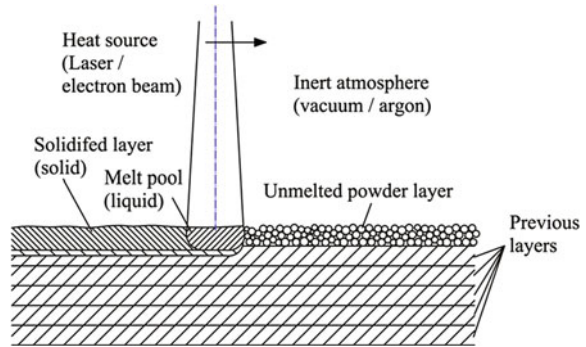
objects. Additive manufacturing avoids tooling and minimizes the wastages. The working principle of selective laser melting and electron beam melting is shown in Fig. 1. The heating source of either laser or electron beam melts the successive layers of metal powder bed and fused with each other to form a 3D finished component. In this paper, the status of research in metal additive manufacturing field has been discussed. The recent trend in metal additive manufacturing has been focusing on two broad categories. Design for additive manufacturing and material properties monitoring through manipulating the process parameters of selective laser melting and electron beam melting processes are those broad categories.

2   Research on Design for Additive Manufacturing

The interesting feature of additive manufacturing is facilitating the design freedom. However, to ensure the quality and reliability of additive manufactured products, few design rules should be incorporated at the design stage itself. Ponche et al. [1] have proposed a new numerical chain based on a new design for additive manufacturing methodology. This new numerical chain has been proposed for Additive Laser Manufacturing of thin walled metal parts. The main objective of this work is to minimize the gap between a CAD model and the corresponding manufactured part. This new method involves part orientation, functional optimization, and manufacturing path optimization as important steps. The part orientation step involves the determination of design area. The functional optimization step involves determining the optimal part geometry which is going to be the initial part geometry. The final step in this methodology is to determine the optimized manufacturing paths. Through these manufacturing paths, the manufacturing program is generated along with the final part CAD model.

Guido et al. [2] explained about the extended design freedoms of technical parts which provides them a new potential with the new project "Direct Manufacturing Design Rules". This research made the design benefits accessible to different user groups. Hence a specific method was defined then design rules were developed for

Fusion Deposition modeling, Laser sintering, and Laser Melting. The results for suitable design for additive manufacturing were summarized in a design rule catalog.

Klhan et al. [3] discussed about the geometrical freedom in design which is utilized to largely improve the functionality of series products by substituting conventional parts with additive manufacturing. Four criteria identified for redesign are integrated design, individualization, lightweight design, and efficiency and it is observed that a product, to be successful, needs to be improved in both a technological and economic direction. On the economic side, the investment in the change of design and process has to pay off either by lower manufacturing costs or by benefits during the lifetime of the product by fully utilizing the geometric freedom in the redesign, impressive increases in performance can be realized. This opens new perspectives in product development.

Cooper et al. [4] exploit the benefits of Additive Layer Manufacturing (ALM) in the weight reduction of internal combustion engines inlet or exhaust valves. CT scan technology was used as a reverse engineering tool. The hybrid manufacturing route was preferred to reduce the manufacturing cost of the vales though ALM. Further investigations are needed to join conventionally manufactured hollow stem to the valve head manufactured by ALM by friction welding route.

3 Research on Effect of Process Parameters of Additive Manufacturing Routes in Metallic Components Manufacturing

Guijun et al. [5] implemented micro-LAAM (Laser Assisted Additive Manufacturing) in layer by layer manufacturing of nickel-based super alloys IN100 which has poor weldability that results in cracking and porosity, the defects were eliminated by optimization and crack free deposition is achieved with minimal heat input, post heated sample was observed with EBSD (Electron Back Scatter Diffraction) and found three size of γ precipitates 0.5–1 µm, 0.1–0.3 µm, 10 µm and the volume fraction of c to γ phase were 60–40 %. After grain refinement the tensile and yield strength were found to be improved than the aerospace requirement specification 5397 for IN100 material.

Yanyan et al. [6] used the hybrid fabrication technique for fabricating TC11 titanium sample alloy for examining the microstructure, micro-hardness, and tensile strength and found that the sample fabricated consist of three typical zone without any defect in metallurgy the zones are called to be the laser additive manufactured zone (LAMZ), the wrought substrate zone (WSZ), and the bonding zone and also found LAMZ has superfine basket-wave microstructure which results in superior tensile properties and HAZ caused by rapid cooling but no recrystallization or grain growth found in HAZ due to the heat effect in $\alpha + \beta$ region micro transition zone has coarse for k-like primary α and fine β microstructure and the TC11 sample

fabricated has tensile strength of 1,033,713 MPa and elongation 6.8 ± 0.2 % and the fracture occurs in substrate which shows mechanical properties of bonding zone is better than the substrate. Micro-hardness in the transition zone was found to be increased noticeably from the WS Z to the LAMZ

Ting et al. [7] fabricated TA2/TA15 graded structural material (GSM) using additive manufacturing (LAM) process and examined the chemical composition, microstructure and micro-hardness of the as-deposited GSM and found that near-equiaxed grains was Widmanstätten α-laths microstructure where β phase volume fraction increase and α phase volume fraction decreases. The part containing large columnar grains was divided into four deposited layers with 3000 μm in width was fine basket-weave microstructure, the graded zone micro-hardness increases from the TA2 part to the TA15 part from 173 to 400 due to the solid solution strengthening and grain boundary strengthening.

Yali et al. [8] simulated the temperature fields in additive manufacturing of AlSi10 Mg by Selective laser melting (SLM) using FEM and investigated the effect of laser power and scan speed on SLM and found cooling rate elevated slightly from 2.13×10^6 to 2.97×10^6 °C/S when laser power increased from 150 to 300 W but when the scan speed increased from 100 to 400 mm/sit enhanced significantly from 1.25×10^6 to 6.17×10^6 °C/s after repeating various combination it is found that a sound metallurgical bonding between the neighboring fully dense layers was achieved at laser power of 250 W and scan speed of 200 mm/s, due to the larger molten pool depth (67.5 lm) as relative to the layer thickness (50 lm).

Konrad et al. [9] attempted to create light weight material for industrial application, and the work focuses on low power fiber laser, feasibility of high strength aluminum alloys, and custom developed powder system with different particle sizes in Al and Cu/Zn particles and found that their size did not change during mixing process. With this customized Al–Cu/Al–Zn composition able to create aluminum alloy composition during laser melting No brittle hard oxidation upper layer was noticed on melted lines, which is very promising for further development of multi additive layer manufacturing process of reactive materials The manufactured additive layers, characterized by a fine microstructure with homogeneously dissolved intermetallic phases in the metal matrix, has a big potential for usability properties of the final manufactured product.

Processing of aluminum and it alloys through Selective Laser Melting is still challenging. Aluminum alloy powders have poor flow ability, high reflectivity, and high thermal conductivity compared to steels and titanium materials [10]. Moreover, difficulties in elimination of oxide layers, porosities, and cracks are major challenges in SLM of aluminum alloy powders [9]. Most of the researches are now focusing on SLM of AlSi10 Mg and AlSi12 Mg alloys (6000 series alloys). The main process parameters are depicted in the following Fig. 2 [10]. Therefore, challenging in processing of aluminum alloy powders through additive manufacturing still persists.

Fig. 2 Process parameters for SLM process
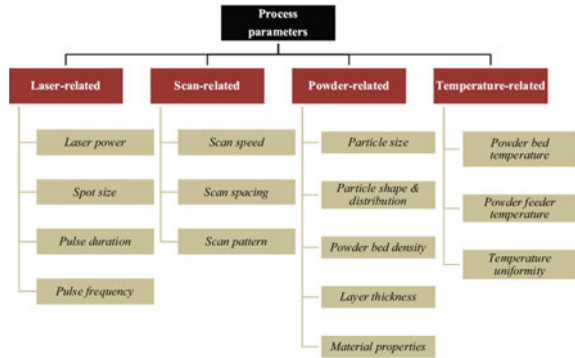
4 Conclusion

With the statistical analysis on research articles, the challenges faced in metal additive manufacturing in design and process parameter control were brought out in this paper. The results of research were analyzed and the research gaps were identified and conclusions are presented.

- New design rules for metal additive manufacturing are derived for repeatability and reliability of parts manufactured by additive manufacturing routes.
- Research on design for metal additive manufacturing is in nascent stage and some of the research works are discussed. Specifically design rule for electron beam additive manufacturing needs to be focused.
- Various research works on metallic components manufacturing through additive manufacturing with various metals are briefly discussed
- Most of the research works are based on Laser additive manufacturing rather than Electron Beam Melting. The wide gap in this area should be bridged with appropriate research works.
- Metal additive manufacturing of aluminum alloys is still challenging and further research works are needed in this area.

References

1. Ponche R, Kerbrat O, Mognol P, vesHascoet J-Y (2014) A novel methodology of design for additive manufacturing applied to additive laser manufacturing process. Robot Comput-Integr Manuf 30:389–398
2. Adama GAO, Zimmer D (2014) Design for additive manufacturing—element transitions and aggregated structures. CIRP J Manuf Sci Technol 7:20–28
3. Klahn C, Leutenecker B, Meboldt M (2014) Design for additive manufacturing—supporting the substitution of components in series products. Procedia CIRP 21:138–143

4. Cooper D, Thornby J, Blundell N, Henrys R, Williams MA, Gibbons G (2015) Design and manufacture of high performance hollow engine valves by additive layer manufacturing. Mater Des 69:44–55

5. Bi G, Sun C-N, Chen H, Lan Ng F, Cho Khin Ma C (2014) Microstructure and tensile properties of superalloy IN100 fabricated by micro-laser aided additive manufacturing. Mater Des 60:401–408

6. Zhu Y, Li J, Tian X, Wang H, Liu D (2014) Microstructure and mechanical properties of hybrid fabricated Ti–6.5Al–3.5Mo–1.5Zr–0.3Si titanium alloy by laser additive manufacturing. Mater Sci Eng A 607:427–434

7. Qian T, Liu D, Tian X, Liu C, Wang H (2014) Microstructure of TA2/TA15 graded structural material by laser additive manufacturing process Trans Nonferrous Met Soc China 24:2729–2736

8. Li Y, Gu D (2014) Parametric analysis of thermal behavior during selective laser melting additive manufacturing of aluminum alloy powder. Mater Des 63:856–867

9. Bartkowiaka K, Ullricha S, Frick T, Schmidta M (2011) New developments of laser processing aluminium alloys via additive manufacturing technique. Phys Proc 12:393–401

10. Aboulkhair NT, Everitt NM, Ashcroft I, Tuck C (2014) Reducing porosity in AlSi10 Mg parts processed by selective laser melting. Add Manuf 1–4:77–86

Multi-response Optimization of Nd:YAG Laser for Micro-drilling of 304 Stainless Steel Using Grey Relational Analysis

Alok Bara, Sarat Kumar Sahoo and Sunita Singh Naik

Abstract The paper addressed an effective approach for the manufacturing of a product using multi-response optimization technique of Nd:YAG laser drilling process parameter of 304 stainless steel. Micro-drilling (diameter less than 1 mm) is a challenging task. Based on orthogonal technique the experiment carried out and grey relational analysis used to optimize the process parameter. The response characteristics, i.e. taper angle, spatter diameter and recast layer is significantly influenced by power, nozzle standoff and assisted gas pressure. The response table and response graph for each level of machining parameter were obtained from grey relational grade. Analysis of variance (ANOVA) was performed to percentage of contribution and significant process parameter during the micro-drilling process. The confirmation experiment has been performed on suggested optimal level of control factor to verify the result. To know the exact combination of Nd:YAG laser parameter, the multi-response technique of is very useful in additive manufacturing.

Keywords Laser micro-drilling · 304 Stainless steel · Characteristics · Grey relational analysis · Multi performance characteristics

1 Introduction

Nd:YAG Laser drilling is an industrial solution for micro hole drilling having hole diameter range less than 1 mm with high aspect (diameter to depth) ratio in wide range of material [1, 2]. The laser drilling is mostly used in industrial and research work on different types of material in manufacturing industries. Laser drilling

A. Bara (✉) · S.K. Sahoo · S.S. Naik
Department of Mechanical Engineering, VSSUT, Burla, Odisha, India
e-mail: bara.alok1@gmail.com

S.K. Sahoo
e-mail: saratkumar222@gmail.com

S.S. Naik
e-mail: naik.sunitasingh@gmail.com

thermal process involves material removal through a combination of both melting and vaporization resulting high intensities process parameter. However, the laser drilling process is complex as it involves approximate manipulation of process parameter to achieve desired holes quality. Effective utilization of the laser to drill high quality of holes for micro holes applications depends greatly upon the proper selection and optimization of factor [3]. The optimization technique is to know the most influencing parameter and parametric combination of machine, towards efficiently manufacturing the product and 3D printing technology. The present paper deals with systematic analysis, methodology for optimizing the pulse Nd:YAG laser micro-drilling to get desired quality of holes and product [4]. A solid Nd:YAG laser beam is typically two modes continuous and pulse-defined according to the means of transferring energy. The pulse laser beam is used herein to precise drill on 304 stainless steel. The selection range of various process parameters is an important issue before conducting set of experiment [5, 6]. The aim of this research was to investigate the effect of laser parameter on the response characteristics such as taper angle, spatter diameter, recast layer of the drilled holes [7, 6]. The laser parameter optimize using multiresponse technique, i.e. grey relational analysis and ANOVA test, to get the percentage of contribution of process parameter on machining [6]. It is clearly shown that the above performance characteristics in laser drilling process can be improved effectively through this approach.

2 Experimental

Laser drilling experiment were carried out using 4 kW Nd:YAG laser and 1.5 mm thick 304 stainless steel plates. The process parameters are average power, nozzle standoff, nitrogen gas pressure and diameter of the hole as the main factors and taper angle, spatter diameter and recast layer as response were studied. The quality of drilled holes was examined by optical microscope. The technical specification is shown in Table 1. A computer numerical control (CNC) machine is used to operate and hold the work piece, position it precisely and move along the drilled path to manufacture the exact shape of micro hole.

Machine details	Description
Laser type	Nd:YAG laser
Wavelength	1064 μm
Mode of operation	Continuous and pulse mode
Beam type	TEM_{00}
Pulse width	700 μm

Table 1 Details of the Nd:YAG laser machine and the constant parameter

Table 2 Composition and properties of 304 stainless steel used for drilling (%)

C	Mn	Su	Ph	Si	Cr	Ni	Fe
0.08	2.0	0.030	0.045	0.75	18.5	8.0	Balance

2.1 Material Selection

The attractive features of 304 stainless steel in terms of corrosion resistance, oxidation resistance, weldability, excellent toughness, even down to cryogenic temperatures which are defined as very low temperatures, such properties useful for fabricating precision component in heavy and light industries. The chemical composition of 1.5 mm thickness 304 stainless steel shown in Table 2.

2.2 Laser Drilling Using Orthogonal Technique

In order to achieve best cutting quality, Taguchi's experimental design, an efficient plan, was used for conducting experiments. For this purpose, L_9 orthogonal array was used for experiment. The nine number of experiment is designed as per L_9 (3^3) orthogonal array [5]. The three level of each of the three process parameters comprised balance comparisons of nine experiment run is shown in Table 3. The orthogonal array of nine experiment run with coded values of process parameter level is shown in Table 4.

Table 3 Factor and their levels for Nd:YAG laser for drilling operation

Process parameter	Level 1	Level 2	Level 3
Average power (kW)	3	3.5	4
Nozzle standoff (mm)	2	3	4
Nitrogen gas pressure (bar)	6	8	10

Table 4 L_9 orthogonal array and experiment response

Expt. sl. no.	Avg. power (kW)	SOD (mm)	Gas pressure (bar)	Taper angle ($\theta°$)	Spatter (mm)	Recast (mm)
1	3	2	6	2.30	2.405	0.0396
2	3	3	8	3.11	4.013	0.0414
3	3	4	10	2.80	3.805	0.0640
4	3.5	2	8	2.34	4.635	0.0382
5	3.5	3	10	2.61	5.120	0.0487
6	3.5	4	6	2.53	4.081	0.0850
7	4	2	10	2.36	4.260	0.0312
8	4	3	6	2.76	4.379	0.0676
9	4	4	8	3.49	4.074	0.0408
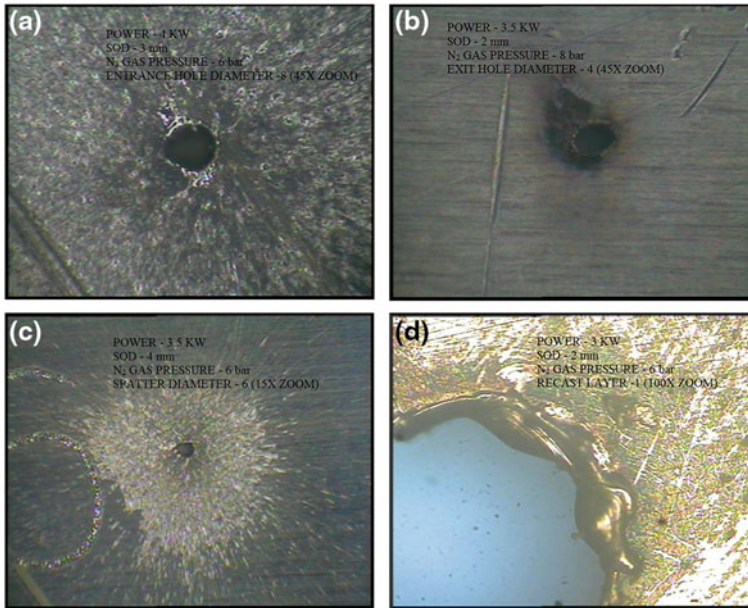
Fig. 1 a Entrance diameter **b** Exit diameter of hole. **c** Spatter diameter. **d** Recast layer

2.3 Scheme for Measuring the Responses

The entry and exit diameter was considered by averaging the hole diameter at six segment divided at 60° angle apart. For calculating taper angle of drilled hole specimen using taper angle formula. The Entry and exit diameter of hole shown in Fig. 1a, b were measured using optical microscope at 45 × zoom. Taper angle (θ).

$$\text{Taper angle } (\theta) \ = \ \tan^{-1}\left(\frac{D_{\text{ent}} - D_{\text{exit}}}{2t}\right)$$

The spatter diameter was considered, where spatter density is more [8, 5]. For calculating spatter diameter of each drilled hole by taking average of six segment at 60° angle apart as shown in Fig. 1c 15 × zoom.

The thickness of recast layer is some amount of melted material again resolidified on the micro-drilled surface which was measured using image analysis software. The recast layer as shown Fig. 1d 100 × zoom.

$$\text{Recast layer thickness} = \frac{\text{Recast layer diameter} - \text{Entry diameter}}{2}$$

The entry and exit diameter, spatter diameter, recast layer of drilled hole measured by optical microscope and imagej analysing software. The response characteristics are as shown in Table 4.

3 Grey Relational Analysis

Grey analysis was first proposed by Dr. Deng in 1982 to fulfil the crucial mathematical criteria for dealing with poor, incomplete, and uncertain system. Grey analysis has been broadly applied in evaluating or judging the performance of a complex project with meagre information. However, data to be used in Grey analysis must be preprocessed into quantitative indices for normalizing raw data for another [2]. Optimization of the laser drilling process with multiple performance characteristics based on orthogonal array with grey relational analysis has been studied. A grey relational grade obtained from grey relational analysis is used to solve the laser process with multiple performance characteristics means the best result for which it should be optimized [6]. In this study the machining parameter, namely average Power, Standoff distance (Nozzle distance from work piece), Nitrogen Gas pressure are optimized with consideration of multiple performance characteristics including taper angle, spatter diameter and recast layer. Experimental result has shown that machining performance in the laser drilling process can be improved effectively through this approach. Linear normalization of the experimental results was performed in the range between zero and unity. The normalized results for 'smaller the better' and characteristics can be expressed by equation

$$x_i^*(k) = \frac{\max x_i^0(k) - x_i^0(k)}{\max x_i^0(k) - \min x_i^0(k)} \tag{1}$$

In deviation sequence, using equation

$$\Delta_{0i}(k) = \left| x_0^*(k) - x_{iwi}^*(k) \right| \tag{2}$$

Grey relational coefficient can be calculated as following Eq. (3):

$$\gamma\left(x_i^*, x_{iwi}^*\right) = \Gamma_i = \frac{\Delta_{\min} - \Delta_{\min}}{x_{0i}^* - \Delta_{\max}} \tag{3}$$

The grey relational grade as following equation:

$$\Delta_{0i}^* = \frac{1}{n}\sum_{k=1}^{n}\Delta_{0i}(k) \tag{4}$$

where $x_0^*(k)$ is the original sequence, $x_i^*(k)$ the sequence after the data preprocessing, max $x_i^0(k)$ the largest value of $x_i^0(k)$, and min $x_i^0(k)$ implies the smallest value of $x_i^0(k)$. x^0 is the desired value. $\Delta_{0i}(k)$ is the deviation sequence of the reference sequence x_i^*.

4   Result and Discussion

In the present study, the work piece taper angle, spatter diameter and recast layer in pulsed laser drilling parameters and the experimental runs are listed in Table 4. Typically, all the response characteristics are smaller the better characteristic (Tables 5, 6 and Fig. 2).

Table 5 The sequences of each performance characteristic after data preprocessing

Expt. sl. no.	Taper angle ($\theta°$)	Spatter (mm)	Recast (mm)
1	1.0	1.0	0.843
2	0.319	0.407	0.810
3	0.579	0.484	0.390
4	0.996	0.178	0.869
5	0.739	0	0.674
6	0.806	0.382	0
7	0.949	0.316	1.0
8	0.613	0.272	0.323
9	0	0.385	0.821

Table 6 The deviation sequence

Expt. sl. no.	Taper Angle ($\theta°$)	Spatter (mm)	Recast (mm)
1	0	0	0.157
2	0.681	0.593	0.19
3	0.421	0.516	0.610
4	0.034	0.822	0.131
5	0.261	1.0	0.326
6	0.194	0.618	1.0
7	0.051	0.684	0
8	0.387	0.728	0.677
9	1.0	0.615	0.179
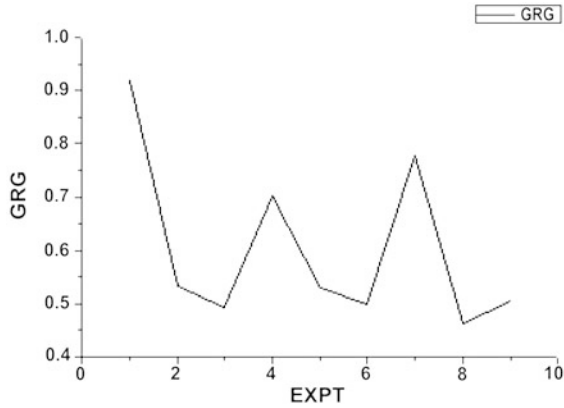
Fig. 2 Graph between grey relational grades with expt. observation

Table 7 The calculated grey relational coefficient and grey relational grade and its orders for nine comparability sequences

Expt. sl. no.	GRC-Taper Angle ($\theta°$)	GRC-Spatter (mm)	GRC-recast (mm)	GR grade	Order
1	1.0	1.0	0.761	0.920	1
2	0.423	0.457	0.724	0.534	4
3	0.542	0.492	0.450	0.494	8
4	0.936	0.378	0.792	0.702	3
5	0.657	0.333	0.605	0.531	5
6	0.720	0.447	0.333	0.5	7
7	0.907	0.442	0.1	0.776	2
8	0.563	0.407	0.424	0.464	9
9	0.333	0.448	0.505	0.505	6

It is obvious from Table 7 that experiment number 1 has the highest gray relational grade value than other experiments. Therefore, it can be concluded that experiment number 1 possesses best multi response characteristics among all the 9 experiments.

The response table of Taguchi method was employed here to calculate the average grey relational grade for each factor level. The procedure was to group the relational grades first for each factor level for each column in the orthogonal array, then average them to get the optimal level.

The optimal combination found from grey relational analysis is A1B1C3. The rank 1, i.e. average power maximum impact on machining condition as shown in Table 8 and Fig. 3.

Table 8 Response table for GRA

Factor/level	Level-1	Level-2	Level-3	Max.–Min.	Rank
A	0.649[a]	0.779[a]	0.628	0.151	1
B	0.583	0.509	0.580	0.074	3
C	0.581	0.499	0.600[a]	0.101	2

[a]Indicates the optimal level
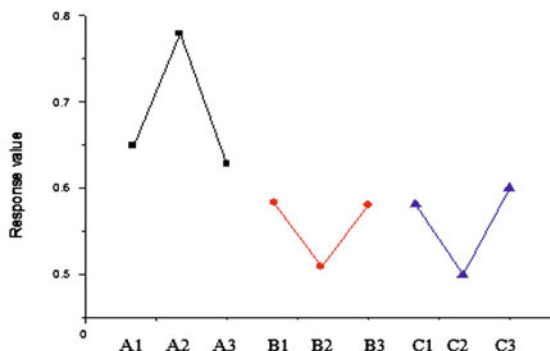
Fig. 3 Variation of response on various level of process parameter

5 Analysis of Variance (ANOVA)

To determine the relative significance of the machining process parameter considered during experimentation, ANOVA test has been performed for the response and result of the performance criteria with calculated F-values of the respective control factor. Comparing F-values with standard F-values in Table 9, it is revealed that avg. power, nozzle standoff, nitrogen gas pressure have significant effect on response parameter at 90 and 95 % confidence interval, respectively. These processes parameters have significant effect on respective machining criteria. Table 9 shows that the percentage contribution of different process parameter on taper angle, spatter diameter and recast layer. Also the Table 9 shows that average power has approximate high percentage of contribution for the machining criteria, i.e. 51 %.

Table 9 Analysis of variance test

Parameter	M/cing parameter	SS	DOF	MS	F	% of contribution
A	Taper angle	0.102	2	0.051	2.833	51
B	Spatter	0.028	2	0.014	0.777	14
C	Recast	0.033	2	0.016	0.888	16.5
Error		0.037	2	0.018		18.5
Total		0.2	2	0.025		100

6 Conformation Test

The predicted value's Overall Desirability at optimum parameter level can be calculated by using Eq. (5)

$$\gamma_m = r_m + \sum_{i=1}^{q} (r_i - r_m)$$

$$= 1.562$$

(5)

7 Conclusion

- Use of the grey relational analysis to optimize the laser drilling process with the multiple-performance characteristics analysis of the workpiece taper angle, spatter diameter and recast layer. The optimal parametric combination found A1B1C3.
- From ANOVA establishes the relative significance of parameters. The average power gives highest contribution towards machining, i.e. 51 %. Comparing F-values with standard F-values in Table 9, it is revealed that avg. power, nozzle standoff, nitrogen gas pressure have significant effect on response parameter at 90 and 95 % confidence interval, respectively.
- Table 10 shows the compared initial and optimal level of control factor. The confirmation experiment has been performed on suggested optimal level of control factor to verify the result. The confirmation result shows that taper angle, spatter diameter and recast layer have been considerably improved by 8.26, 7.90 and 21.46 %, respectively.
- This technique can be used for better analysis in additive manufacturing and 3D printing process parameter.

Table 10 Comparison between initial and optimal level

Optimal parametric combination			
	Initial	Optimal	Improvement (%)
Setting level	$A_1B_1C_1$	$A_1B_1C_3$	
Taper angle	2.30	2.11	8.26
Spatter diameter	2.405	2.215	7.90
Recast layer	0.0396	0.0311	21.46

References

1. Arrizubieta A, Lamikiz S, Martinez EU, Tabernero I, Girot F Internal characterization and hole formation mechanism in the laser percussion drilling process
2. Mishra S, Yadava V Modeling and optimization of laser beam percussion drilling of nickel-based super alloy sheet using Nd:YAG laser
3. Yung WKC, Wu J, Yue TM, Zhu BL, Lee CP Nd:YAG laser drilling in epoxy resin/AlN composites material
4. Bandyopadhyay S, Gokhale H, Sarin Sundar JK, Sudaranjan G, Joshi SV A statistical approach to determine process parameter impact in Nd:YAG laser drilling of IN718 and Ti-6Al-4V sheet
5. Pandey AK, Dubey AK Taguchi based fuzzy logic optimization of multiple quality characteristics in laser cutting of duralumin sheet
6. Kibiria G, Doloi B, Bhattacharyya B Experimental investigation and multi objective optimization of Nd:YAG laser micro turning process of alumina ceramic using orthogonal array and grey relational analysis
7. Bharatish A, Narasimha Murthy HN, Anand B, Madhusoodana CD Characterization of hole circularity and heat affected zone in pulsed CO_2 laser drilling of alumina ceramics
8. Romoli L, Rashed CAA, Fiaschi M Experimental characterization of the inner surface in micro-drilling of spray holes: A comparison between ultraspot pulsed laser and EDM
9. Kacar E, Mutlu M, Akman E, Demir A, Candan L, Canel T, Gunay V, Sınmazceli T Characterization of the drilling alumina ceramic using Nd:YAG pulsed laser

Additive Manufacturing at French Space Agency with Industry Partnership

Sébastien Begoc, Sandrine Palerm, Raphaël Salapete, Marie Theron and Jérôme Dehouve

Abstract   As an introduction, the role of CNES (Centre National d'Études Spatiales, the French Space Agency) in France is defined as well as its involvement in the European context. The first part details the organization of research and technology activities dedicated to additive manufacturing (AM) for liquid-propellant rocket engines and its associated objectives, which are conducted together with SNECMA of SAFRAN group. This work is orchestrated around two axes, one dealing with design aspects, realization, justifications which are as much as possible transverse to the second one, which covers the applications of this technology. Our strategy aims at developing additive manufacturing mainly to reduce costs and manufacturing cycles. It results in some actions that will be developed in a second part. Among them, we find the characterization of materials, the related processes to improve surface finishing and to address issues related of anisotropy and porosity. Controllability aspects, deformation (by simulation), design rules (taking account residual stresses) are also presented. Next, examples of parts made by additive manufacturing for launchers are presented. To ensure these innovative technologies lead to significant benefits (both from cost and mass savings point of view, and from manufacturing flexibility and production cycle), key challenges must be overcome. These are presented in a dedicated part. Such challenges are related mainly to the design (design rules and tools), manufacturing (size machine, standardization of powders, new materials, simulation tools) and qualification (qualification methods, process optimization, range acceptable defects, surface treatment and normative framework).

Keywords   Additive manufacturing · Liquid-propellant rocket engines

S. Begoc (✉) · S. Palerm · M. Theron · J. Dehouve
CNES, French Space Agency, 52 rue Jacques Hillairet, 75612 Paris, France
e-mail: sebastien.begoc@cnes.fr

R. Salapete
SNECMA, SAFRAN Group, Forêt de Vernon, 27200 Vernon, France
e-mail: raphael.salapete@snecma.fr

1 Introduction

AM (Additive Manufacturing) is a process with rich promises and a rapid growth, for the space activities and beyond. One of CNES missions is to communalise information, methods, and resources to establish a coordinated roadmap especially with the French industrials active in this area. Furthermore, at national and European level, and in the ESA (European Space Agency) framework, various groups are created, with various funding opportunities. The coordination managed by CNES allows defining a common strategy for better competitiveness and leads to give a greater consideration to the French space ambitions.

This article presents the main research and technology activities as well as the actions and challenges to meet the cost and manufacturing cycle reduction targets. In conclusion, applications for space engines are presented.

2 Context

Today, lowering the costs of manufactured parts is critical in a highly competitive environment. The main potential benefits of AM are the lowered costs of realization of a part, the reduction in cycle time, the simplification of the supply chain and the improvement of performance allowed by the freedom given to designers.

CNES conducts many studies related to AM, with several industrials and for different targets such as satellites and launchers. However, in the next chapters, only the liquid propulsion applications conducted together with SNECMA Company, for engine components such as injectors, injection heads and turbo-pumps housings are presented. Among the various AM processes existing for direct metal fabrication, two have been used for those applications, considering technological and geo-metrical constraints: Electron Beam Melting (EBM) and Laser Beam Melting (LBM). The best potential of these process for optimizing the design of selected components are used to manufacture parts. The next step is, first, to control the geometry, and second, to characterize materials (Inconel 718 and TA6V ELI). Activities to improve the surface condition and to optimize the controllability of the parts produced have also been initiated. The resulting hardware is then tested in representative functional conditions. The first results of this work allow to validate the ability of the process (material properties, dimensional aspect and functional results), for the needs of the targeted applications.

3 Research and Development Activities

These activities are organized today around two axes: the first corresponds to the realization and justification aspects, which is as much as possible transverse to the second one, which concerns the applications of this technology.

3.1 Realization, Dimensioning, Justification

Four main steps are needed to achieve these objectives, mechanical characterization, surface finishing, controllability and finally, dimensioning and justification to successfully qualify the produced parts.

(1) *Mechanical characterization* The aim is to get the mechanical characterization of the materials used for the targeted applications. Test specimens made by LBM are characterized (tensile strength and endurance tests), at different temperatures (20–300–950 K) for different materials (Inconel 718, 625, Hastelloy-X, Aluminium, 316L and AS7G06). Similarly, TA6V test specimens made by EBM process are also characterized (tensile strength and endurance tests), at different temperatures (20–300 K).

(2) *Post-treatment (surface condition, removal of the supports, heat treatment…)* The main objective of this activity is to find a solution to improve the surface quality of the manufactured parts. Different techniques are investigated such as mechanical polishing, chemical dissolution and electrolytic polishing.

   Some works has been done on the heat treatments, to ensure geometric stability of the parts, and especially to homogenize the mechanical characteristics (isotropic). The completion of heat treatment during manufacturing is also studied to reduce the number of post-processing steps. The Hot Isostatic Pressure (HIP) also ensures dimensional stability to the parts, by limiting the deformation stresses and potentially reduces the degree of porosity like the optimization of the process parameters.

   The removal of supports must be made with great attention because of the risk of pollution in the subsequent use of the part. This operation can be performed before or after heat treatment, which can be performed before or after removal the part of its plate.

(3) *Controllability* Samples are implemented for each manufacturing to complement the Non-Destructive Inspection (NDI) on the part and to detect possible defects. It is interesting to benefit from the construction method by layer of a few tens of microns for a mapping of the final part and to limit checking operations afterwards. This control mode also allows real-time adjustment of some parameters, such as the power of the laser during the merger of the sensitive layers.

(4) *Dimensioning* This activity involves the simulation aspect, especially the impact of the AM process on the life of the components. Two work axes are needed to achieve this aim. First, an identification of defects, of surface finishing and residual stresses is performed. Second, logic is proposed to include defects, surface finishing and residual stresses in the AM parts design. The objective is therefore to define a methodology for parts qualification.

3.2 Feasibility and Design

Concerning the application, the objectives are first, to identify what is possible and interesting to realize in additive manufacturing and second, to design and manufacture these parts using the best potential of these processes.

The work consists in assessing this technology on titanium and Inconel parts representatives of the targeted applications. The key areas addressed are:

- Assessment of dimensional tolerances
- Assessment of achievable thickness
- Assessment of surface quality (off finishing)
- Assessment of cost for each pairs: part/material
- Definition of rules and design constraints
- Characterization of processes for each material at different temperatures
- Assessment of finishing methods

The potential of AM for making mesh structures and bi-materials parts is also investigated.

4 Examples of AM Parts

In this chapter, the specific definition that led to perform injection elements and turbo-pump housings, for liquid propulsion engines is presented. For these two concrete examples, a comparison of the materials characterization results between the additive manufacturing and the conventional process is shown. The research to improve the surface condition of these parts by chemical mechanical polishing is also presented, as well as a state of the art on the controllability.

Injection components are traditionally manufactured by welding and brazing numerous machined parts. AM allows manufacturing a direct part without those joint processes, which are costly (realization, inspection) and time consuming. Housings for turbo-pump (TP) are heavy and the introduction of titanium-based alloys enables to lower the weight of the hydrogen TP dramatically. For those reasons, the realization of those components with EBM and LBM is studied. In order to evaluate the whole process, the mechanical properties and geometrical reliability, are investigated together with the post-processing phase.

4.1 Injection Elements

(1) *Definition* An evaluation of the specific modifications to be applied on existing injection elements has been performed, in order to produce them by LBM process. Design adaptation must take into account process constraints (down

Fig. 1 Injection elements in Inconel 718 made by LBM **a** as built **b** welded on the bench interface for fire test

(a) **(b)**
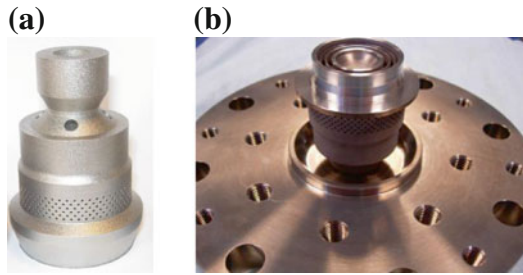
Fig. 2 Injector in Inconel 718 made by LBM

skin zone, contour zone), while minimizing dimensional modifications of fluid veins of injection elements.

Hypothesis taken to optimize the design were driven by process constraints. The direction of construction of the part was also studied in order to avoid internal supports. Careful attention was finally given to the definition of the entry zone of the injection element, in order to minimize post machining operations. The final geometry obtained is presented on Fig. 1.

After succeeding in this first fabrication test, an injector (e.g. Fig. 2) was designed and manufactured following the same guidelines.

(2) *Dimensional control* Calibration of injection elements is a crucial point for functional aspects of the engine. A high accuracy of the injector lips dimensions is then required. A picture of the different diameter to be analysed is presented on Fig. 3.

Fig. 3 Injector diameter of interest to study dimensional repeatability
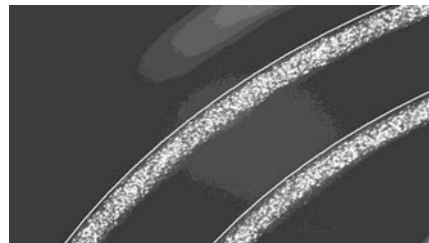
Table 1 Min values comparison between forged and LBM Inconel 718 tension test at 300 K

Value	Unit	Forged Inconel 718	LBM Inconel 718
Yield strength	MPa	1075	980
Rupture limit	MPa	1320	1180
Elongation	%	11	10

The diameters of hydrogen and oxygen vanes were analysed. A good reproducibility was demonstrated which is compatible with functional need for injectors.

(3) *Mechanical properties* In order to fire test these parts, mechanical properties have to be close to those of forged parts.

Mechanical tests in tension and fatigue have been performed on specimens manufactured with the LBM process on a M270 EOS machine. Specimens were heat treated with solution treating and age hardening and machined before tests. Comparative results at ambient temperature, between forging and LBM results, are presented in Table 1. Cryogenics test for tension and fatigue follow the same trend.

A 10 % decrease between forged and LBM results is observed. From a mechanical point of view such a decrease is acceptable to envisied fire tests.

4.2 Turbo-Pump Housing

(1) *Definition* Turbo-pump housings made by EBM process were built with small modifications from the existing one made by casting process. A 0.75 scale part was made on an Arcam A1 machine because the full scale did not fit in the production chamber. A CAD file of the raw part was prepared including:

- A bigger thickness in functional zones which has to be machined after EBM process
- A bigger thickness in the supported zones

The produced part can be seen on Fig. 4.

(2) *Mechanical properties* Turbo-pump housing was fabricated by EBM process in TA6V. Mechanical test were performed in order to compare mechanical properties between casting and EBM process. Results at ambient temperature are presented in the Table 2.

Results at cryogenics temperature are good enough compared to the requirements.

Fig. 4 Turbo-pump housing made in TA6V by EBM process

Table 2 Average value comparison between casting and EBM TA6V tension test at 300 K

Value	Unit	Casting TA6V	EBM TA6V
Yield strength	MPa	896	932
Rupture limit	MPa	1000	1005
Elongation	%	8	15

4.3 Post-Processes and Controllability

(1) *Post process* The produced parts cannot be used with the surface roughness inherent to both processes. Several elements are used to define the surface state obtained by EBM and LBM processes. Three levels are retained in order to characterize the surface aspects:

- Level 0: supports
- Level 1: un-melted attached particles on the surface (e.g. Fig. 5)
- Level 2: general roughness (Ra and Rt parameters)

Depending on the fluid flow requirements and the mechanical sensibility of a zone, several techniques can be implemented depending on the accessibility of the zone.
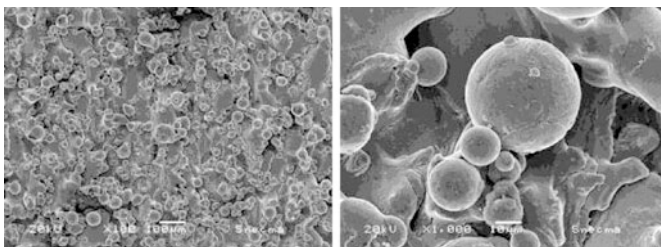
Fig. 5 As built surface of Inconel 718 LBM injectors
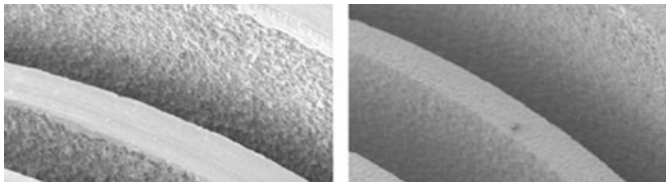
Fig. 6 MEB analysis of the lips of injectors before and after chemical etching

For level 0, as no supports are present inside the injector, machining was only performed on the lips of it.

For level 1, the risk of detachable particles during fire tests results in applying a chemical etching onto the component in order to eliminate those particles. The results of such chemical etching can be seen on Fig. 6. The benefits of the post-process have been proved by illustrating the elimination of the un-melted attached particles.

The level 2 roughness obtained with chemical etching was sufficient for this application.

On the TA6V EBM turbo-pump housing, all the functional zones are accessible to machining. Therefore, no specific post-treatment was applied on those zones.

(2) *Controllability* Manufactured parts can present several defects linked to different types of process problems. Typical internal defects in LBM parts are distributed micro-porosity, projected un-melted particles and cracks. Surface defects can also be presents. In EBM parts, the same defects can be encountered. Risk of cracks is lower and surface defects are generally bigger due to poor roughness.

Different NDI and destructive techniques can be used in order to detect the defects. One issue encountered with the NDI control of the injector, was the lack of resolution of the classical X-Ray technique to pass through successive wall thickness of the internal geometry (Inconel 718 material density was prohibitive). Though, in a development framework, micro-tomography was used in order to capture internal defects. No internal defects greater than a few tens of millimeters were observed with micro-tomography. Those results were confirmed by destructive tests.

For EBM turbo-pump housing, NDI tests are currently performed.

Controllability of complex powder bed parts made by LBM and EBM by classical NDI is thus complicated in a production perspective. Therefore, process qualification and process monitoring are two key milestones to develop in order to guarantee flying defect free parts.

Fig. 7 LBM Inconel 718
injector fire tests
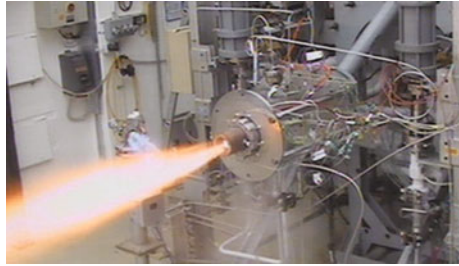
4.4 Injector Fire Tests

An injector made by LBM process was tested at fire on a combustion bench (e.g. Fig. 7). The expertise showed a nominal comportment that provided confidence in the reliability of LBM parts.

5 Prospects

5.1 Design Challenges

The engineers training, to integrate the capabilities offered by additive manufacturing has to be developed. This also requires standardization of design rules.

Current design tools do not necessarily allow to take into account the potential of additive manufacturing, it is necessary to work on the integration of topological optimization in the modeling tools.

5.2 Manufacturing Challenges

As for design, future machine designers need to be trained to meet the growing dimensional needs and thus to increase the manufacturability potential of parts by this new technology.

Moreover, it is necessary to use quality standards for powders, to ensure the reliability and reproducibility of the manufactured parts. New materials to be used specifically in AM should also be developed.

5.3 Challenges of Qualification and Validation

Conventional qualification methods cannot necessarily be applied to parts produced in additive manufacturing. Monitoring samples are not always representative of the

health of the part material. Methods of non-destructive inspections have to be established and qualified (monitoring in real time).

Optimization and qualification of additive manufacturing processes is essential, to minimize the potential defects (porosity, crack, inclusion…). The range of acceptable defects has to be determined and taken into account in the design rules.

6   Conclusions

These new processes are now considered as real means of production. However, to obtain the intended benefits, great challenges remain and are tackled by the research and development activities conducted together with SNECMA.

The confidence in the process capability is growing for space engine applications. Since the injector testing, other components are investigated.

Additive manufacturing is a young technology, which may require greater maturity. This technology can make an indelible imprint on the future for design and manufacturing, and could radically change the production habits in the coming years.

Reference

1. Bégoc S, Palerm S, Salapete R, Cornu D, Venard M, Guichard D (2014) Additive manufacturing: processes, materials and applications for liquid engines. Space propulsion 2014. Cologne, Germany

Wear Characterization of Direct Steel–H20 Specimens Produced by Additive Manufacturing Techniques

**Usaid Mohammed Baig, A.R. Anwar Khan
and D. Ramesh Rajakumar**

Abstract Quality assurance and health monitoring of rotating and sliding components are very significant in order to prevent the catastrophic failures. One of the inputs for this process is wear rate of the materials at different working conditions. An attempt has been made to use additive manufacturing technology for aerospace components since this process is bring down manufacturing time, cost effective and flexible for intricate shapes and contours. Before the actual manufacturing of the components, test specimens were manufactured using additive manufacturing route (Rapid prototype technique-RP) for wear characterizations study. Taguchi's orthogonal array was used for wear test study to find out the parametric effects with less number of experiments. The loads, speeds and track diameters were varied for wear test study in RP produced test specimens. The most dominant parameter contributing to wear was found to be load and less significant was speed. The load under the combination of 15 N-200 rpm-35 mm track diameter gave volume loss of 0.3262 mm^3 and speed gave volume loss of 0.05978 mm^3 with the combination of 10 N-200 rpm-30 mm track diameter. The track diameter (which affects the sliding distance) has negligible effect on the wear, this may be because after a certain point the surfaces become smooth and also the wear particles from the pin deposit on the disc, and hence, the roughness is reduced and causes negligible wear further on. The load was very dominant because it increases contact area of surfaces and very high stresses at peaks and valleys of the surface finish are resulted in higher order of wear rates.

Keywords Additive manufacturing · Taguchi's orthogonal array · Wear rate and wear co-efficient

U.M. Baig (✉)
Ghousia College of Engineering, Ramanagara 562159, KA, India
e-mail: usaydbaig@gmail.com

A.R. Anwar Khan
Department of Mechanical Engineering, Ghousia College of Engineering,
Ramanagara 562159, KA, India

D. Ramesh Rajakumar
CSIR-National Aerospace Laboratories, Bangalore 560017, India

1   Introduction

Wear rate measurements are vital parameter for failure mode and effect analysis of rotating components. Additive manufacturing/Rapid prototype method is a promising and cost effective for intricate shapes and profiles of aero components. Before manufacturing of functional components for aerospace applications using additive manufacturing (AM/RP) route, test specimens were manufactured by AM methods for wear analysis. Wear characterization of AM produced test specimens are discussed in this paper. Intensive research is going on wear analysis of newly formed material using innovative process and manufacturing methods. Kruth [1] has proposed a tentative classification and nomenclature for the rapid prototyping techniques. The author states that this is a promising manufacturing technique which can be applied to computer-integrated manufacturing but requires more research and development to bring the techniques to maturity.

Ramesh Rajakumar et al. [2] have tested the mechanical properties of H20 steel specimens produced by direct metal laser sintering method. The authors observed that the surface produced by this method gave maximum values, such as Ra: 10.7084 µm, Rt: 43.1248 µm and Rz: 9.4519 µm roughness. A slight variation in hardness was also observed and a deviation of −0.035 mm for a contour of 10 mm radius was measured. The ultimate tensile strength of the specimen was found to be suitable for only subsonic component for wind tunnel applications. Luo et al. [3] have adopted the use of rapid prototyping for rapid tooling. Here, tool temporary or permanent tool moulds are created my rapid prototyping methods. Software and hardware components of the rapid tooling system are introduced and equations are derived which give reference data for the experiment and expect to manufacture the rapid tooling part with better quality.

Ranjit Roy [4] has proposed the design for experiments using the Taguchi Approach which was developed by Dr. Genechi Taguchi to improve the quality of products by using orthogonal arrays developed by Taguchi, i.e. L4, L8, L9, L12, L16, L′16, L18, L25, L27, L32, L′32, L50 we can design the experiment combinations to reduce the size of experiment but get accurate results at the same time. Further, the Author has developed a software tool to facilitate the calculation of complicated equations and easy computation of complicated data like performing the analysis of variants and displaying accurate results in form of tables or graphs. Wang [5] has suggested the use of orthogonal arrays developed by Dr. Genechi Taguchi to achieve high quality. The author proposes a procedure the use of orthogonal arrays in such a way that some new factors can be added to the experiment even after designing so that the entire experiment would not have to be restructured. This method used modified orthogonal arrays in the order 1,12,2,13,23,123,23,3,14,124,24 … 4,1k, …, k Marwaha et al. [6] have tested Al/Sic/Gr metal matrix hybrid composite for analysis of wear parameters by using Taguchi method. The influence of the parameters on wear rate and co-efficient of friction was determined using analysis of variants or ANOVA also the best combination for least wear was also determined.

A pin on disc tribometer was used to test the wear parameters. It contains three control parameters, load, sliding speed, and track diameter varied over three levels. Using orthogonal arrays the experiment size was reduced from 27 trials to 9 trials using an L9 orthogonal Array. After analysis of variants it was observed that the track diameter had the largest effect on the co-efficient of friction while speed of the disc had the least effect.

This technology has a lot of advantages in terms of reduction in time and ease of production, a lot of study has been done on polymer materials but very less on direct metals. This motivates a study of wear characteristics of Direct Steel H20 models produces by this method in order to get an insight on how the models behave when subjected to friction and wear.

2 Description of Present Work

2.1 Machine and Process Parameters

A test piece and a few tensile specimens were fabricated using Directsteel H20 at CMTI (Center for Manufacturing Technology Institute) Tumkur Road, Bangalore, using DMLS- method. The machine is shown in the Fig. 1. The details of machine and process parameters are listed below.

2.2 Details of Machine

Machine: EOSINT M250 Xtended Rapid Prototyping Machine

Make: EOS GmbH, Germany
Laser: CO_2 Laser

Fig. 1 EOSINT M250 Xtended rapid prototyping machine (CMTI)

Fig. 2 Photograph of
machined pin/test specimens

Fig. 3 2D drawing of
pin/test specimens
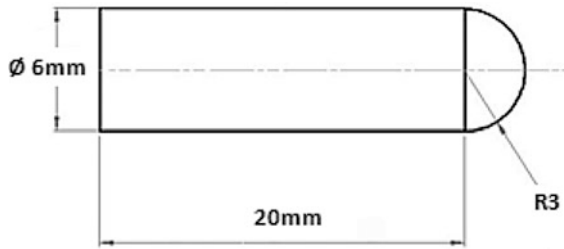
2.3 Process Parameters

Laser power	200 W
Layer thickness	0.040 mm
Laser scan speed	100 mm/s
Hatch width	5 mm
Hatch spacing	0.25 mm

2.4 Machining of Test Piece into Pin Samples

The test piece was machined by EDC (electron discharge machining) at CMTI (into nine pin samples with hemispherical ends for the pin on disc wear testing and photographs and 2D drawings are shown in Figs. 2 and 3.

3 Results and Discussion

The wear analysis was performed on TR-201 DUCOM wear and friction monitor at SED (Surface Engineering Department) at NAL (National Aerospace Laboratories), Bangalore. The experimental equipment is shown in Fig. 4.

The design of experiment was done by Taguchi approach by using L9 Orthogonal Array. The load, speed and track diameter were considered as very significant

Fig. 4 Wear and friction monitor TR-201

Table 1 Taguchi's orthogonal array (L9)

SI no.	Load (N)	Speed (rpm)	Track diameter (mm)	Wear loss (μm)	COF
1	5	100	30	90	0.274
2	5	150	35	86	1.297
3	5	200	40	147	2.281
4	10	100	35	155	1.222
5	10	150	40	109	0.582
6	10	200	30	80	0.462
7	15	100	40	154	1.348
8	15	150	30	130	0.566
9	15	200	35	188	0.692

parameters for wear measurements. The parameters ranges and result of this investigation are shown in Table 1.

The combined effect of the different parameters is depicted in Fig. 5.

It is observed that minimum and maximum wear occurs at samples 6 and 9, respectively. The loss in height of hemispherical pin with respect to time in these two pins is depicted in Fig. 6.

Fig. 5 Combined effect in wear loss (mm^3)
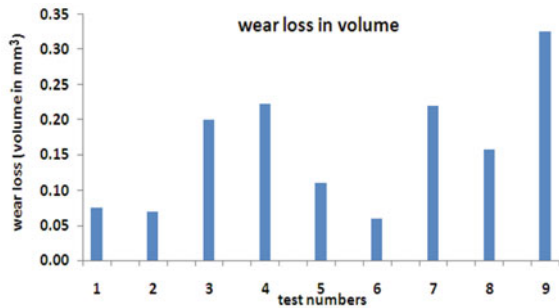
Fig. 6 Minimum and
maximum wear
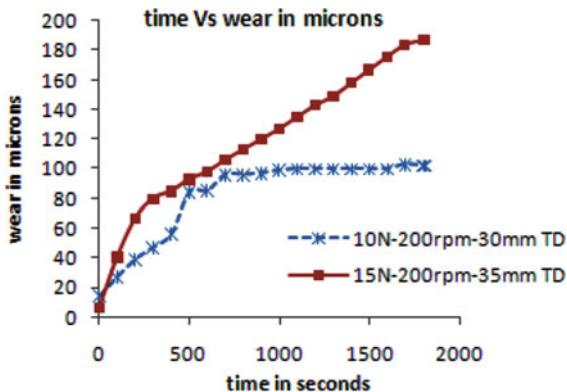
As observed from Fig. 6, for trial 6 the wear keeps increasing up to a point and then the slope reduces to almost a straight line, so beyond this point, the wear is negligible.

As for trial 9, the wear keeps increasing throughout. The load under the combination of 15 N-200 rpm-35 mm track diameter gave volume loss of 0.3262 mm^3 and speed gave volume loss of 0.05978 mm^3 with the combination of 10 N-200 rpm-30 mm track diameter.

The individual effect of the parameters is depicted in the Fig. 7.

It is observed that the wear only keeps increasing with increase in the load as depicted in Fig. 7 since loads. The load is very dominant because it increases contact area of surfaces and very high stresses at peaks and valleys of the surface finish are resulted in higher order of wear rates.

The increase in speed to level 2 (SP2) drops the wear and then there is an increase in the wear as speed further increases.

As the track diameter increases, increase in wear is observed up to a certain level, further increase in track diameter results in reduction in wear.

The effect of dry sliding wear on the surface of the pin and disc is studied through the surface microstructure as shown in Figs. 8 and 9.

Fig. 7 Individual effects
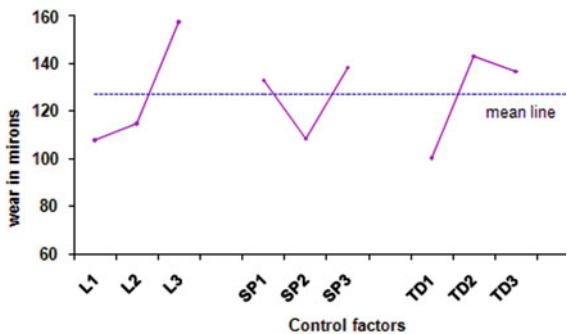
Fig. 8 Pin and disc surface for trial 6 (microscopic image for minimum wear)
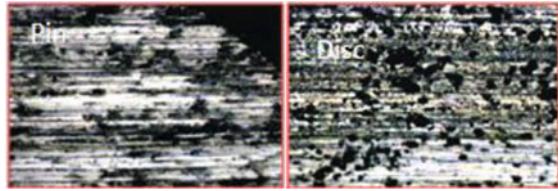
Fig. 9 Pin and disc surface for tril 9 (microscopic image for maximum wear)

The track surface for test no 6 reveals a lot of binder particles visible as black color spherical shapes. These particles were used as binders in the metal powers during manufacturing of the test specimens. These particles come from the wearing of the pin specimen. The particles are present in spite of the track being continuously cleaned. This results in the pin specimen sliding against particles of its similar kind, hence there is reduction in wear.

The disc track surface for trail 9 reveals lesser binder material as compared to trial 6 due to higher temperature generated between contact surfaces and this temperature transform the binders into other type of components. More contact area of the pin slides against the disc and results in increasing wear. Direction of the lay of materials is clearly visible in horizontal directions in photograph of pin in Fig. 9.

4 Conclusions

In this wear analysis test on H20 specimens produced by additive manufacturing techniques, the following conclusions were drawn

1. Load was found to have the greatest effect on the wear. 1. This is because it increases contact area of surfaces and increases stresses in the peaks and valleys of the surface finish resulted in higher wear rate.
2. The track diameter was found to have the less effect on the wear. As the pin slides on the disc, after a certain point in the wear particles from the pin deposit on the disc track in spite of being cleaned continuously. This causes surfaces to become smooth, and hence, the roughness is reduced and causes negligible wear further on. This means that, further increase in sliding distance (or track diameter) will have negligible wear loss

3. The combination of 15 N load −200 rpm speed −35 mm track diameter gave the highest volume loss of 0.3262 mm^3 and the combination of 10 N load −200 rpm speed −30 mm track diameter gave the lowest volume loss of 0.05978 mm^3.
4. The binder particles from the pin deposit on the disc track and cause reduction in wear by reducing the roughness of the pin.

References

1. Kruth JP (1991) Material incress manufacturing by rapid prototyping techniques. Katholieke University Leuven/Belgium, Annals of the CRIP vol. 40/2/1991
2. Ramesh Rajakumar D, Rajeev G, Tushar P (2014) Mechanical characterization of steel specimens produced by rapid prototyping techniques for wind tunnel model applications. National Trisonic Aerodynamic Facilities, National Aerospace Laboratories, Bangalore
3. Luo RC, Chen C-C Tzou J-H (2004) The development of direct metallic rapid prototyping system. IEEE
4. Ranjith Roy K (2001) Design of experiments using Taguchi approach. Wiley-Interscience Publication
5. Wang PC A simple method to design good experiments. Department of Industrial and Business Management, Chang University, Taiwan
6. Marwaha R, Dev Gupta R, Jain V, Sharma K (2013) Experimental investigation and analysis of wear parameters on Al.Sic/Gr-metal matrix hybrid composite by Taguchi Method. Global J Res Eng Mech Mech Eng 13(9)

Rapid Manufacturing of Customized Surgical Cutting Guide for the Accurate Resection of Malignant Tumour in the Mandible

Sandeep W. Dahake, Abhaykumar M. Kuthe, Mahesh B. Mawale and Ashutosh D. Bagde

Abstract A case report of malignant tumour in mandible is discussed in this paper. The innovative rapid prototyping (RP) assisted customized surgical cutting guide (CSCG) has developed for the accurate resection of the malignant tumour in the mandible. Computer tomography (CT) scan data in DICOM format is utilized for the development of CSCG. Mimics 14.11 used for image processing to develop diseased model. 3Matics 6.0 software is used for the virtual surgical planning (VSP) and computer-aided design (CAD) of customized implant and CSCG. Finally, CSCG developed by using fused deposition modelling (FDM), a technique of rapid prototyping (RP) in ABS material. The testing of the RP assisted CSCG was performed by mutually fixing it on the patient's diseased model developed by the same RP. This paper describes the novel methodology for the development of the RP assisted CSCG and its application to accurately resect the malignant tumour in the mandible. This approach shows good results in designing and manufacturing of the CSCG. Using advanced tools like VSP, CAD and RP, manufacturing of CSCG for the accurate resection of tumour and placement of customized implant may possible easily in actual surgery.

Keywords Virtual surgical planning · Computer-aided design · Rapid prototyping · Customized surgical cutting guide

S.W. Dahake (✉) · A.M. Kuthe · M.B. Mawale · A.D. Bagde
Mechanical Engineering Department, VNIT, Nagpur 440010, India
e-mail: sandeepdahake@students.vnit.ac.in

A.M. Kuthe
e-mail: amkme2002@yahoo.com

M.B. Mawale
e-mail: mbmawale@gmail.com

A.D. Bagde
e-mail: bagde.ashu@gmail.com

1 Introduction

The customized surgical cutting guide (CSCG) is a jig designed and manufactured by an engineer with surgeon input in complex surgeries using computer-aided design/computer-aided manufacturing (CAD/CAM) and rapid prototyping (RP) technology. Design and manufacturing of such a CSCG are conducted according to the pre-operative virtual surgical planning (VSP) of an engineers and surgeons with the aim to accurately transferring this plan into the operating theatre [4, 8]. To understand the patient's diseased anatomy and preparation of the CSCGs preoperative planning using advance software plays vital role. The CSCG consists of intraoperative instruments which are enough capable to exactly transfer VSP into actual surgery for exact resection of tumours and accurate placement of the customized implant in resected area. This process helps to improve the patient's quality of life by improving the functionality and aesthetics [6].

In this paper, author reported the application of CAD/CAM based technologies for the innovative designing and RP based FDM technique for manufacturing the CSCG to finalize the mandibular rehabilitation in the surgery, i.e. resection and reconstruction. This paper only focuses on the development of CSCG using FDM technique for accurate resection of the malignant tumour in the mandible and accurate placement of customized implant.

2 Materials and Methods

2.1 Case Report: Background

In this paper, the previous data of patient (27 years old female) has taken for the study. She complained of swelling in the right side of mandible from about 9 months. In the biopsy test that swelling was confirmed as malignant tumour. Initially that tumour was small and increased up to present size gradually [1].

Surgeon used conventional methodology for operation. They used manual surgical planning and without using any guide resected the tumour as well as filled the gap by placing the metallic implant which was fabricated prior to the actual surgery. Postoperative they noted that

- Inaccurate cutting of tumour because of no guiding instrument used while cutting.
- The placement of the metallic implant was not accurate as required for proper fixation.
- At the time of actual surgery, for the planning of tumour cutting and implant placement taken more time.
- So actual surgery lengthen up to 4 h.
- Implant design and manufacturing was time consuming, tedious and costly.

Table 1 Design methodology of customized surgical implant and CSCG

S. No.	Methodology
1	Radiology
2	Image processing
3	VSP
4	CAD of customized implant
5	CAD of CSCG
6	Export CAD file in RP compatible STL format

To avoid these problems author used new advanced CSCG for the accurate cutting of the tumour directly which also help to exact placement of the metallic implant at the desired site. Mimics 14.11 used for image processing and 3Matics 6.0 for VSP, CAD of customized implant and CSCG. RP used for manufacturing of CSCG. The adopted methodology is given in Table 1.

2.2 Radiology

In this study, spiral CT scan of diseased mandible in DICOM format adopted with thickness of slice 0.6 mm, pixel size 0.332 mm, resolution 512×512, total slices 146, tube current 89.1 mA and tube voltage 100 kV.

2.3 Image Processing

Mimics 14.11 (Materialise NV, Leuven, Belgium) software is used for image processing and conversion of DICOM file into STL file for further CAD design. 3D reconstruction of diseased model is generated by using few steps in software. Exact threshold value for bone was selected to separate the particular desired anatomy. A 3D model of diseased mandible was quickly and easily created with by performing the segmentation. In this case, for reconstruction of the diseased mandible required half an hour, which includes detail removing of the unwanted tissues, surface cleanness and smoothness of model. For the accurate VSP and CAD the appropriate model development is very important. Diseased reconstructed 3D model in STL format is shown in Fig. 1.

2.4 VSP

3Matic 6.0 software is used for VSP and CAD (customized implant and CSCG). Various advanced tools available in the software used to overcome the inaccuracies
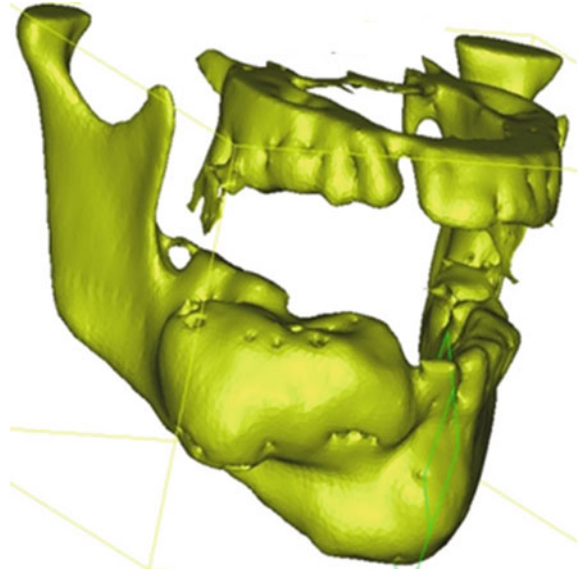
generally seen in conventional surgery planning. Elimination of various surgical
steps like finding implant location, intraoperative planning and tumour cutting
measurement also easily possible using this software [9]. VSP plays vital role
before design the customized implant and CSCG [5]. Resection was planed vir-
tually by considering additional 5 mm distance for surgical margin from both the
side of tumour portion.

Bad surface on the mandible model removed with taking measurements of the
holes by using the advanced tools in the 3Matic 6.0 (Fig. 2). Two cutting planes
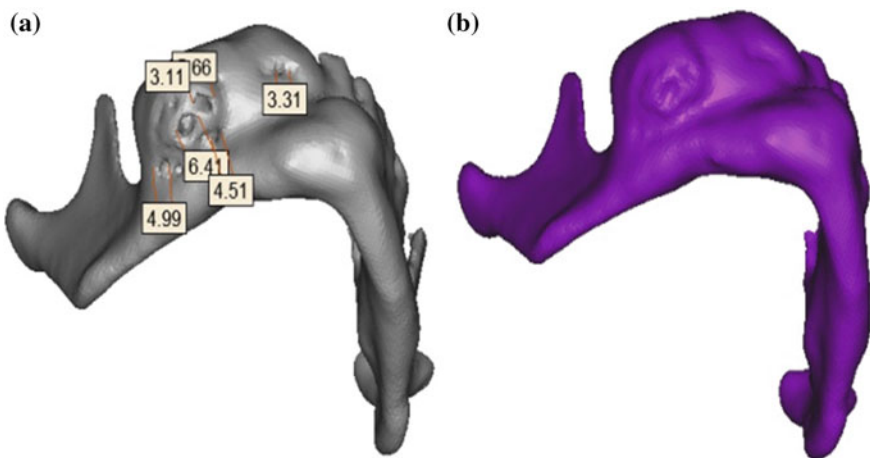
Fig. 2 a Measurement of gap (bad surface) and **b** filled gap on mandible in 3Matics 6.0

Fig. 3 VSP for tumour cutting as well as customized implant and CSCG design
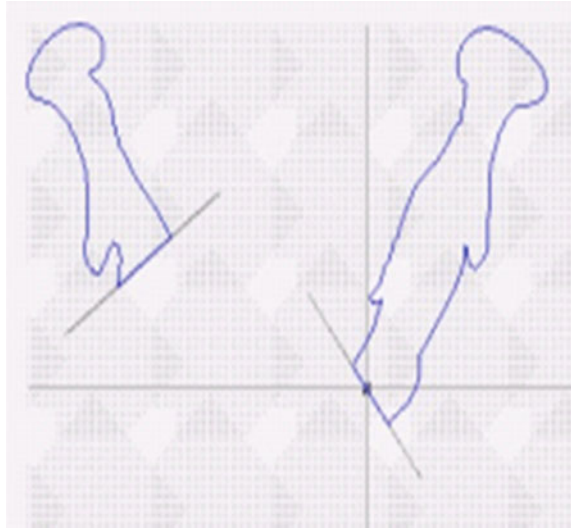
selected which decided the tumour cutting and implant size and shape (Fig. 3). VSP significantly decreases the laborious manual steps as compare to the traditional planning [10].

For design of CSCG, first the VSP and design of customized implant is very important. Because the end sides of customized implant are used as cutting planes for tumour resection. These cutting planes are useful for design of cutting slots for CSCG. So before design of CSCG the design of customized implant was done in this study. The size of implant, thickness of implant, screw positioning of implant, shape of implant, and exact match of the implant (location and orientation), as well as plan for design of CSCG, i.e. cutting slot, retention plate, screw holder, etc. finalized using this software. First implant was designed and then plate is attached on it using Boolean operation tool by transferring exact mandible surface contour on the plate fixation area. The provision of screw fixation was also given on the plate by considering the mandibular nerve and teeth roots. All details of customized implant are shown in Fig. 4.

2.5   CAD of CSCG

After completion of the VSP and CAD of customized implant on the diseased CAD model of patient's mandible the CSCG development starts. The cutting planes as planned in VSP were utilized to design final CSCG (Fig. 3).

To create this CSCG, the mandible surface was inverted which assured of a perfect fit. The cutting slots are developed at the location of the cutting plane. The cutting slot is designed in this study in such a way that 0.89 mm thickness scalpel can easily move inside. The advanced tools in 3Matics are used to design the CSCG

Fig. 4 Customized implant
position in mandible
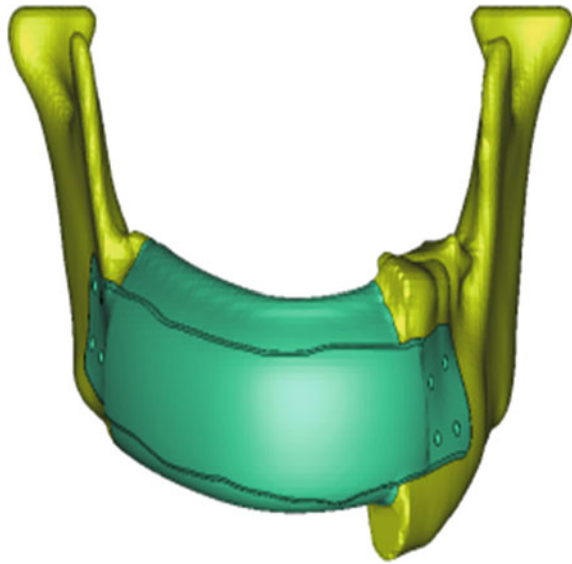
Fig. 5 Designing of the
CSCG on the diseased
mandible
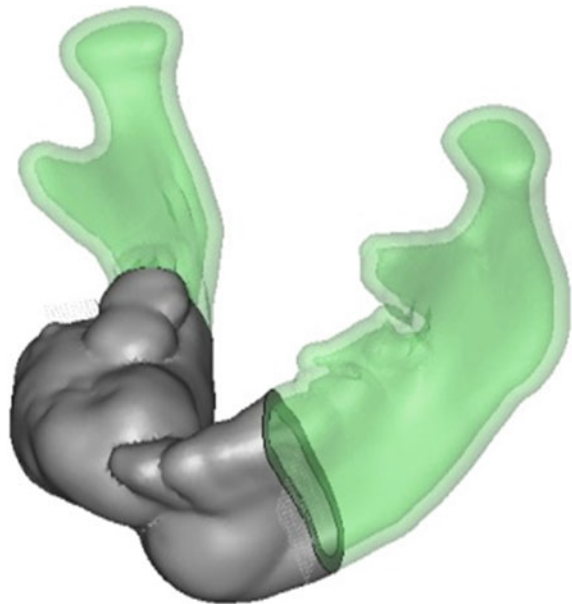
by accurately transferring the mandibular contour on the guide (Fig. 5). Table 2
shows the different elements and their functions of the CSCG. This CSCG designed
by considering surgeons and patient convenience, cutting saw. As per surgical
recommendation, CSCG provide most accurate site for resection and implant
placement [3]. The complete CSCG is shown in Fig. 6.

Table 2 Elements of CSCG and their function

S. No.	Elements of CSCG	Function
1	Cutting planes	Used for the design of cutting slots
2	Upper guide	For fixation of the upper half of the mandible
3	Lower guide	For fixation of the lower half of the mandible
4	Cutting slots	For cutting saw movement and exact cutting of the mandible
5	Screw holder	Mutual positioning of the upper and lower portion of CSCG while cutting
6	Retention plate	To maintain the same gap between cutting slot while cutting

Fig. 6 Upper portion and lower portion of CSCG positioned on the mandible
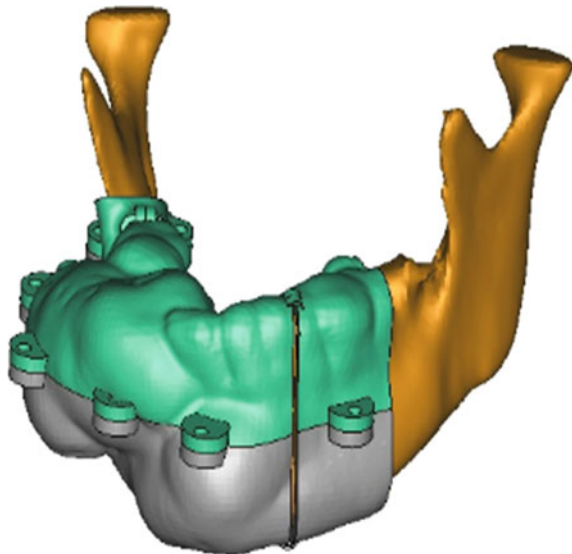
2.6 Manufacturing of CSCG

There are various RP techniques are available to manufacture the CSCG in various materials. Now a day different biomaterials are available to manufacture the CSCG. In this study FDM technique of RP (uPrint, Stratasys) (Fig. 7a) is used to fabricate CSCG in ABS material. For the accurate placement of the CSCG on the diseased mandible proper finishing is required. Agitation tank (Biosonic) (Fig. 7b) is used for removing support material after fabrication of the CSCG. The manufacturing procedure of the customized implant and CSCG is given in "Table 3".

Fig. 7 **a** RP FDM machine (uPrint, Stratasys), **b** agitation tank (Biosonic)

Table 3 Manufacturing methodology of the customized implant and CSCG

S. No.	Manufacturing process steps
1	Import STL CAD file of customized implant and CSCG in Catalist EX software
2	Slice STL CAD file and link with RP (FDM) machine
3	RP using ABS material
4	Finishing using agitation tank

3 Testing of CSCG on Diseased Mandible

Virtually, mandible and CSCGs fitted well but for conformation, mutual positioning test was performed on RP assisted diseased mandible using RP assisted CSCG (Fig. 8). This test conformed the accurate fitting of the CSCG on the mandible and helps to improve the confidence of the surgeons. Cutting planes were obtained exactly on RP assisted diseased mandible through the cutting slots of CSCG. This experimental feasibility test showed that RP assisted CSCG is simple to use and fit well in resection of the tumour. If surgeon satisfied with this test the CSCG can be use in the actual surgery after sterilization with standard autoclave.
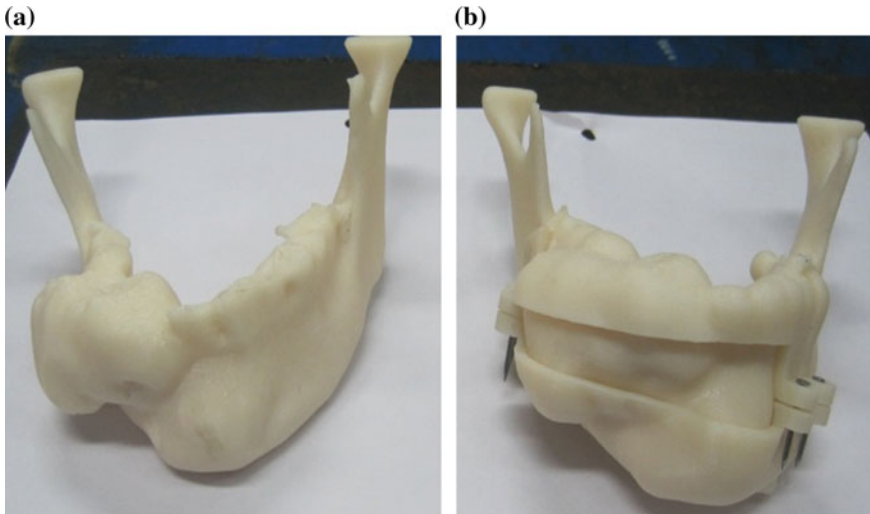
Fig. 8 a FDM assisted diseased mandible, **b** FDM assisted diseased mandible with CSCG

4 Discussion

It is really very easy to find the best fit for positioning the CSCG manually on the mandible, because no significant motion in between the CSCG and the mandible was seen in the feasibility test. RP assisted CSCG requires clean bone surface preparation to fit properly. But it is seen that this technique still better than other techniques. The major advantages of CSCG in mandibular reconstruction are as follows.

- Before to the actual surgery surgeon can decide the implant position, angulations and size by considering the size and the shape of the mandibular tumour.
- Use of CSCG in the surgery is very simple, so surgeons do not require any specific skills.
- No need of costly instruments as well as lengthy surgical procedures in the surgery hence reduces the surgery time.
- While placing the implant, screws positioning can be done precisely by considering the delicate adjacent tissues.
- Fluoroscopy can be avoided using the CSCG, which reduces the radiation exposure to people inside the operation theatre [2, 7].
- In surgery CSCG improves the confidence of the surgeons.

5 Conclusion

This case study proved that FDM is a feasible rapid manufacturing technique to develop effective CSCG for accurate resection of the mandibular malignant tumour and exact placement of implant. Because of the high accuracy, safety in surgery, cost effective RP technique, this type of CSCG have expected to use largely in the future for tumour resection and placement of customized implant in mandible. 3D reconstruction of diseased mandible using Mimics 14.11, VSP and CAD of customized implant and CSCG using 3Matics 6.0 and manufacturing using RP (FDM) technique is a powerful and useful tool for mandibular reconstruction surgery. This technique may simplify and improve accuracy of the complicated surgical procedure of mandibular reconstruction.

References

1. Arora A, Datarkar A, Borle R, Rai A, Advani D (2013) Custom made implant for maxillofacial defects using rapid prototype models. J Oral Maxillofac Surg 71:e104–e110
2. Cansiz E, Arslan Y, Turan F, Atalay B (2013) Design and production of a novel computer assisted patient specific sagittal split osteotomy guide and soft tissue retractor. J Med Biol Eng
3. Dérand P, Rännar L, Hirsch J (2012) Imaging, virtual planning, design, and production of patient-specific implants and clinical validation in craniomaxillofacial surgery. Craniomaxillofacial Trauma Reconstruct 5(3):137–144
4. Fantini M, Crescenzio F, Ciocca L (2013) Design and manufacturing of customized surgical devices for mandibular rehabilitation. Int J Interact Des Manuf 7:227–237
5. Hsu S, Gateno J, Bell R, Hirsch D, Markiewicz M, Teichgraeber J, Zhou X, Xia J (2013) Accuracy of a computer-aided surgical simulation protocol for orthognathic surgery: A prospective multicenter study. J Oral Maxillofac Surg 71:128–142
6. Logan H, Wolfaardt J, Boulanger P, Hodgetts B, Seikaly H (2013) Exploratory benchtop study evaluating the use of surgical design and simulation in fibula free flap mandibular reconstruction. J Otolaryngol—Head Neck Surgery 42(42):1–9
7. Lu S, Zhang Y, Shi J, Chen Y, Xu X (2012) Accuracy and efficacy of thoracic pedicle screws in scoliosis with patient-specific drill template. Med Biol Eng Comput 50:751–758
8. Oliveira M, Hussain N, Dias A, Lopes M, Azevedo L, Zenha H, Costa H, Santos J (2008) 3-D biomodelling technology for maxillofacial reconstruction. Mater Sci Eng, C 28:1347–1351
9. Polley J, Figueroa A (2013) Orthognathic positioning system: intraoperative system to transfer virtual surgical plan to operating field during orthognathic surgery. J Oral Maxillofac Surg 71 (5):911–920
10. Schepers R, Raghoebar G, Lahoda L, Meer W, Roodenburg J, Vissink A, Reintsema H, Witjes M (2012) Full 3-D digital planning of implant-supported bridges in secondary mandibular reconstruction with prefabricated fibula free flaps. Head Neck Oncol 4(2):1–6

Implant Analysis on the Lumbar-Sacrum Vertebrae Using Finite Element Method

A. Kavitha, G. Sudhir, T.S. Ranjani., V. Sarah Rajitha Thilagam and S. Vinutha

Abstract Disc degeneration is a common phenomena occurring due to ageing and is observed as changes occurring in the anatomical and physiological functioning of the disc. Degenerative Disc Disease (DDD) occurs when the inner core leaks out through the outer portion of the disc which places pressure on nearby nerves or the spinal cord. Intervertebral discs deteriorate and grow thinner as age progresses, which cause lower back pain. In many cases this is treated with medication and in severe cases surgery is preferred. In surgical procedures, for the fusion of bone in degenerated regions, pedicle screw implant has gained more importance. But in post-operative condition, loosening of screw occurs in the lower lumbar spine L5-S1 region. This is due to the high stress developing on the screws post surgery. The objective of this work is to compare the stress developed in the normal and abnormal subjects for various loads using finite element analysis. The data was acquired from two subjects (Normal −1, aged 43 and the other abnormal −1 diagnosed with DDD aged 61). A 3D model was generated from CT images by identifying the regions of interest. In addition to it volume and surface rendering techniques were employed in obtaining a 3D model. Intervertebral disc for L5-S1region was generated and pedicle screw implant was designed. The screw along with the vertebrae was subjected to stress analysis using Finite element method. Analysis was carried out for various loads applied on the L5-S1 region. It was observed that the stress values varied from 1.979e+02 to 1.371e+04 without screws and from 5.831e+04 to 6.936e+05 with the screws for normal subject. For the abnormal subject, it has been observed that the stress values varied from 1.337e+02 to 6.269e+03 for mild degeneration and from

A. Kavitha (✉) · T.S. Ranjani. · V. Sarah Rajitha Thilagam · S. Vinutha
Centre for Healthcare Technologies, Department of Biomedical Engineering,
SSN College of Engineering, Rajiv Gandhi Salai (OMR), Kalavakkam,
Chennai 603110, India
e-mail: Kavithaa@ssn.edu.in

T.S. Ranjani.
e-mail: ranjanisivaperumal@gmail.com

G. Sudhir
Orthopedic Surgeon, Sri Ramachandra Medical College and Research Institute, Chennai,
Tamil Nadu, India

1.029e+02 to 5.051e+03 for severe degeneration without the screws. Further, it has been noted that the stress values varied from 1.792e+04 to 2.130e+05 for mild degeneration and from 5.831e+04 to 6.936e+05 for severe degeneration with the implant placed. This study proves to be clinically highly relevant in addressing post-surgery issues due to placement of implants and in analysing the subjective appropriateness of the implant being used.

Keywords Degenerative disc disease · Implant design · Finite element analysis · Lumbar-sacrum vertebrae

1   Introduction

An intervertebral disc lies between each vertebrae keeping them separated in the spinal column. It can act as a shock absorber and tend to protect the nerves in the spinal column. Prescher et al. describes that as the pressure on the spine is due to the jelly-like protective covering called the mucoprotein gel, which moves inside the outer disc and redistributes itself to absorb the impact of the pressure [13]. The mucoprotein gel dehydrates due to ageing and the spine does less work as a shock absorber. In children, they begin to solidify as part of the normal ageing process. During early adulthood, the disc becomes less flexible as the blood supply stops and the soft inner material begins to harden. By middle age, the discs act like a hard piece of rubber and they become quite unyielding. These changes make the discs prone to more injury as the outer layer weakens followed by deterioration and begin to rip, causing chronic back pain for some people which emanates as Degenerative Disc Disease (DDD).

DDD in the lumbar region refers to a syndrome in which a degenerated disc causes lower back pain. When the lumbar discs between the vertebrae begin to break down, it can cause both inflammation and instability in the lower back, bringing about pain, muscle spasms and sometimes sciatica. DDD is one of the most common causes of low back pain and also one of the most misunderstood. The disc is impaired of blood supply and when injury occurs it cannot repair itself the way other tissues in the body can. An otherwise insignificant injury to the disc is the degeneration followed by wearing out of the disc. Degenerative disc disease is highly a commonly occurring phenomenon, and it is estimated that **at least 30 % of people aged between 30 and 50 years** will have some degree of disc space degeneration. Further, it has been observed that, once a patient reaches 60, some level of disc degeneration is a normal finding on an MRI scan in most of the cases considered for evaluation [15].

At young ages, people experience back pain due to strain in the lower back muscle or within the disc space itself. Spinal cord injuries occur due to ageing, falls, weight falling on back, stress developed over the L5-S1 vertebrae, road accidents. Lifting a heavy object, twisting or a sudden movement can develop microscopic tears and can cause the muscles or ligaments to stretch. In India, the ratio of men to women sustaining spinal injuries was 3.6:1 and most of the patients belonged to the

age group of 20–39. The different levels of spine that were subjected to injuries were cervical spine (36.2 %), thoracic spine (34.3 %) and lumbar spine (29.5 %). Injury occurred from patients who fall from height (58.9 %), fall of weight (7.2 %), motor vehicle accident (21.3 %) and non-traumatic causes (12.6 %) [16].

Pedicle screw placement has become an increasingly common method for the treatment of spine deformity, degenerative disease, trauma and tumours in the past two to three decades. Pedicle screw fixation provides more rigid fixation than sub laminar wires or hooks as they are successful. Despite the advantages of pedicle screw systems, screw breakage, loosening, pullout can still be considered as problematic. Proper application of pedicle screw requires a complete study of pedicle screw biomechanics including screw characteristics and insertion techniques as well as an understanding of bone quality, pedicle morphometry and salvage options. The pedicle contributes approximately 80 % of stiffness and 60 % of pullout strength at bone-screw interface. The lumbar pedicle is located at the converging location of the middle of the transverse process, the superior facet and the pars interarticularis [11].

This work is mainly concerned with pre-surgical treatment to check for abnormalities. The objective of this work is to evaluate the stress developed in normal and abnormal subject (one with degenerative disc disease). The stress analysis is carried out for various loads using finite element method. The finite element analysis includes determination of the geometrical parameters, the creation of a mesh, definition of the material properties and all procedures should be associated to the given subject. The common method for creating a subject-oriented mesh of the vertebrae is the direct conversion of image voxel to tetrahedral mesh elements. In this method, the segmented region of the image is extracted and each image voxel is directly converted to a brick element in the mesh. Material properties are defined on an element-by-element basis using densities derived from the image data. And the optimal screw position for various loading conditions is found and results are analyzed.

2 Methods

2.1 Data Acquisition

For creating a 3D model of the Lumbar-sacrum spine, the input data to the input data to the modelling software should be in DICOM (Digital Imaging and Communication in Medicine)format. The CT or MRI scan DICOM images of same gender will be most suitable for the analysis. CT spine images of 43 years old, female patient (normal) and 61 years old female patient (abnormal) diagnosed with DDD were collected. As the number of slices increases, the 3D model would be most accurate and analysis can be done precisely. The images are acquired from Indian Scan, Chennai.

2.2 3D Model of L5-S1 Vertebrae

For creating a 3D model of the Lumbar-sacrum spine, the input data to the modelling software (MIMICS) has to be in DICOM format. The CT or MRI scan DICOM images are the most suitable ones. 110 images are the most suitable ones. The planar views in Mimics include Coronal, Axial and Sagittal. In order to create accurate three-dimensional model of L5-S1, it is essential to discern regions containing bone tissue [7]. Thus, image segmentation has to be done by setting threshold values of CT number for bone tissue. The pixels having CT numbers in the threshold range were treated as bone tissue and collected in a segmentation mask [7]. The segmentation is done in axial view and it is copied to the other views using appropriate options. Segmentation is removal of unwanted information which is done using multiple slice edit tool and the floating pixels are removed using region growing tool. After every operation, the 3D object from the mask is calculated.

Further the segmentation is done by subtracting the L5 or S1 from the whole assembly (L5 + S1). This results in two separate entities, which have to be imported in 3-Matic. The 3D model is wrapped and smoothened for obtaining accurate precision. Same procedure is being carried out for both normal and the patient diagnosed with DDD.

2.3 Intervertebral Disc in 3-Matic

In the next step of geometric modelling of the vertebrae, intervertebral disc is generated in between the L5 and S1 section of vertebrae. After performing masking, multiple slice editing, region growing, the 3D model generated is exported to 3-matic to design the disc. Smoothing operation was performed to remove sharp edges. Vertebra was wrapped for creating an enclosed region. A surface was created using smooth curve on the lower side of first vertebra and upper side of second vertebra. This procedure was repeated for both the subjects. Disc was created by contouring the two surfaces. Hence the 3D model and disc are merged together. The segmented L5-S1 section for both the subjects is converted to a single entity for screw placement.

2.4 Implant Modelling

(1) *Designing of the implant* Pedicle screw implant has been designed using Solidworks. Currently used Monoplanar screw has better compression strength than Polyaxial and Monoaxial. Screw has 5 parts—pedicle, swivel, top head, conforming washer, setscrew, distraction rod.

(2) *Screw dimensions* Length 45 mm, diameter 6.5 mm, pitch (distance the screw would move for one revolution) 2.3 mm, Swivel top head 5 mm, Conforming washer 5 mm. These specifications are calculated from the CT radiographic images. In the axial view, the diameter of the pedicle is calculated so that it matches the diameter of the screw. Length of the screw is 80 % of the vertebrae length. Pedicle screws traverse in all three columns of the vertebrae and they stabilize both the ventral and dorsal aspects of the spine. The pedicle represents the strongest point of attachment of the spine and thus significant forces can be applied to the spine without failure of the bone-metal junction. Furthermore, the rigidity allows incorporation of fewer normal motion segments in order to achieve stabilization of an abnormal level.

(3) *Material* Titanium of Young's Modulus 110 GPa has been chosen as material. The implant should not have very high Young's Modulus as it increases its stiffness. The other normally used material like stainless steel has young's Modulus of 210 GPa which is not suited for pedicle screw implant. Also the titanium elasticity matches with the bone elasticity. Screws are placed in pedicle portion of the vertebrae. Pedicle is actually the joining of vertebrae and discs.

(4) *Assembly of vertebrae and pedicle screw implant* The screw is assembled into vertebrae using interactive translation and interactive rotation. Both screw and vertebrae are imported as different parts into 3-Matic. Then the screw is positioned inside the vertebrae by translating the object coordinates. The coordinates are translated linearly using interactive translation and rotated using interactive rotation. Now the screw and vertebrae are assembled together using Boolean union. Then the meshing is done for the combined assembly Fig. 1.

2.5 Finite Element Analysis

(1) *Importing into ABAQUS* The Vertebrae model is imported into ABACUS in INP, a pre-meshed format.

(2) *Material property Definition* The screws and bone are defined by homogeneous linear elastic properties. The material properties assigned have been

Fig. 1 Work flow representation
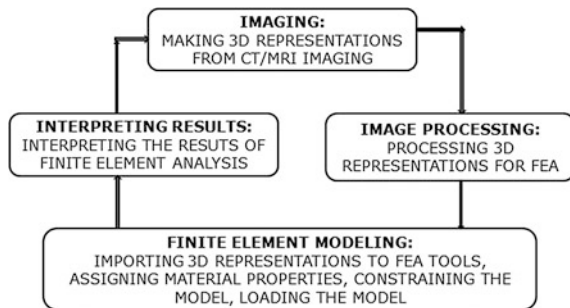
Table 1 Material properties

Material properties	Model	E (MPa) Young's modulus	γ Poisson's ratio
Cortical shell	Linear elastic, isotropic	5000–15,000	0.2–0.3
Trabecular bone	Linear elastic, isotropic	100–500	0.2–0.3
Nucleus pulposus	Poro elastic	1.5	0.49
Intervertebral disc	Normal	1.1	0.49
Intervertebral disc	Severe degeneration	2.5	0.32
	Mild degeneration	1.3	0.42

listed in Table 1. Sections have been created in ABAQUS with material properties assigned to each of them and then the sections have been assigned to the corresponding parts of the constructs. The screws are given the material properties of Titanium which is the commonly used metal for human body implants.

(3) *Creation of instances* Instances are used to define the dependency of the model. Since, a meshed model is imported it is automatically designated as dependent.

(4) *Formation of step models* Step models are created which defines the general nature of the analysis. In this static analysis is performed.

(5) *Definition of load and boundary conditions* Boundary conditions are to prevent rigid body motion. It is to constrain a region by effecting zero displacement. This option allows joining the finite elements with a common border shared by the two sections meaning and thus they were not allowed to move freely in six degrees of freedom. Symmetric boundary conditions are applied to the bone and assembly mesh models. Different pressures are given as loads on the top of the L5 region and analysis is done for every single pressure given in order to find the stress developed in different regions accordingly. In this analysis 100, 600, 1200, 3400 N are the different pressure values assigned.

(6) *Verification of mesh* The mesh is verified for errors and warnings in the next step. Any unwanted or disconnected meshes can be found in this step.

(7) *Job creation and processing* A static linear analysis is carried out in ABAQUS. A new job is evoked. The meshed file in ABAQUS CAE is automatically saved as.inp file. This file is transferred internally to ABAQUS Standard, the analysis module. The user then requests an output from ABAQUS Standard to be visualized in CAE. In order to start the analysis, first the given data must be checked for correctness with the help of data check. Before that a job has to be created to run the data check and analysis. Once the data check is successful, the values are submitted for analysis. Separate jobs are created for various pressures.

3 Results and Discussion

Figure 2a, b refer to the DICOM images of normal and DDD affected abnormal lumbar spine segments respectively. The exclusive L5-S1 segments of the normal and abnormal subjects are shown in Fig. 3a, b.

The intervertebral disc and the vertebrae with the intervertebral disc for normal and abnormal subjects after they have been designed from the original images are shown in Figs. 4 and 5a, b respectively. The single entities for normal and abnormal images are presented in Fig. 6a, b respectively.

Figures 7 and 8 show the model of a pedicle screw and the screw designed as per the specifications respectively. Finally, the screws were placed and the images of normal and abnormal images after screw placement are shown in Fig. 9a, b respectively. Figure 10a, b show the stresses developed in each region differentiated with colour variations for normal and abnormal subjects respectively. Displacement variation and stress variation for various pressures and the two models are analyzed and the results are verified.
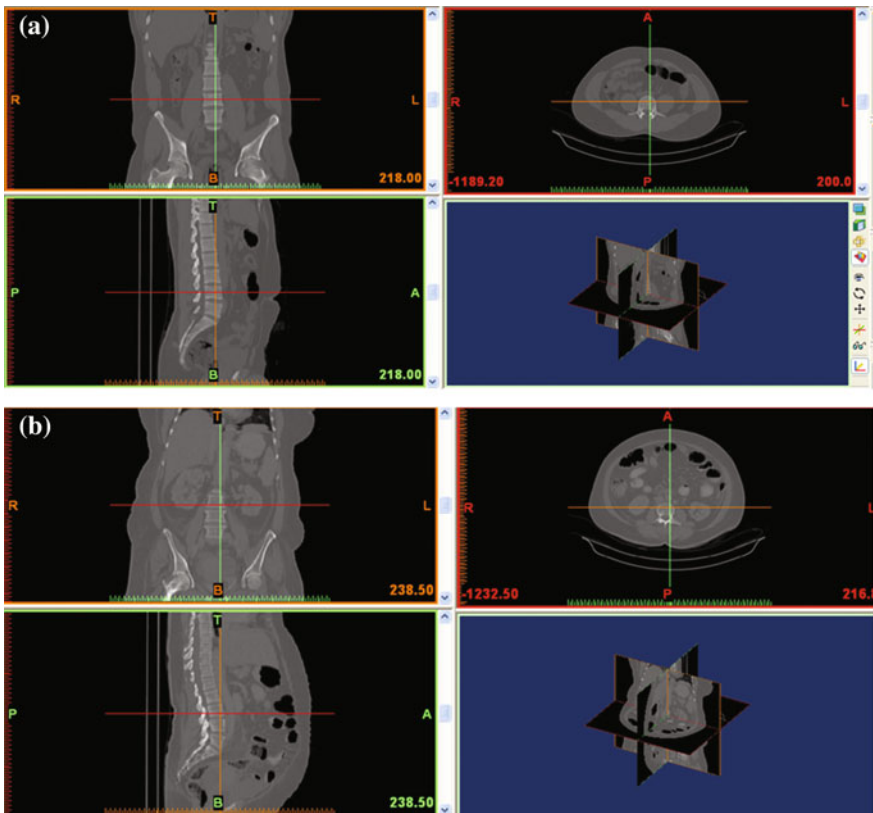
Fig. 2 **a** Normal lumbar spine segment. **b** Abnormal lumbar spine segment affected by DDD

Fig. 3 a Segmented L5-S1
(normal). b Segmented L5-S1
(abnormal)
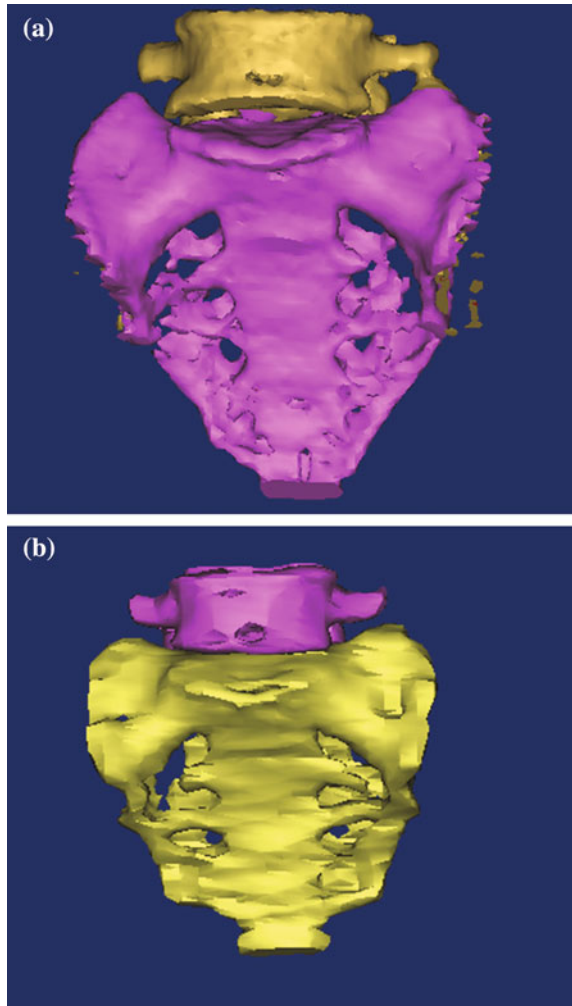
Fig. 4 Intervertebral disc

Fig. 5 a Vertebrae with intervertebral disc (normal). **b** Vertebrae with intervertebral disc (abnormal)
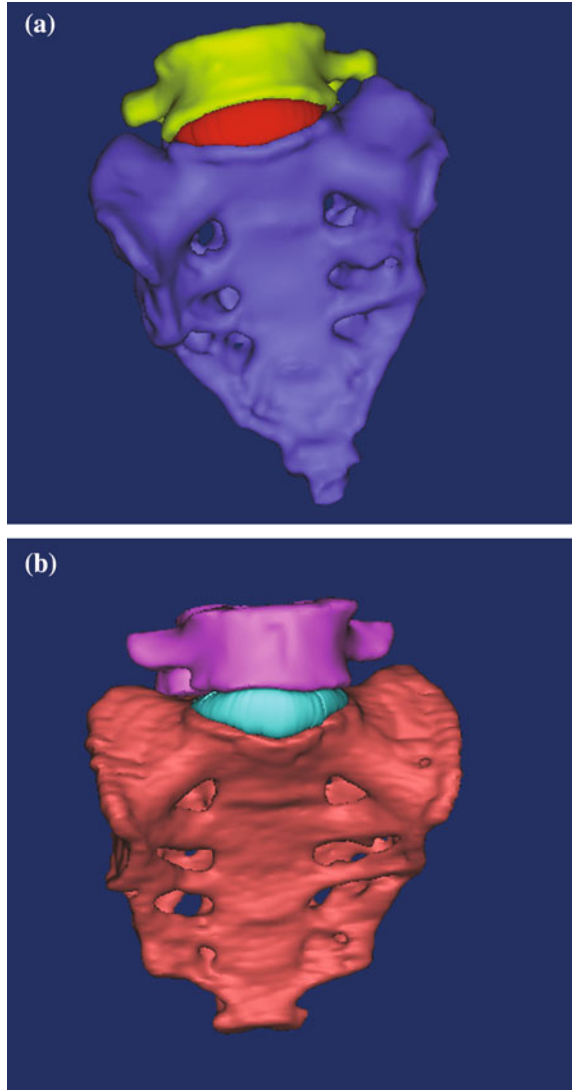
3.1 Analysis Without Placing the Screw

The results of normal stress analysis performed for the vertebrae without the insertion of screw are given below in Table 2. The increase in the stress at the L5-S1 region with the increase of the normal stress can be visualized. By assigning different material properties to Mild degeneration and severe degeneration to the disc and screw, the load is applied to the subject on the surface of L5-S1 region and the place that is subjected to stress is constrained.
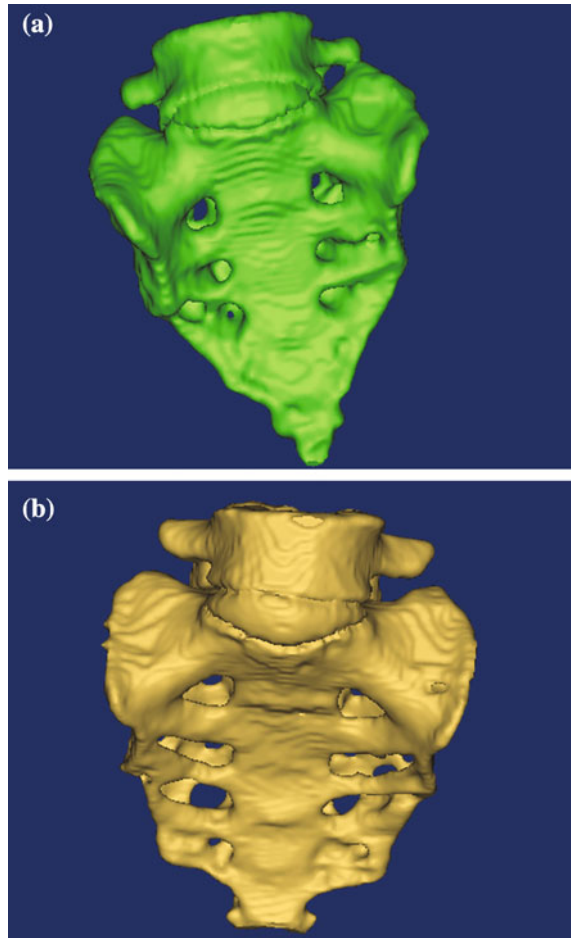
Similarly, Analysis is done for 600 N (Fig. 11a), 3400 N (Fig. 11b) and 1200 N (Fig. 11c), respectively and the stress developed was studied.

Without Screws By performing a comparative analysis between normal and abnormal subject, we conclude that the stress is more for normal subject compared to the one with degenerative disc disease. While looking at the stress value of subject with mild and severely degenerated disc, mild degenerated disc is more prone to stress than severely degenerated one. The minimum stress for mild and severely degenerated disc are 1.337e+02 and 1.029e+02 for load of 100 N, whereas for normal subject it is 1.979e+02. The maximum load that a subject can withstand is 3400 N, when subjected to such a load, the normal subject experiences a maximum stress of 1.371e+04 on contrary the subject with mild and severe degeneration is subjected to stress of 6.267e+03 and 5.051e+03 respectively. It is also noted that on increasing the load the stress in normal subject keeps on increasing.

Fig. 7 Pedicle screw

set screw

conforming washer

swivel top head

Distraction rod
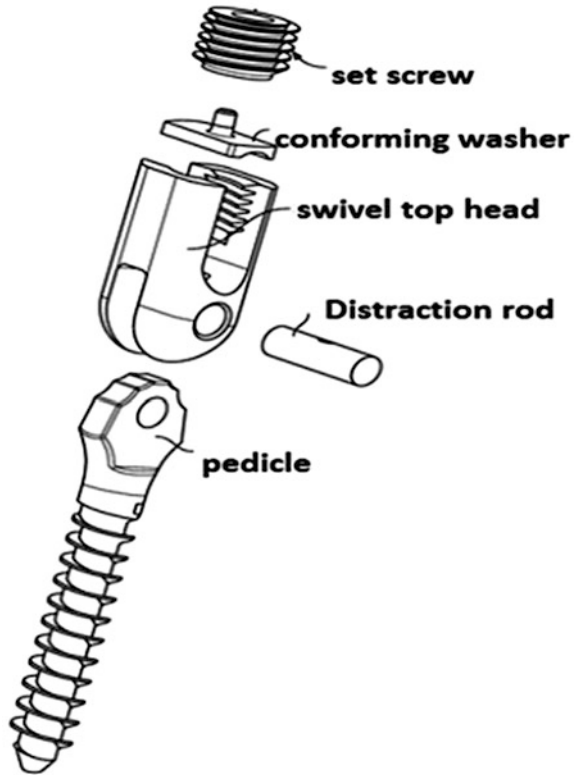
pedicle

Fig. 8 Pedicle screw designed as per specifications
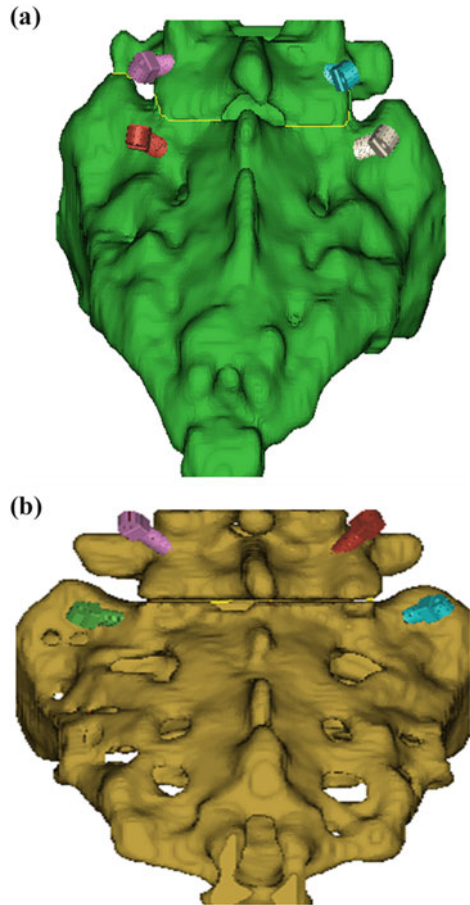
3.2 Analysis After Inserting the Implant

The results of stress analysis after placing the implant into the vertebrae are shown below. The decrease in the stress level at the L5-S1 region and increase in stresses at pedicle region, i.e., near implant can be visualized. Similarly, Analysis is done for 100, 600, 1200 N, respectively, and the stress developed was studied.

Similarly, Analysis has been done for 100, 600, 1200 N respectively and the stress developed was analyzed. The corresponding results are shown in Table 3.

With Screws After insertion of screws into the pedicle region of the vertebrae the subject is applied force in steps of 100, 600, 1200, 3400 N. Normal subject experiences more stress compared to one with Degenerated Disc Disease as seen in Table 4. The minimum and maximum stress a normal subject experiences is 7.326e+05 and 8.025e+06 respectively. Subject with severely degenerated disc experiences a stress of about 6.998e+05 and mild degenerated disc is subjected to 2.150e+05. The decrease in

Fig. 10 a Meshed model
(normal). **b** Meshed model
(abnormal)
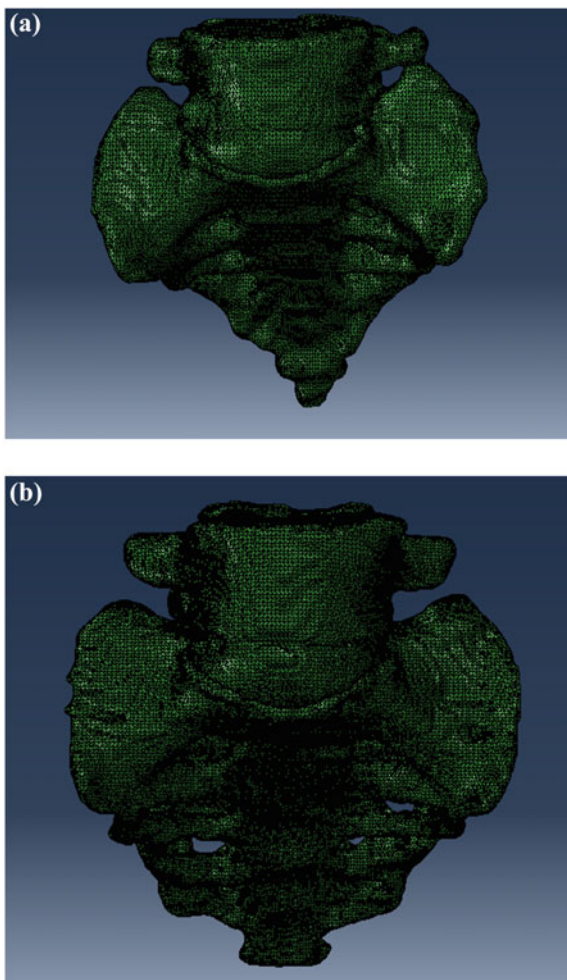
Table 2 Stress distribution in abnormal subject without screws

Force (N)	Stress without inserting screws for mild degenerated disc (Pa)		Stress without inserting screws for severely degenerated disc (Pa)	
	Minimum	Maximum	Minimum	Maximum
100	1.337e+02	1.605e+03	1.029+02	1.235e+03
600	1.730e+02	2.076e+03	1.685e+02	2.021e+03
1200	2.998e+02	3.987e+03	2.555e+02	3.065e+03
3400	5.224e+02	6.267e+03	4.209e+02	5.051e+03
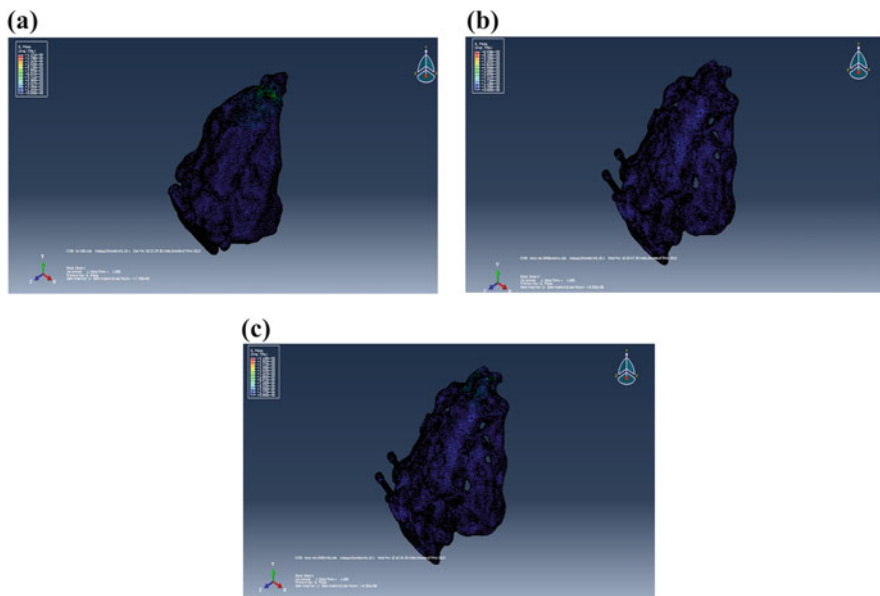
Fig. 11 **a** Stress developed when compression force of 600 N applied (normal). **b** Stress developed when force of 3400 N was applied (severe degeneration). **c** Stress developed when force of 1200 N was applied (mild degeneration)

Table 3 Stress distribution of abnormal subject after insertion of screws

Force (N)	Stress after inserting screws for mild degenerated disc (Pa)		Stress after inserting screws for severely degenerated disc (Pa)	
	Minimum	Maximum	Minimum	Maximum
100	1.792e+04	2.150e+05	5.831e+04	6.998e+05
600	1.791e+04	2.149e+05	5.829e+04	6.994e+05
1200	1.784e+04	2.140e+05	5.804e+04	6.964e+05
3400	1.775e+04	2.130e+05	5.780e+04	6.936e+05

Table 4 Stress distribution in normal subjects

Force (N)	Stress without inserting screws (Pa)		Stress after inserting screws (Pa)	
	Minimum	Maximum	Minimum	Maximum
100	1.979e+02	2.375e+03	7.992e+05	8.025e+06
600	2.080e+02	2.496e+03	7.871e+05	8.001e+06
1200	2.495e+02	2.994e+03	7.532e+05	7.871e+06
3400	1.14e+03	1.371e+04	7.326e+05	7.745e+06

stress at L5-S1 region with increase in force is observed in both normal subject and the one with degenerative disc disease.

The boundary conditions are given by constraining the region of stress developed and various force values of 100, 600, 1200, 3600 N have been applied. Force simulations have been imposed with spine in standing positions of the subject static analysis. The bone fusion process can be achieved best using pedicle screws since it is reducing the stress at L5-S1 junction.

4 Conclusion

Degenerative disc disease that affects nearly 30 % of people aged 30–50 years is a serious issue as it leads to severe back pain. With advancement in technology pedicle screws are preferred for treating degenerated disc and spine deformity in spite of screw breakage, loosening and pull out. It is inferred that Pedicle screws are the best implants to reduce the stress developed at the junction of the L5-S1 in disc degenerative disease. However, there is development of more stress on the screw and at the region near the screw. Hence the screws are inserted at the pedicle region. The pelvic parameters under stress conditions can give more accurate results regarding loosening of the screws. By performing comparative stress analysis it is seen that stress is high in normal subject compared to the subject diagnosed with DDD. The positioning of the screw also plays a major role. So the analysis can be performed by placing the screw at different positions. For the patient with abnormal pelvic parameters, first the stress analysis is performed and the region with less stress is chosen for the placement of screws. This reduces the risk of loosening of screws. Analysis has yielded valuable results and stress is high in normal subject compared to the one with degenerated disc.

References

1. Jean-Marc Mac-Thiong P (2011) Age- and sex-related variations in sagittal sacropelvic morphology and balance in asymptomatic adults. Eur Spine J
2. Guan Y (2008) Internal and external responses of anterior lumbar/lumbosacral fusion: nonlinear finite element analysis. J Spinal Disord Tech
3. Znne P (2003) Factors influencing stresses in the lumbar spine after the insertion of intervertebral cages: finite element analysis. Eur Spine J
4. Sharma, Pure flexion extension moments using a pair of concentrated axial loads on top of the upper vertebra. In: Spine surgery, 3rd ed., Chap 22
5. Kumaresan S, Wheeldon JA Pure moments by using a force couple acting on the rigid plate attached to the superior vertebra. In: Spine surgery, 3rd ed., Chap. 22
6. Park (2012) biomechanical effects of the number of ventral fixation rods, with or without dorsal fixation, on the spinal stability of thoracolumbar burst fracture constructs. Spinal surgery 2

7. Jovanovic JD, Jovanović M Lj (2010) Finite element modeling of the vertebra with geometry and material properties retrieved from CT-Scan Data
8. Kang S-H, Kim K-T, Won Park S, Kim Y-B (2011) A case of pedicle screw loosening treated by modified transpedicular screw augmentation with polymethylmethacrylate. J Korean Neurosurg Soc
9. Cho W, Cho SK, Wu C (2011) The biomechanics of pedicle screw-based Instrumentation. Korean Neurosurg Soc
10. Li H (2011) An approach to lumbar vertebra biomechanical analysis using the finite element modeling based on CT Images. In: Theory and applications of CT imaging and analysis, Chap 10, pp 165–180
11. Lehman RA, Kuklo TR, O'Brien MF (2002) Biomechanics of thoracic pedicle screw. Sem Spine Surgery 14(1):8–15
12. Singh Roop, Sharma Sansar Chand, Mittal Rajeev, Sharma Ashwini (2003) Traumatic spinal cord injuries in haryana: an epidemiological study. Indian J Commun Med 28:184–186
13. Prescher A (1998) Anatomy and pathology of aging Spine. Eur J Radiol 181–195
14. Zhang QH, Teo EC (2008) Finite element application in implant research for treatment of lumbar degenerative disc disease. Med Eng Phys 30:1246–1256
15. Adams M, Freeman BJC, Morrison HP, Nelson LW Spine 25:1625–1636
16. Agarwal P, Upadhyay P, Raja K (2007) A demographic profile of traumatic and non-traumatic spinal injury cases: a hospital-based study from India. J Int Spinal Cord Soc 597–602

An Automated Acupressure Glove for Stress and Pain Relief Using 3D Printing

Anjali P. Rajan, A.V. Mulay and B.B. Ahuja

Abstract Acupressure is the non-invasive form of acupuncture; a complementary and alternative medicine based on the concept of life energy which flows through "meridians" in the body and uses point pressure to stimulate acupoints instead of needles. Though acupressure is not a mainstream approach in medical treatment, its efficiency on providing effective relief from stress and strain has held its evidence for ages. There are a range of acupressure devices available, all with the fundamental design of having spiked surfaces; mostly rollers, rods or balls. Time required in achieving relief and manual mode of operation is hindering their popularity. Also as pressure needs to be applied for considerable time, stretching application of pressure by spiked roller/rod/ball causes discomfort and pain, thereby making individual reduce the periodicity of application of pressure leading to less effective relief. Hence the idea of developing an automated acupressure glove was conceptualised so as to develop a simple biomedical device that provides utmost relief from stress and pain with least effort by the user. This new design consists of a dual layered glove and a programmed electronic module. This smart bio medical wearable device provides auto-stimulation of acupressure points on the hands-palm and fingers using pressure build up in the potential chamber developed in between the two layers of the glove. The inner layer is made from a combination of liquid resin material and generated using rapid prototyping based on PolyJet technology. The outer layer is an air proof material and creates a potential chamber for pressure build up in between as both the layers are attached along its margins. The concept design being very simple and smart can be used by anyone and anywhere as it does not require supervision of a medical professional. Following ergonomics at every level of design, the acupressure glove is a revolutionary yet

A.P. Rajan (✉) · A.V. Mulay · B.B. Ahuja
Biomedical Engineering & Technology Incubation Centre,
College of Engineering Pune, Pune, India
e-mail: anjalirmenon91@gmail.com

A.V. Mulay
e-mail: avm.prod@coep.ac.in

B.B. Ahuja
e-mail: bba.prod@coep.ac.in

155

simple biomedical device that is developed from a combination of 3D modelling, rapid prototyping and microcontroller programming.

Keywords Acupressure · Rapid Prototyping · Biomedical · PolyJet technology · Ergonomics · Wearable · Medical devices

1 Introduction

In a world where the tag of being called a patient is always bothersome and to tackle such mentality, medical devices are being redesigned to suit the needs of the user so that they are the master of their devices, be it their gadgets or their medical diagnosis. The core endeavour of this project is to develop a biomedical device that helps the society to obtain utmost effectiveness of Acupressure therapy with a self-controllable device that satisfies the need of each user just as a custom-made solution.

There are a plenty of acupressure devices in the market, mostly based on the spiked design concept. However, the widely used products are those to be operated manually and hence involve more effort and time. Furthermore, the simple designs do not provide the acupressure effect to the fullest. Nevertheless, it requires considerable amount of time and effort to bring out best results and hence cumbersome for usage by the working professionals. The electronic versions of these products are inspired from the concept of massager effect and would necessitate limiting the mobility of the user during its operation. There are a couple of patents on the concept of designing a glove device for providing the acupressure effect [1, 2]. The current device design is not the most advanced model yet is of better potential as the design has scope to be redesigned at different levels of complexity.

Among the various forms of acupressure devices, all proven effective methods require medical supervision or a second skilled practitioner. Majority of the methods that keeps us free from doubts on efficiency involves complex and higher medical technology, towards which the common man always possess a natural inertia. The conventional acupressure objects like spikes rollers, balls and others have their efficiency still on questionable grounds since the application of pressure is patient specific.

In this regard, a medical professional in the field of naturopathy and acupuncture, put forward the need for a user-friendly automatic device for acupressure therapy that can be used at table top, so that the psychological condition of the patient is not affected as during the conventional procedure and its derivatives are performed. The usual practice requires a lot of effort and time by the medical practitioner and witnessing which develops a tiring mentality in the patient too. Thus, after in-depth study, a portable yet effective solution that seemed advantageous over the requirement put forward for a table top device was conceptualised. Designing an automated glove that provides acupressure therapy more effectively and has the potential of being used as a general solution as well as patient specific,

custom made device is developed from the simplest yet smartest methodology that ensures the users of a safe stress buster they can carry and use on the go.

The proposed glove has the following features (1) Wearable with hand-held control (2) Dual layered with inner adaptable 3D printed spike layer and outer pocket that is airtight (3) A safe and compact encased portable electronic unit with a voltage regulator section to prevent excess current from being drawn (4) A durable connective tube for air passage (5) Provision for pressure selection and control and (6) Smart plug- and play-based charging of device.

This basic model suits as an on the go stress buster as it can be miniaturised to a size that can be carried along. It can be utilised for a minimum of 3 times before the battery is drained and the electronic capsule is required to be put to charge.

The material composition of the glove is designed so as to accommodate one's hand comfortably. It is a safe and general solution as acupressure therapy possesses no harmful side effects [3]. The novelty of this concept of automated acupressure glove lies in the potential of this basic model to be modified upon and to prove efficiency at its higher levels of design.

2   Literature Survey

Acupressure, derived from traditional Chinese medicine, is a form of treatment for pain that involves pressure on particular points in the body known as "acupressure points".

Acupressure philosophy is based on the same principles as Acupuncture. Using pressure instead of needles, acupressure works to stimulate specific reflex points located along the lines of energy which run through the body, called meridians. There are 14 main meridian lines, each of which corresponds to an individual organ of the body. When the vital energies are able to flow through the meridians in a balanced and even way the result is good health. When you experience pain or illness it is an indication that there is a block or leak in the energy flow within your body [3]. Acupressure is a very powerful technique and most of the ailments are relieved by it.

Following the need that arose from the side of medical practitioner, an in-depth background research was done on acupressure therapy, the different forms and available devices. It was put forward by a naturopath and acupressure therapist the need for a user-friendly device that reduces the time consumed and effort that is otherwise required to be taken during treatment. The conventional methods require time and effort to be taken by the clinician and portability and effectiveness does not go hand-in-hand. Acupressure is mostly used as a complementary or parallel form of treatment to enhance recovery. Since the aim was to make the process simpler, a variety of self-operated devices was studied. The effective methods always involved medical supervision or higher technologies. The structural and functional aspects of the acupressure devices available in the market were researched upon. The most commonly used portable devices were acupressure rollers, balls and rods. The designs

were more or less the same or just slight modifications of the same concept of closely spaced spikes of wooden or hard rubber materials. The electronic versions were more of massagers, which were again not again a carry along kind of devices. Some other methods of using magnets in association with the therapy is not advisable as they cause exhaustion to the particular area of the body on prolonged exposure to it.

A number of patents in the field of acupressure devices were also studied, along with the market study to provide the background information and hence shed light on the significance of the benefits and novelty of the current invention [4, 1, 2, 5].

Among the self-administered devices that are in the form of a glove, US Patent No. 5405357 is an "Acupressure glove device" that facilitates self-stimulation of acupoints using direct pressure. This involves selective placement of nodules that presses against the acupoints [2]. This requires manual effort and hence does not provide the benefit of minimising time and effort taken.

Another is U.S. Pat. No. 5067478, a glove attached to a transcutaneous electrical nerve stimulation unit (TENS) that is used to provide TENS, massage or acupressure to a second person by a skilled clinician. The in-built detriment of this form lies in its necessity of a second skilled person to administer. Also, rather than stimulation of specific points it provides a general electric current through the hand which may in turn cause superficial burns.

U.S. Pat. No. 4233966 is an "Appliance for Use in Acupressure Therapy" that consists of protuberances contained holder that involves applying finger pressure required to produce pressure on particularised areas. The limitation of this invention where the user is to lay atop the holder is its requirement of the user to have sufficient knowledge on the anatomical landmarks and acupressure therapy.

U.S. Pat. No. 4520798 is a wall-mounted acupressure apparatus with adjustable arms a knob for pressing against with one's body. The constraint here is its non-portability and the requirement of knowledge about anatomy and location of acupressure points. Further it does not include the acupoints on the hand.

After the much comprehensive survey and evaluating the existing solutions from various aspects, it was analysed that each invention had its own share of pros and cons over one another.

A summary of the analysis drawn on comparison of the real requirement over the features of the available devices resulted in formulating the desired functional and structural parameters of the invention as follows.

2.1 Requirements to Overcome Current Challenges

- Covering majority of acupoints on the palm.
- Least effort and time expended.
- Efficiency with least complex mechanism.
- Optimum pressure that the effect produced hurts good.
- Ergonomic and Modular Design.
- Durability.

2.2 Desirable Features

- Automated solution that reduces time and effort.
- Minimising the size of the device that it is compact and portable.
- Pressure control provision.
- Safe preset pressure limits.
- Easy charging.
- Simple and smart operation.

The extensive literature survey, experiments and medical consultation resulted in collaborating various techniques to build the basic model which has scope of being a device with higher potential and advancement.

3 Project Idea

In relation to the concept of reflexology, acupressure works based on the principle that all organs have their respective connection points on the palm and feet, and so application of pressure at these points would eventually clear the blockage in the corresponding organ. During treatment, physical pressure is applied to acupuncture points by hand, elbow or special devices [3].

Syncing portability and effectiveness was the key to curb the problems of time and effort consumed for the therapy. Hence, designing a wearable was the solution to an effective self-administrable method of acupressure therapy. The uniqueness accounts to the simple method to apply pressure over controlled time, release and to reapply pressure.

Collaborating advanced technologies of 3D modelling, Rapid Prototyping, medical electronics and ergonomics, an automated biomedical device is conceptualised that facilitates acupressure therapy with utmost effectiveness. The device is designed in the form of a dual layer ergonomic glove with an external compact electronic module connected to it. The basic mechanism involved being that the steady and continuous pressure build up and release in the internal chamber between the two layers of the glove, that in turn causes the spikes of the inner layer to press onto the acupoints when inflated and release from contact with acupoints when deflated. This continuous cycle facilitates auto stimulation of acupoints.

The basic idea of the automated acupressure glove is to revolutionise the trend of ergonomic concepts of the conventional medical techniques for acupressure therapy devoid of the need for medical supervision.

3.1 Mechanical Design

- Dual-layered glove
- Spiked Inner layer to face palmar and dorsal area of hand palm

- Expandable material to contain range of sizes
- Air proof Outer Pocket
- Compactly cased electronic module
- Ergonomic design using lighter weight counterparts

3.2   Medical Design

- Exert optimum pressure at acupoints to provide acupressure therapy effectively.
- Pressure control provision with a preset safer upper limit as pressure threshold varies with age.
- Safe material composition that does not cause irritation and other negative impact due to use in contact with the skin.

This project presents a design overcoming the drawbacks in designing a smart biomedical device with perfect ergonomics and hence grows into an affordable potential innovation in the smart wearables category.

4   Design Methodology

The design of the automated acupressure glove comprises of a mechanical and electronics section. Based on in-depth study on the structural and functional requirements, they were formalised as described in the following sub-sections.

4.1   The Glove

The hardware design is further divided into the mechanical unit and electronic unit.

The Glove forms the mechanical section. The glove was engineered to be a dual-layered unit with each layer unique on structural and functional specifications. The inner layer was designed based on dimensions of a surgical glove designed for loose-fit. The sketch of a normal glove was taken and dimensions were sketched onto a graph paper so as to obtain accurate measurements for the designing using CAD software. An outline of the palm was reconstructed more accurately and neatly by converting the sketch into those with accurate arcs, lines and angles at the areas of curvature (Fig. 1). The inner layer being the most crucial layer from medical aspects was designed using the Autodesk Inventor Professional software (Fig. 2). The design involves a basic sheet of 2 mm thickness in the shape of the outline of a palm (Fig. 1). Over the base layer, a series of spikes are constructed.

Fig. 1 Base sheet of inner layer reconstructed from original glove sketch
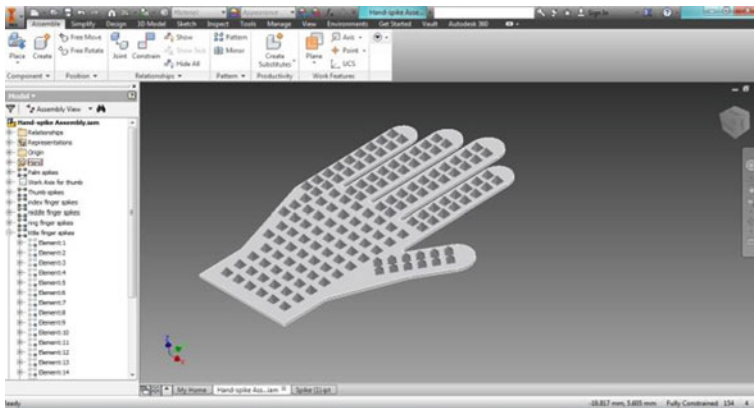
Fig. 2 Isometric view of spike layer

These spikes were chosen to be of square pyramid structure of 6 mm height, over a wide range of geometries studied to provide pressure exertion onto the points on the palm. After consultation with medical professionals along with the research on currently available acupressure devices, it was concluded that the square pyramid structure with a slightly blunt tip was the most effective for acupressure therapy.

Fig. 3 A 3D printed inner spike layer prototype
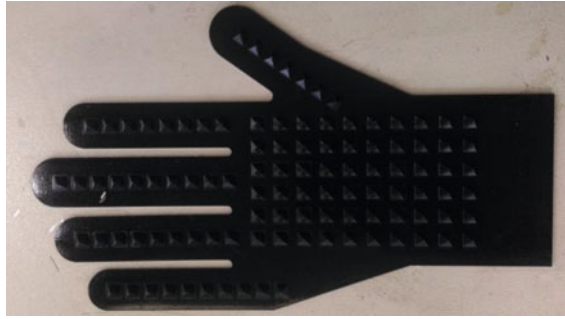
The 3D model developed using Inventor software was then printed using Stratasys Connex 350 (Fig. 3). The 3D printer that uses PolyJet technology helps creating rapid prototypes with a variety of material combinations. The palmar layer was printed with base sheet of shore hardness A50 of Tangoblack+material, which is a kind of rubber material. The spikes were made with shore hardness of A90, which is tougher (Fig. 3). For the dorsal layer which was designed by mirroring the palmar layer, the spikes were assigned material of lower shore hardness of A70. The two layers are to be joined into a single glove by sticking it onto an elastic material like nylon spandex, which then forms a glove.

The outer layer has the purpose of providing bounding for the potential chamber into which the air pressure is allowed to build up. The outer layer should be airproof so that the pressure is controlled only via the programmed unit. It is suggestive of material like neoprene or Teflon hybrid fabric that is airtight. The two layers are sealed along the margin of the hand palm outline forming a dual-layered glove that acts as a single unit.

4.2 The Controller Unit

The other hardware counterpart of the product is the controller unit. This comprises of all the electronic elements for the functioning of the Acupressure Glove . It consists of an arduino programmed unit, a Lithium Polymer battery (LiPo), a mini air pump and solenoid valve.

The LiPo powers the whole unit. A mini air pump of maximum output pressure of 1.5 bar acts as the source of pressure and the solenoid valve serves the purpose of exhaust valve. The electronic circuitry is basically designed to work on a timer mechanism that facilitates pressure build up and release in a cyclic manner. A switch is provided for switching on/ off the system and a knob is provided for pressure control using which the user can vary through a range of pressure and choose the desired level of pressure one is comfortable with. A pressure sensor of BMP085 is used for the calibration. The upper threshold of the pressure is set to

safer limit of 1.2 bar which is not harmful to the human body. It is programmed to cause inflation for 5 s, hold the pressure for another 5 s and followed by releasing the built-up pressure, which takes about 4 s.

At the base of the glove, an opening is provided that lets a plastic tube to be inserted. The tube is the element that connects the electronic unit to the glove. The tube ends in the gap between the two layers of the glove. On activation, the pump exerts pressure through the tube causing the pressure to build up in the potential chamber. This inflates the chamber which in turn causes the spikes of the inner layer to press against the acupoints and stays intact for duration of 5 s. Following this, the chamber then deflates as it releases the pressure built-up via a solenoid valve and gradually causes the spikes to release from tight contact with the skin. This process repeats continuously and steadily until the user switches off the system.

The entire unit works based on an arduino programme that runs to inflate/deflate the glove in a continuous and rapid manner causing auto stimulation of the acupoints. A simple timer mechanism with an upper threshold set to 1.2 bar after calibration, it ensures the device to be a safely operable. Programming includes one that was used for calibration of pressure sensor and another for controlling the motor speed.

4.3 Integration

The inner spike layer set of palmar and dorsal pieces are pasted onto an elastomer fabric, like nylon spandex with its outline bigger than that of the outline of the hand on which the spikes were designed on, so as to include the thickness of the layers and an average human palm to be contained in between them. This can be done by considering the height of the printed model (height of Base sheet + height of spike = 2 mm + 6 mm= 8 mm) and then providing clearance enough for a hand to be inserted in such a way that the spikes of dorsal piece would be in contact with the upper side and that of the palmar piece would be in contact with the palm. This glove can be fabricated so, by providing openings along the edge of the thumb and tiny finger from the base of the cloth, which can be closed using Velcro or zip.

The electronic module, comprising of the power source, air source and microcontroller with the electronic circuitry is encased to form a compact module with openings on the surface for battery outlet, the switch, tube and pressure control knob (Fig. 4). The casing for the electronic module is again printed using 3D printing based on fused deposition method, wherein the model is developed from fusing the wire of ABS plastic.

A durable plastic tube connects the controller unit to the glove, which can be detached when the battery needs to be charged. Since the power source is embedded in the casing, only the controller encasing need to be plugged in to charge.

Fig. 4 Assembly of basic functional prototype

5   Results and Discussions

Following several clinical survey and design experimentation, the requirements specified by acupuncturist led the research to redefine the problem as a smart wearable—an automated (with facility to choose the desired level of operation), making it portable as well as effortless. Designing the inner layer of the dual-layered glove was taken up after gaining an insight into the acupressure and reflexology concepts, and review of existing devices.

After consultation with medical professionals, it was concluded that providing a general uniformly spaced array of spikes would cover 80 % of the acupoints distributed on the palm. Next aspect of research was the geometry of the spike. Conical and square pyramid spikes of varying hardness and dimensions were printed to select the most appropriate geometry. The geometry required to be one that provided a pressure that hurt good, i.e. a feeling between firm and outright pain, when the spikes were pressed against the acupoint. The pressure requirement varying from person to person and among acupoints too led to choosing a square pyramid geometry of dimensions that let the sufficiently blunt tip to exert optimum pressure when pressed against the skin. The variety of materials for the outer layer, which needs to be airproof was tried. A number of design concepts were evolved, and a rapid prototype was fabricated in flexible (elastomer) material (Fig. 4). The electronics were also developed, which involved integrating the pressure source and microcontroller programming to enable pressure build up as well as release. The effectiveness of this automated acupressuredevice is theoretically proven advantageous over the currently available and affordable devices in the market for the purpose of self-use that are moreover just a supportive therapeutic device, since its significance has not been proven sufficient to gather the social beings into trusting this generations old form of medicine.

Advantages of the automated acupressure glove over the prior art products are as listed:

- Inexpensive
- Portable
- Ease of usage: Automated and zero complexity makes it a threat-free choice of a device for stress/pain relief and a device for the common man as they can be free of fear from the complexity or related dangers of an electronic product.
- Flexible usage and size: The expandable rubber material of inner layer makes it suitable to incorporated a range of palm sizes and; provision to chose and set desired pressure level to be applied enables flexible usage as patient can reduce or increase pressure at any point of operation.
- Ergonomic design: The materials used being soft and durable promotes portability as it is lighter among the counterparts.
- Compact
- Customizable
- Least effort: The wearable with its external electronic unit and the operation/working of which can be controlled by the user by merely using a knob.
- Lesser time consumed: Including that needed to go up to the doctor, taking an appointment, the time to carry out the treatment and the follow-up.
- Simple mechanism: The exclusion of any complex technology enables its use by any individual without the requirement of a medical professional.
- Safe operation: The voltage regulator acts as a protection from excess current being drawn by the motor, so does the pressure control provision provide user to select desired pressure value. The voltage protection circuitry disables the unit if at all the maximum limit of current draw is crossed.

Unlike most other case studies where effectiveness of acupressure therapy was established through randomised controlled trials, the product developed here is decided to follow standard clinical trials to draw more accurate experiment results.

For future advancements, the first improvement to be made in this model to its next level of design would involve minimising the size of electronic module using a double headed micropump that would provide the same required pressure despite of its small size. Next would be fabricating the glove as a single mould using injection moulding, which can be put to practice only while converting this idea into a new product line in the market. The advanced technology of 3D printing has facilitated development of prototypes within a minimum time period. Facing challenges at different levels of development, starting from the validity of concept to procurement and miniaturising the size of the device, the basic model was finally implemented as a functionally sound product, which now awaits clinical trials.

6 Conclusions

Designing a device to effectively provide acupressure therapy without consuming time and effort has been the aim of redesigning the acupressure devices for ages. By this project, a solution to the majority challenges in the acupressure devices is conceptualised and itself have made its first step into the field of wearables. This simple compact device in its very basic prototype form has proved its efficient functioning and durability through its smart and simple working mechanism.

In short the following are the limitations in the previous products which were overcome with this invention:-

(1) The effective products and methods are time-consuming and requires more effort; The completely automated operation of this invention with provision for pressure control by user solves this limitation.
(2) Other effective products and methods involve complex techniques and require supervision of medical professional; A predefined rate of air flow into the predefined volume of chamber is the simplest means to achieve effective compression and relaxation of the chamber that ultimately facilitates acupressure therapy.
(3) Simpler devices in market are mostly the same basic design and stimulation of acupoints is not facilitated with maximum effectiveness. The unique and modular design makes it more ergonomic and reliable with the benefit that it can be carried along.

The automated acupressure glove has a 3D printed inner layer that is a rubber hybrid material and hence flexible to accommodate a wider range of sizes. Again, the consistent collaboration and discussion with medical professionals shed light in deciding the duration of pressure application and other medical aspects. The provision of pressure control with the safer upper limit already set adds on to the user friendliness and usability to varying age category. But, only following the statistical analysis drawn after clinical trial can the upper threshold for each category be decided so as to provide an in-built safer limit for each age category. The pump used facilitates pressure build up rapidly in the volume of pressure chamber between the two layers of glove with its flow rate of 3 litres per minute. This facilitates the volume of the hand to be covered in just a matter of seconds.

An ergonomic on-the-go usable medical product is hence invented using the collaboration of advanced technologies of 3D printing, CAD modelling, medical electronics and microcontroller programming. Having implemented the initial model, this concept has already discovered its scope of advancement into a perfect ergonomic wearable medical device with a customisable potential.

7　Future Scope

With the wearable medical devices growing as the next big thing in the global market and the prevailing trend of wearable electronics, the need for engineering a solution for the need of the hour increasingly demands simplicity, portability and ergonomics just as much as the functional priorities of any biomedical wearable device. Living in an era where the work-obsessed humans do not prefer medical consultation unless and until the health condition starts to take over their physical productivity, our concern should be in redesigning medical devices from that which requires a medical supervision to a form where it can be self-administered. This is where the Complementary and Alternative Medicine, the simplest and yet effective one of which, Acupressure, can be one's saviour.

The core potential of this concept lies in its design, capable of transformation from a general device to a customizable one. The concept discussed above being just the basic functional prototype (Fig. 4) implemented, this automated acupressure glove can be modified to form a much advanced model which can reasonably revolutionise the concept of acupressure devices.

All the further enhancements formulated being patented along with this basic demonstrative model, this design provides a modular template onto which a number of mechanisms can be experimented to provide acupressure therapy in an effective manner. Redesigning with predefined tracts for passage of air, using piezoelectric, electromagnetic effect within safer limits and using microelectronics are some of the areas where development foresees potential scope. Provision for external medium for selection of particular areas of acupoints is another method that can be incorporated to facilitate auto stimulation of acupoints of a desired area alone.

References

1. Gavish S, Abramson G (2011) U.S patent US 20110178360 A1. Acupressure magnetic therapy glove, 21 Jul 2011
2. Rowe-Lanzisera L, Lanzisera F (1995) US 5405357. A Acupressure glove device, 11 April 1995
3. Reed Gach M (1990) Acupressure's potent points. Bantam Books, Dec 1990
4. Yoo TW (1995) U.S Patent US5405310 A. Acupressure gloves adhered acupressure devices. 11 April 1995
5. Akcasu F (2012) US 8292915 B2 Hand-held acupressure device, 23 Oct 2012

Development and Optimization of Dental Crown Using Rapid Prototyping Integrated with CAD

P.J. Kale, R.M. Metkar and S.D. Hiwase

Abstract Conventionally dental crown manufacturing was done by investment casting. This work presents the Rapid Prototyping as a best tool for dental prosthesis and crown manufacturing. It also represents the static structural analysis of dental crown with FEM software, ANSYS 14.5. Crown Models are constructed with dental wings client software and mimics. FEM compatible models were constructed using Remeshing and Volume meshing tool of 3-matic software. Masticatory force 350 N was applied downward perpendicular to surface of molar crown with boundary conditions. Five materials such as Ti-6Al-4V, Stainless steel, Cobalt-Chromium, Zirconia and Titanium are selected for analysis. Zirconia and Cobalt-Chromium are found to be the best materials amongst the five. ANSYS results show that the optimum crown thickness ranges from 1.75 to 2.25 mm. Directional deformation is very less for the crown model developed with dental wings. Tooth preparation is the main parameter which affects the strength of crown 3D printing is the most promising tool for Dental Prosthesis manufacturing. It can be manufactured with selective laser sintering, ink-jet printing. This model is manufactured with Desktop CNC milling in Cobalt-Chromium metal.

Keywords Dental · Crown · CAD · ANSYS · Meshing · Zirconia · CT scan · MIMICS

P.J. Kale (✉)
Mechanical Department, Jawaharlal Darda Institute of Engineering & Technology,
Yavatmal 445001, MS, India
e-mail: pankajkale888@gmail.com

R.M. Metkar
Mechanical Department, Government College of Engineering,
Amravati 444604, MS, India
e-mail: rajeshmetkar@yahoo.co.in

S.D. Hiwase
Samrachana Software Solutions Ltd, Hyderabad 500005, India
e-mail: hiwases@gmail.com

1   Introduction

Rapid prototyping is generally known as the 3D printing technology. It manufactures any complex-shaped component provided it must have a 3D CAD model developed. This technology is mostly helpful in medical field where it is impossible to manufacture the human body implant by any means of conventional mechanical manufacturing processes. Stereolithography was the first 3D printing system introduced in 1987. Till today lots of research is done in the field of RP machine and material. Owing to its advanced techniques and materials, it can also manufacture the metallic part. 3D printers help to manufacture any complex shape component without tooling.

Today this technology is used for manufacturing of mandible implants made from titanium. This 3D printed model helps Doctors for dental surgery and dental implant fixation and exact positioning. This paper gives the alternate procedure to get the 3D CAD model of the crown. This process integrates the old process with a new one and reduces the complexity, time and cost. Rapid Prototyping Dental CNC desktop milling system is used to manufacture the functional crown. This 3D printed crown is ready to fit in patient's mouth after post processing treatment. EOS companies EOSINT M 270 3D printer manufacture metallic implant with titanium Ti64 and Cobalt Chrome SP_2. Any biocompatible material can be used for dental crown manufacture with 3D printing but requirement is that material in powder form. Layer thickness and particle size decide the surface finish of the crown, and post processing treatment. FEM is the best tool for the analysis of any system before going to actual manufacturing. ANSYS provides direction for correcting the design of the system at early stage.

2   Methodology

The methodology adopted for dental crown design, optimization and manufacturing is given in Fig. 1.

Today lots of dental lab, manufactures tooth crowns manually. This total process requires minimum 2 weeks to deliver it to patient or doctor. During that time period, doctor provides the temporary crown with stainless steel material. This temporary crown cannot be used in mastication process. Patient faces various problems with this temporary crown during this period of manufacturing of crown.

Each human tooth has different surface profiles. But the tooth profile for the all humans with same tooth is nearly same. Maximum enamel thickness range for molar tooth is 1.5–2.5 mm, which is maximum as compared to other teeth. Two types of crown model are developed for analysis. One model developed with actual scan of cast model and second with CT scan. 3-matic software is used for the model preparation for FEM analysis. In boundary conditions, base and side surface were made fixed and 350 N downward masticatory force were applied. Analysis is

Fig. 1 Methodology


```
Identification of Problem
        ↓
Data Collection
        ↓
Developement of Crown Models
        ↓
FEM Model Preparation for Analysis
        ↓
Selection And Application of Boundary
Conditions
        ↓
Fem Analysis with Ansys 14.5
        ↓
Manufactured with R P Technique
```
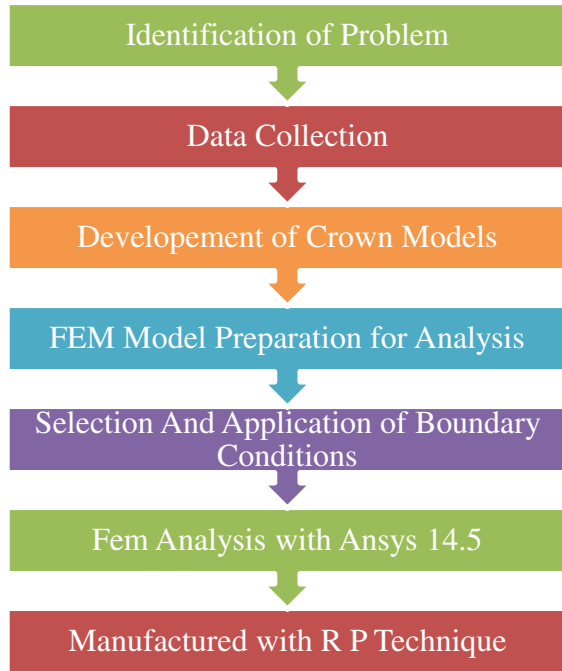
completed in ANSYS Workbench 14.5. Crown developed with dental wings client software is manufactured with Desktop CNC milling for time and cost analysis.

3 CAD Model Development with 3D Scanner

3D laser scanner was used to get the geometry of the existing model but the requirement is to get the missing geometry. Patient's cast model of mandible and maxilla were scanned using dental wings 3S series laser scanner. The data capture was used to get the crown for particular tooth with the help of dental wings client software. Dental wings client software provides the necessary tool for model development. Steps to get 3D CAD model after cast model developed is shown in Fig. 2.

As shown in Fig. 1 total dental cast model after selecting tooth number is scanned using 3S laser scanner. Only half portion of teeth layout is selected for the further processing which contains the prepared tooth. Reason behind to select only half portion for further processing is to avoid unnecessary processing time and memory. Some points are selected for the positioning of upper tooth profile with lower one. Shoulder and Ditching Optimization tool is used which places the Green margin line automatically. Software containing CAD tool in which final prosthesis, i.e. crown model is developed and exported as .stl
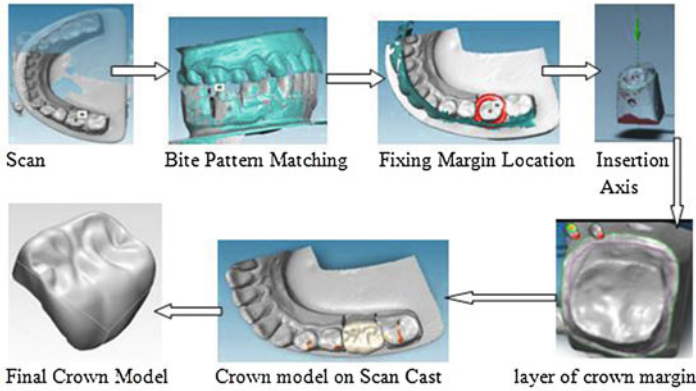
Fig. 2 Crown developed on dental wings client software interface

4 CAD Model Development from DICOM Images

CT scan images were imported in MIMICS software. Thresholding was used for the separation of other body tissues from required part. Automatic thresholding is used for Enamel. The thresholding value ranges from 1553 to 2850. 3D model is developed for the enamel parts. It includes all the teeth with mandible and maxilla part. Single molar tooth is separated from total 3D model of teeth using lasso tool, which separates mask in 3D. This 3D molar tooth is exported to .stl file format (Fig. 3).

Molar 3D model is imported to 3-matic software. Different thickness crowns are developed with Wrapping command and some Boolean operations. Figure shows the sequential procedure for the crown model development. The molar tooth model of .stl file is imported in 3-matic. Tooth is wrapped with required thickness. The section plane had drowned with required height. Molar tooth is cut through the section line. Boolean operation subtraction is used for the crown model development. The crown model are developed with 1, 1.5, 1.75, 2, 2.25, 2.5 mm

Fig. 3 Steps to get crown model in 3-matic
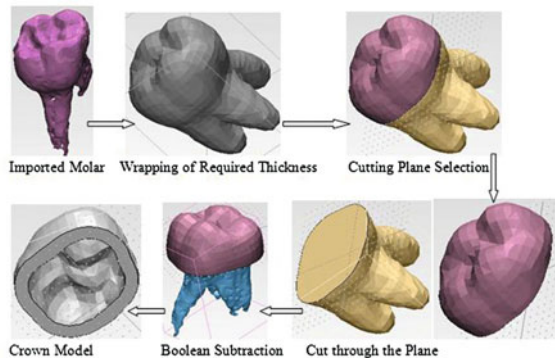
Mimics model   Mimics model After Remeshing
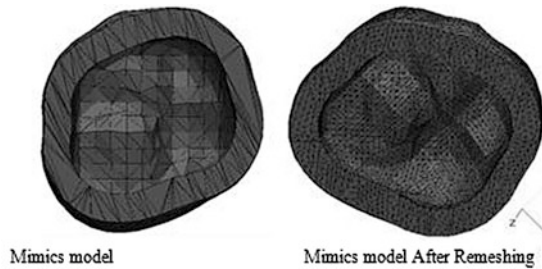
5 FEM Model Preparation with 3-Matic Software

The model was constructed with Dental wings Client software and MIMICS and both the models had triangular meshing with irregular edge length. The remesh operations enable quickly and easily transform badly shaped triangles into more equilateral triangles (Fig. 4).

The more geometrically regular triangles are the better and more reliable for the results of the FEA. Volume meshing is used to convert surface meshing into solid. Converted volume mesh has element type Linear Tetrahedral, its name in ANSYS APDL is Solid 185.

6 Static Structural Analysis

The geometry of crown model is exported in ANSYS compatible file format which is of .cdb. This file is imported through FE modeller. FE modeller helps to divide the geometry for the application of boundary conditions. Crown model is divided into four parts and given different names. Four parts are base part, two side parts which is in contact with adjutant tooth and top surface of crown. This FE model is updated and transformed to the Static Structural Analysis tool of the ANSYS workbench.

Engineering data were set for the analysis. Table shows the material and material properties were used for analysis. Out of this five material Ti-6Al-4V, Cobalt-Chromium and Titanium are available in powder form and can be manufacture using selective laser sintering technique. Zirconia can be manufactured using CNC desktop milling which is subtractive RP machine (Table 1).

After THE addition of material, boundary conditions are applied. Side surface and base surface were made fixed, where 350 N force is applied on the crown top surface which is acting in the downward direction. Three parameters were selected for analysis, i.e. total deformation, directional deformation and Von Mises stress. Following figure shows the ANSYS results for the crown constructed with dental wings client software for material Cobalt-Chromium is Shown in Figs. 5, 6 and 7.

Following figures shows the ANSYS results for 3-Matic Crown Model with 2 mm Thickness (Figs. 8, 9 and 10).

Table 1 Material properties

Material	Young's Modulus GPa	Poisson's ratio (μ)	Density (ρ) kg/m³
Ti-6Al-4V	113.8	0.34	4430
Stainless steel	200	0.285	7750
Cobalt-Chromium	230	0.30	8500
Zirconia	200	0.22	5680
Titanium	110	0.33	4510

Fig. 5 Total deformation in dental wings crown model
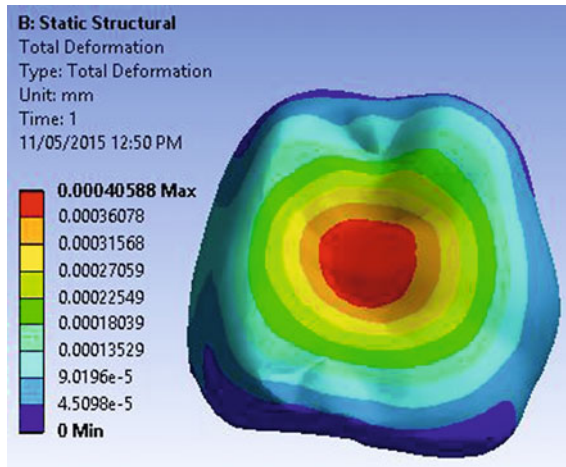
Fig. 6 Directional deformation in dental wings crown model
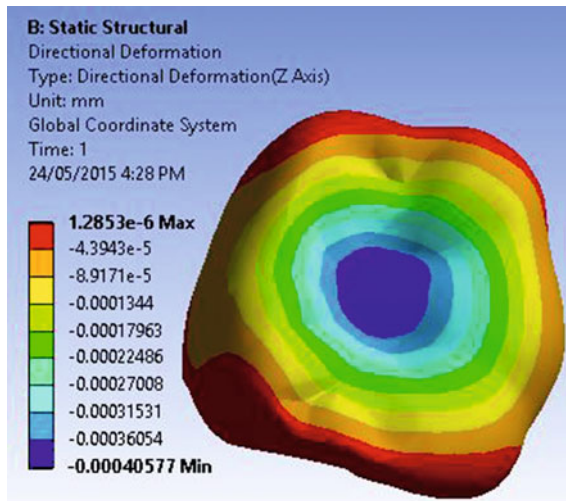
Fig. 7 Von Mises stress in
dental wings crown model
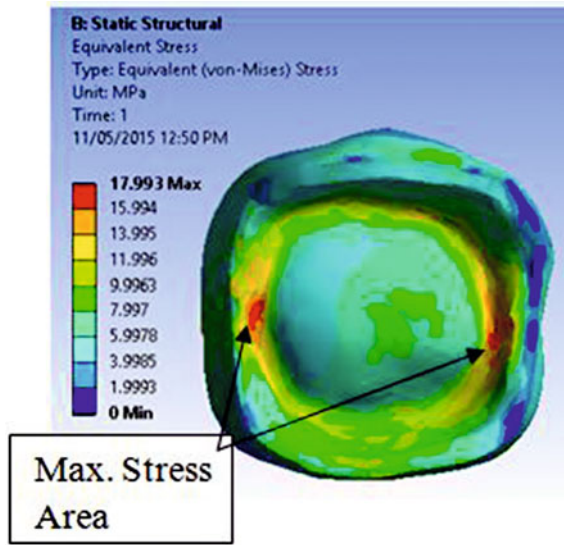
Fig. 8 Total deformation in
3-matic crown model with
2 mm thickness
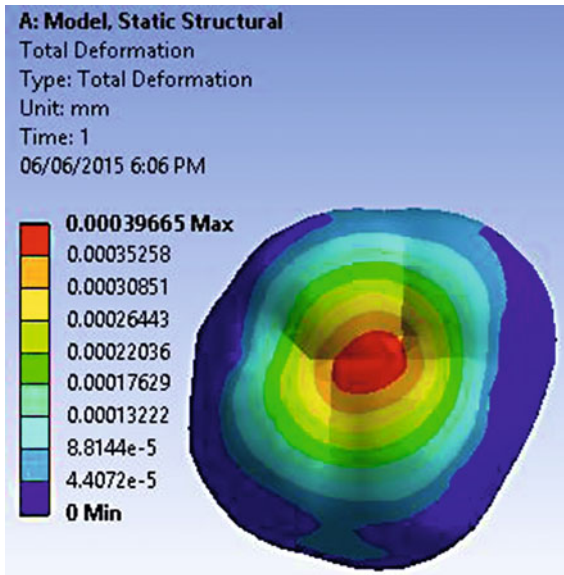
7 Result and Discussion

Total analysis is done for 7 Crown models. Each model was solved with five
materials. Comparison is done for the 1.75, 2, 2.25 mm, and crown model developed with dental wings client software (Tables 2, 3 4 and 5).

Fig. 9 Directional
deformation in 3-matic crown
model with 2 mm thickness
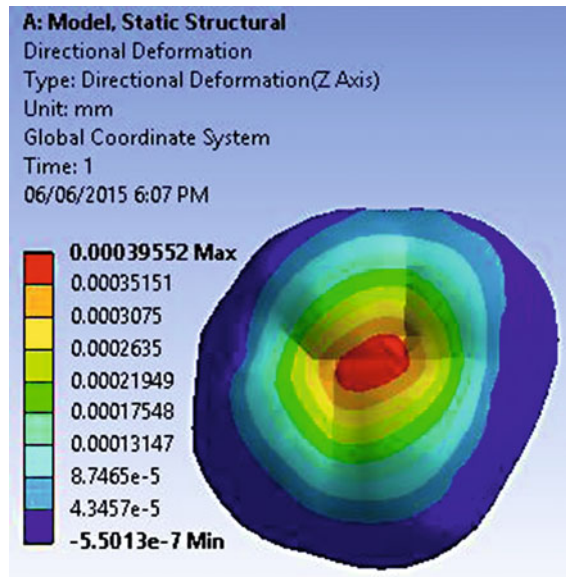
Fig. 10 Von Mises stress in
3-matic crown model with
2 mm thickness
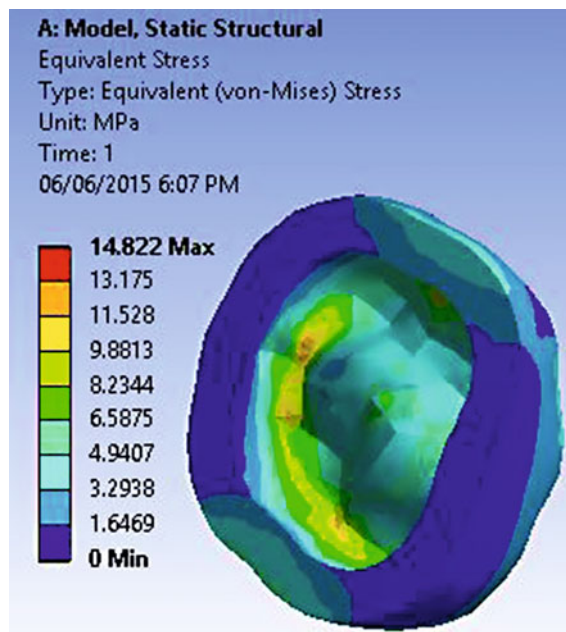
Table 2 Results for dental wings client crown model

Material	Mass (kg)	Total deformation (µm)	Directional deformation (µm)	Von Mises stress (MPa)
Ti-6Al-4V	1.3651	801.21	1.927	17.345
Stainless steel	2.3881	470.7	1.628	18.239
Cobalt-Chromium	2.6192	405.8	1.285	17.663
Zirconia	1.7503	482.9	2.3297	19.536
Titanium	1.3897	834.4	2.1627	17.506

Table 3 Results for 1.75 mm thickness crown

Material	Mass (kg)	Total deformation (µm)	Directional deformation (µm)	Von Mises stress (MPa)
Ti-6Al-4V	2.3535	1025	1024	14.93
Stainless steel	4.1174	605.6	604.8	15.5
Cobalt-Chromium	4.5158	522.0	521.4	15.35
Zirconia	3.0176	622.8	621.8	16.10
Titanium	2.396	1096.6	1068.5	15.04

Table 4 Results for 2 mm thickness crown

Material	Mass (kg)	Total deformation (µm)	Directional deformation (µm)	Von Mises stress (MPa)
Ti-6Al-4V	2.7978	776.9	774.9	14.073
Stainless steel	4.894	460.69	459.32	15.088
Cobalt-Chromium	3.3682	396.6	395.5	14.822
Zirconia	3.5872	476.5	475.0	15.18
Titanium	2.8483	810.7	808.5	14.26

Table 5 Results for 2.25 mm thickness crown

Material	Mass (kg)	Total deformation (µm)	Directional deformation (µm)	Von Mises stress (MPa)
Ti-6Al-4V	3.2673	727.7	726.0	11.858
Stainless steel	5.7156	430.3	429.4	12.709
Cobalt-Chromium	6.269	370.7	370.1	12.485
Zirconia	4.1892	445	442.9	13.657
Titanium	3.3263	758.9	757.82	12.02

8   Graphical Interpretations

Figure 11: mass variation with material and thickness. Model constructed after tooth preparation has mass as compared to other model. The thickness of the Dental wings model ranges from 2 to 2.25 mm other model constructed with mimics software have even thickness, hence there mass increases with increasing thickness of the model.

Figure 12: variations in total deformation with different crown thicknesses. Total deformation is maximum for 1.75 mm and minimum for 2.25 mm thickness. Total deformation of Dental wings model matches with 2 mm thickness crown.

Figure 13: variations in directional deformation in downward direction with different Crown thicknesses and materials. Direction deformation is reduced for Mimics model with less value but for dental wings model it reduces up to 2 μm, i.e. negligible.

Figure 14: Indicates the variations in von Mises stress with different crown thicknesses. Maximum stress pattern is observed on top surface of the Mimics model and it is concentrated at centre. Maximum stress value is observed in dental wings model but area for the maximum stress as compare with mimics model is very less.

Fig. 11 Comparison of mass of materials with thickness
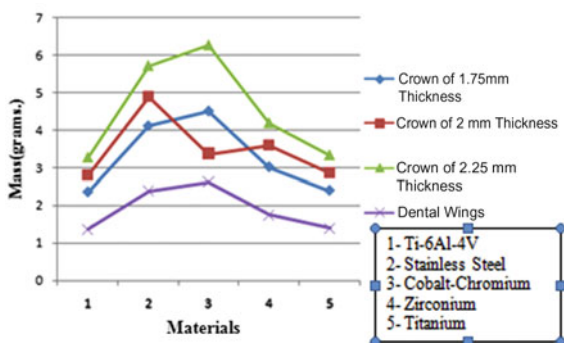
Fig. 12 Comparison of total deformation of materials with thickness
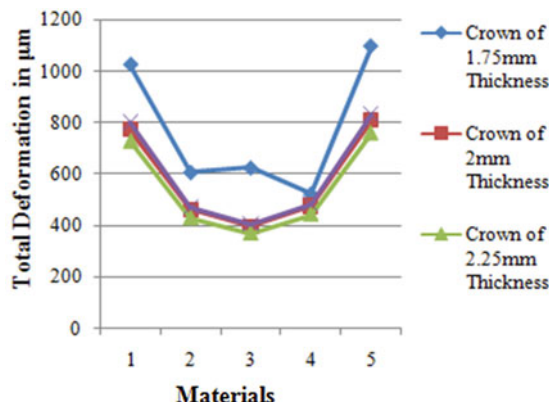
Fig. 13 Comparison of directional deformation of materials with thickness
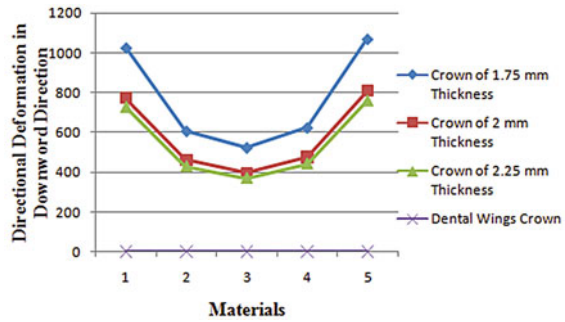
Fig. 14 Comparison of von Mises stress of materials with thickness
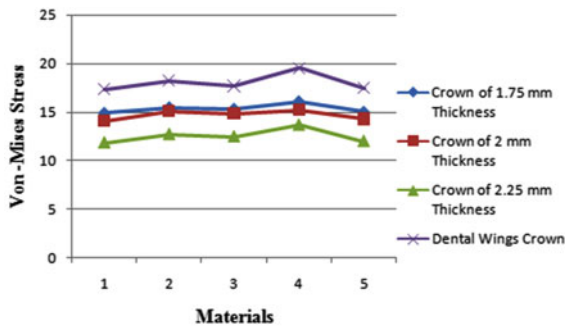
When the results of three models are compared with Dental wings crown model, the stress is more in Dental Wings model but that maximum stress occurs at small section which is shown in Figure. It is also very less compared to yield stress. This maximum stress area can be reduced by increasing small amount of material at that place. The stress value ranges from 17.345 to 19.536 M Pa. Designed dental crown model with Dental wings client software is the optimum design. Directional deformation in downward direction is negligible. Also crown profile exactly matches with upper tooth and gives perfect bite pattern. Also mass is less as compared to alternate crown model. Results show that tooth preparation is important step for crown designing. It affects the strength of the crown and hence teeth also. The variation of the von Mises stresses is very less. Material does not affect the selection of crown. Total deformation and directional deformation are nearly same for the model constructed with Mimics software.

9   Manufacturing of Dental Crown

Zirconia and Cobalt-Chromium are the best materials among the five materials. Model developed with dental wings client software is manufactured from Imaginarium India Pvt. Ltd. Mumbai. The cost for single crown is nearly about Rs.

Fig. 15 Manufacture
Cobalt-Chromium crown

800–1000. It is manufactured in Cobalt-Chromium. Manufacturing of zirconia is very simple as compared to other material. Manufacturing cost of zirconia single crown is minimum Rs. 2000 (Fig. 15).

10 Conclusion

ANSYS is the good software for structural analysis of the system. Result pattern of the actual patient specific model with dental wings client software matches with MIMICS model. Directional deformation is negligible in Dental Wings model. Tooth preparation plays a very important role to give strength to crown. The maximum stress for Cobalt-Chromium and Zirconia, respectively, is 17.663 and 19.536 Mpa. The area for maximum stress is very less and it can be removed by doing small changes during tooth preparation. The directional deformation is negligible in Dental wings model. Grzegorz Milewski is the researcher from Institute of Applied Mechanics, Cracow University of Technology, Poland. He performed FEM analysis for molar tooth and validated it with actual experimentation with strain gauge and found 12 % error between ANSYS result and actual experimentation. This error may also reduce if experimental setup and surrounding environment are monitored as per boundary condition of human tooth. The values obtained from stress analysis are very less from breaking stress. From this, it is clear that result obtained with ANSYS is acceptable. It is impossible to develop CAD model of tooth with any CAD design software. This methodology can be used for the development of 3D model for dentistry and human body part. Cobalt-Chromium is the good material if cost matter otherwise zirconia is the best for single crown. Its dimensional accuracy is very high.

11 Future Scopes

In the present work, static structural analysis of molar crown for stress stain analysis is done with ANSYS. Results obtained are verified with the results obtained by previous researcher with molar tooth analysis. Not a single researcher applied FEM

tool for tooth crown strength analysis. In future, if tooth crown fatigue analysis is performed, it will help to know the life of crown and factor affecting to reduce the crown life. Today's Crown life is nearly about 10–15 year, it may extend after this analysis. Also the strength of 3D printed crown and investment casting crown can be analysed only with experimental analysis. Experimental analysis is required for this because the grain structure may vary due to manufacturing process.

References

1. Bammani SS, Birajdar PR, Metan SS (2012) Dental crown manufacturing using stereolithography method. In: Proceedings of international conference on advances in industrial and production engineering 2012
2. Chougule VN, Mulay AV, Ahuja BB (2013) Three dimensional point cloud generations from CT scan images for bio-cad modeling. In: Proceedings international conference on additive manufacturing technologies—AM 2013
3. Baradeswaran A, Joshua Selvakumar L, Padma Priya R (2014) Reconstruction of Images into 3D Models using CAD Techniques. European J Appl Eng Sci Res 3:1–8
4. Chromy A, Zalud L (2014) Robotic 3D scanner as an alternative to standard modalities of medical imaging. SpringerPlus a Springer Open J 3:1–10
5. Jin GQ, Li WD, Gao L, Popplewell K (2013) A hybrid and adaptive tool-path generation approach of rapid prototyping and manufacturing for biomedical models. Elsevier Comput Indus 64:336–349
6. Gomes Ferraz E, Costa Safira Andrade L, Rode dos Santos A, Rabelo Torregrossa V, do Rosario Santos Freire M, Almeida Sarmento V (2011) Effect of different surface processing protocols in three-dimensional images for rapid prototyping. Elsevier Adv Eng Softw 42:332–335
7. Wanga C-S, Wangb W-HA, Lin b M-C (2010) STL rapid prototyping bio-CAD model for CT medical image segmentation. Elsevier Comput 84 in Indus 61:187–197
8. Lauwagie T, Vanhollebeke F, Pluymers B, Zegels4 R, Verschueren4 P, Dascotte1 E (2010) The impact of high-fidelity model geometry on test-analysis correlation and FE model updating results. In: Proceedings of ISMA 2010, pp 2679–2688
9. Singare S, Li Dichen L, Bingheng LY, Zhenyu G, Yaxiong L (2004) Design and fabrication of custom mandible titanium tray based on rapid prototyping. J Med Eng Phys 26:671–676
10. Gebhardt A, Schmidt F-M, Hotter J-S, Sokalla W, Sokalla P (2010) Additive manufacturing by selective laser melting the realizer desktop machine and its application for the dental industry. J Phys Proc 5:543–549
11. Bammani S, Birajdar P, Metan S (2013) Application of CAD and SLA method in dental prosthesis. AMAE Int J Manuf Mater Sci 3:14–18
12. Varun Desai S, Venkateshkashyap KG, Thomas TO, Siddartha S, Ramesh CS (2013) Rapid prototyping of dental tool. In: Proceedings 3rd International Conference on Additive Manufacturing Technologies—AM 2013, Bangaluru
13. Costa Safira L, Costa Bastos L, Estevao Beal V, Almeida de Azevedo R, Eduardo Francischone C, Almeida Sarmento V (2013) Accuracy of rapid prototyping biomodels plotted by three dimensional printing technique: ex vivo study. Adv Comput Tomogr 2:41–45
14. Choi Y-J, Koak J-Y, Heo S-J, Kim S-K, Ahn J-S, Park D-S Comparison of the mechanical properties and microstructures of fractured surface for Co-Cr alloy fabricated by conventional cast, 3-D printing laser-sintered and CAD/CAM milled techniques. http://dx.doi.org/10.4047/jkap.2014.52.2.6785

15. Pan H, Li L, Tao J, Xurong X, Mao C, Gub X, Tang R (2008) Repair of enamel by using hydroxyapatite nano particles as the building blocks. J Mater Chem 18:4079–4084
16. Ozcan M, H¨ammerle C (2012) Review-titanium as a reconstruction and implant material in dentistry: advantages and pitfalls. J Mater 5:1528–1545
17. Malshe A, Bartolo P, Rajurkar K (2012) Biomedical production of implants by additive electro-chemical and physical processes. CIRP Ann Manuf Technol 61:635–655
18. Guti´errez Rubert SC, Meseguer Calas MD, Bellera Sosa J, Folguera Arbas, F.b (2013) Analysis of variability in the manufacture of Cr-Co fixed partial dentures by geometric comparison. Procedia 63:481–488
19. Satoko T, Soshu K, Mitsuyori S, Taiji S (2011) Particle size effect and mechanical properties of alumina dental crown fabricated by stereolithogrphy. Trans JWRI, I 40:85–87
20. Palamara JEA, Palamara D, Messer HH (2002) Strains in the marginal ridge during occlusal loading. Aust Dent J 47(3):218–222
21. Milewski G (2005) Numerical and experimental analysis of effort of human tooth hard tissues in terms of proper occlusal loadings. Acta of Bioeng Biomech 7:47–59
22. Raoofi S, Khademi Reza Amid M, Kadkhodazadeh M, Reza Movahhedi M (2013) Comparison of the effect of three abutment-implant connections on stress distribution at the internal surface of dental implants: a finite element analysis. J Dental Res Dental Clinics, Dental Prospects 7(3):132–133
23. Uddanwadiker Rashmi (2012) Study of various molar crown designs and their assessment. J Biomed Sci Eng 5:629–633
24. Biswas BK, Bag S, Pal S (2013) Biomechanical analysis of normal and implanted tooth using biting force measurement. Int J Eng Appl Sci 4(2):17–23
25. Weisskircher HW (2013) Maximum bilateral masticatory forces in patients with and without pain. J Craniomandibular Function 5(1):19–39

Index